

POLITEHNICA UNIVERSITY TIMIȘOARA  
Civil Engineering Faculty  
Department of Steel Structures and Structural Mechanics

# EFFECTS OF CYCLIC LOADING ON THE MECHANICAL PROPERTIES OF STEEL

---

Author: Pierre Darry VERSAILLOT, Civ. Eng.

Supervisors: Assoc. Professor Aurel STRATAN, Ph.D.  
&  
Lect. Ioan BOTH, Ph.D.



Universitatea Politehnica Timisoara, Romania

Study Program: **SUSCOS\_M**

Academic year: **2015 / 2017**

# EFFECTS OF CYCLIC LOADING ON THE MECHANICAL PROPERTIES OF STEEL

---

By

Pierre Darry VERSAILLOT

February 2017



## JURY MEMBERS

- President: **Professor Dan DUBINA, PhD**  
**Member of the Romanian Academy**  
Politehnica University Timișoara  
Srada Ioan Curea, 1  
300224, Timișoara, Timiș, Romania
- Members: **Assoc. Professor Aurel STRATAN, PhD**  
(Thesis Supervisor)  
Politehnica University Timișoara  
Srada Ioan Curea, 1  
300224, Timișoara, Timiș, Romania
- Professor Adrian CIUTINA, PhD**  
Politehnica University Timișoara  
Srada Ioan Curea, 1  
300224, Timișoara, Timiș, Romania
- Professor Viorel UNGUREANU, PhD**  
Politehnica University Timișoara  
Srada Ioan Curea, 1  
300224, Timișoara, Timiș, Romania
- S.I. Dr. ing. Cristian VULCU**  
Politehnica University Timișoara  
Srada Ioan Curea, 1  
300224, Timișoara, Timiș, Romania
- Secretary: **Assoc. Professor Adrian DOGARIU, PhD**  
Politehnica University Timișoara  
Srada Ioan Curea, 1  
300224, Timișoara, Timiș, Romania

## ABSTRACT

Laboratory experiments were performed on four European mild carbon steel grades i.e. S275, S355, S460 and S690 to investigate their stress-strain and low cycle fatigue behavior under cyclic loading. The coupons were tested at room temperature and at 0.2%/sec constant strain rate for three different loading protocols: Monotonic tensile, variable strain amplitude, and constant strain amplitude of  $\pm 1\%$ ,  $\pm 3\%$ ,  $\pm 5\%$  and  $\pm 7\%$ . Charpy V-notch impact tests were also performed at 20°C and -20°C to determine the amount of energy absorbed by each steel grade at fracture.

For the monotonic tensile tests, the steels with lower yield strength have shown higher ductility. Interestingly, recorded mechanical properties such as yield strength, proof stress, ultimate tensile strength and true fracture strength increased while the Young's modulus and the ductility decreased from S275 to S690. When comparing the monotonic to cyclic stress-strain curves, cyclic hardening was evident in both S275 and S355. In contrast, cyclic softening was evident in the high strength steel, S690. However, S460 exhibited a combination of cyclic softening within the first cycle followed by cyclic hardening within the remaining cycles. At the beginning of each cyclic loading, changes in cyclic deformation behavior were more visible but steady-state condition reached with continued cyclic for all the steel grades. For each steel grade, the number of cycles to failure decreased with increasing constant strain amplitude. S355 exhibited higher fatigue life than all the other steel materials but overall they exhibited roughly the same fatigue life behavior. Based on the results from Charpy V-notch impact tests, the energy absorbed at fracture by all the steel materials exceeded significantly the minimum energy required for traverse orientation.

Aimed at validating the experimental results, numerical analysis was also performed using Finite Element Software ABAQUS. The numerical results for selected coupons revealed close agreement with the experimental results.



## ACKNOWLEDGMENTS

I wish first to express my heartfelt thanks and deep appreciation to both my thesis supervisors Assoc. Professor Aurel STRATAN, Ph.D. and Lect. Ioan BOTH, Ph.D. of the Department of Steel Structures and Structural Mechanics at POLITEHNICA UNIVERSITY TIMIȘOARA (Romania). Whenever I had questions, their office doors were always open. Their valuable comments and contributions to complete this dissertation were more than important. In every single meeting, Prof. STRATAN always inspired me to organize my work. This valuable skill will be useful for my Ph.D. studies.

I would like to thank Ph.D. student Ciprian Zub. Without his passionate help, material calibration for the cyclic tests could not have been successfully conducted. I also express my sincere thanks to Ph.D students Cosmin and Adina as well as Dr. Ing. Ioan Mărginean.

I would also like to acknowledge the SUSCOS coordinator in Romania, Professor Dan DUBINA and Professor Adrian CIUTINA for their generous help and very valuable comments on this thesis. I also want to put on record my appreciation to every single administration staff I met and lecturer I had during the whole study period coming from the University of Coimbra (Portugal), Université de Liège (Belgium), University of Naples FEDERICO II ( Italy), Czech Technical University in Prague (Czech Republic) , Lulea University of Technology (Sweden), and Politehnica University of Timisoara (Romania).

I spent the whole study program with my colleagues Jie Xiang (from China) and Ghazanfar Ali Anwar (from Pakistan). Very special thanks go to them for their consistent support.

I am unable to express in words my gratitude to my girlfriend Ing. Lovely Polynice, my colleague Ing. Johane Dorcena and my friends Claude Siméus, Samenta Mentor, Fania Alexis, among others for their constant encouragement.

Last, but certainly not least, I must express my very profound gratitude to my family for providing me with unfailing support and continuous encouragement throughout my years of study abroad.

This accomplishment would not have been possible without each of you. Thank you very much.

# Contents

<b>JURY MEMBERS.....</b>	<b>3</b>
<b>ABSTRACT .....</b>	<b>4</b>
<b>ACKNOWLEDGMENTS .....</b>	<b>5</b>
<b>Contents .....</b>	<b>6</b>
<b>List of Tables.....</b>	<b>11</b>
<b>List of Figures .....</b>	<b>12</b>
<b>SECTION 1.....</b>	<b>14</b>
<b>INTRODUCTION .....</b>	<b>14</b>
1.1    Cyclic Loading and Low Cycle Fatigue .....	14
1.1.1    Notable Low Cycle Fatigue Failures .....	15
1.2    Objectives .....	16
1.3    Introduction to the Mechanical Properties of Steel .....	18
1.3.1    Yield Strength.....	18
1.3.2    Ductility.....	19
1.3.3    Toughness.....	20
1.3.4    Weldability .....	21
1.3.5    Other Mechanical Properties .....	22
1.4    Some Applications of Steel .....	22
1.5    Research Framework (RFSR-CT-2013-00021 EQUAL JOINT) .....	24
1.6    Thesis Outline.....	25
1.7    Limitations of Tests and Numerical Results.....	26
<b>SECTION 2.....</b>	<b>27</b>
<b>REVIEW OF LITERATURE .....</b>	<b>27</b>
2.1    Review of Analytical Models for Cyclic Behavior .....	27
2.1.1    Engineering and True Stress and Strain.....	27

2.1.1.1	Engineering and True Stress .....	27
2.1.1.2	Engineering and True Strain .....	28
2.1.1.3	Relationships between Engineering and True Stress and Strain.....	29
2.1.1.4	True Fracture Strength.....	29
2.1.2	Elastic and Plastic Deformation .....	30
2.1.2.1	Elastic Deformation.....	30
2.1.2.2	Plastic Deformation .....	31
2.1.3	Cyclic Plasticity.....	31
2.1.3.1	Bauschinger Effect .....	32
2.1.3.2	Isotropic Hardening Model.....	32
2.1.3.3	Kinematic Hardening Model .....	35
2.1.3.4	Combined Isotropic-Kinematic Hardening Model .....	40
2.1.4	Ramberg-Osgood Relationship.....	41
2.1.5	Fatigue Strain-Life Relationship .....	44
2.2	Summary of the Low Cycle Fatigue Steel Research .....	47
<b>SECTION 3 .....</b>		<b>50</b>
<b>EXPERIMENTAL TESTS FOR CYCLIC RESPONSE ASSESSMENT .....</b>		<b>50</b>
3.1	Equipment.....	50
3.2	Test Coupons Arrangement and Dimensions .....	50
3.3	Steel Material Details .....	51
3.4	Chemical Composition of the Steels .....	52
3.5	Load History Types .....	53
3.6	Coupons Grouping for the Testing .....	53
3.7	Specimens Nomenclature and Data Processing.....	54
<b>SECTION 4 .....</b>		<b>56</b>
<b>CYCLIC STRESS-STRAIN BEHAVIOR .....</b>		<b>56</b>
4.1	Results from Monotonic Tensile Tests.....	56

4.2	Results from Variable Strain Amplitude Tests .....	58
4.2.1	Results Comparison with Literature .....	60
4.3	Results from Constant Strain Amplitude Tests .....	61
4.4	Cyclic and Monotonic Stress-Strain Curves Comparison .....	66
4.5	Recorded Properties from Constant Strain Amplitude Tests.....	68
4.6	Results from Charpy Impact Tests .....	71
4.6.1	Standard, Methodology and Specimens .....	71
4.6.2	Tests Temperature and Materials details .....	73
4.6.3	Energy Absorption Capacity .....	73
<b>SECTION 5</b>	.....	<b>76</b>
<b>LOW CYCLE FATIGUE (LCF) BEHAVIOR</b>	.....	<b>76</b>
5.1	Recorded Fatigue Life .....	76
5.1.1	Variation of the Recorded Fatigue Life .....	77
5.2	Low Cycle Fatigue of the Steel Grades .....	79
5.2.1	For Each Steel Grade.....	79
5.2.2	For all the Considered Steel Grades .....	81
5.2.3	Comparison and Summary of the Results .....	82
5.3	Determination of the Strain-Life Fatigue Properties .....	83
5.3.1	Results and Comparison with Literature .....	84
5.5	Transition Fatigue Life .....	86
<b>SECTION 6</b>	.....	<b>88</b>
<b>FINITE ELEMENT MODELING (FEM)</b>	.....	<b>88</b>
6.1	FEM for Monotonic Tensile Tests.....	88
6.1.1	Part.....	88
6.1.2	Material Definition .....	89
6.1.3	Step .....	90
6.1.4	Load Definition.....	91

6.1.5	Mesh Definition.....	91
6.2	Numerical Results for Monotonic Tensile Load History .....	92
6.3	FEM for Cyclic Tests .....	95
6.3.1	Assumptions and Parts.....	95
6.3.2	Material Definition .....	95
6.3.2.1	Isotropic Hardening .....	96
6.3.2.2	Kinematic Hardening.....	98
6.3.3	Step .....	101
6.3.4	Load Definition.....	101
6.3.5	Mesh Definition.....	102
6.4	Numerical Results for Cyclic Load History .....	103
<b>SECTION 7 .....</b>		<b>108</b>
<b>CONCLUSIONS AND COMMENTS .....</b>		<b>108</b>
<b>SECTION 8.....</b>		<b>110</b>
<b>REFERENCES .....</b>		<b>110</b>
<b>APPENDIX .....</b>		<b>112</b>
1.	Results from monotonic tensile tests for S275 .....	112
2.	Results from constant strain amplitude tests for S275.....	113
3.	Results from variable strain amplitude tests for S275 .....	125
4.	Results from monotonic tensile tests for S355 .....	128
5.	Results from constant strain amplitude tests for S355.....	129
6.	Results from variable strain amplitude tests for S355 .....	140
7.	Results from monotonic tensile tests for S460 .....	143
8.	Results from constant strain amplitude tests for S460.....	144
9.	Results from variable strain amplitude tests for S460 .....	155
10.	Results from monotonic tensile tests for S690 .....	158
11.	Results from constant strain amplitude tests for S690.....	159

12. Results from variable strain amplitude tests for S690 ..... 170

## List of Tables

Table 1. 1: Variation of the minimum yield strength (MPa or N/mm <sup>2</sup> ) at ambient temperature [5] .....	18
Table 1. 2: Variation of the tensile strength (MPa or N/mm <sup>2</sup> ) at ambient temperature [5].....	19
Table 3. 1: Some Properties of the Steel Grades Used.....	52
Table 3. 2: Chemical Composition of the Considered Steel Grades [Source:AZO Materials] .....	52
Figure 4. 1: Stress-Strain from Monotonic Tensile Tests for all Steel Grades Considered .....	57
Table 4. 1: Recorded Mechanical properties of the Steel Grades Considered from Monotonic Tensile Tests.....	57
Figure 4. 2: Stress-Strain from Variable Strain Amplitude Tests for the steels .....	59
Table 4. 2: Mechanical Properties of the Steel Grades Considered from Variable Strain Amplitude Tests .....	60
Table 4. 3: Normalized Maximum Stress Ratio of the Steel Grades Considered Tests from Literature [16] .....	60
Table 4. 5: Recorded Properties from Constant Strain Amplitude Tests .....	70
Table 4. 7: Tolerances on specified test piece dimensions [ISO 148-1 : 2009 (E)] .....	72
Table 4. 8: Maximum permissible values of element thickness t in mm [EN 1993-1-10 : 2005 (E)] .....	72
Table 4. 9: Materials dimension at 20°C.....	73
Table 4. 10: Materials dimension at -20°C.....	73
Table 4. 11: Energy absorption capacity of the steel materials at 20 °C.....	74
Table 4. 12: Energy absorption capacity of the steel materials at -20 °C .....	74
Table 5. 1: Reversals to Failure (2N <sub>f</sub> ).....	76
Table 5. 2: Fatigue Life Coefficients from Literature [16].....	85
Table 5. 3: Fatigue Life Coefficients of the Considered Steel Grades .....	86
Table 5. 4: Comparison between Transition Fatigue Life and Reversals for the Steel Grades Considered.....	87

## List of Figures

Figure 1. 3: Building collapsed during the earthquake as a result of LCF [3, 4] .....	15
Figure 1. 9: Use of S275 and S355 steels in typical railway and highway bridges [8] .....	23
Figure 1. 10: Structural steel plates applications in bridges and buildings [8].....	23
Figure 1. 12: Structural steel plates applications in hydro power stations and boilers and pressure vessels [8].....	24
Figure 1. 13: Structural steel plates applications in storage tank and machinery [8].....	24
Figure 2. 1: Engineering and true stress versus engineering and true strain [9].....	28
Figure 2. 2: Elastic and plastic range of the stress-strain curve [11].....	31
Figure 2. 3: Description of the Bauschinger effect [9].....	32
Figure 2. 8: Graphic representation of the saturated stress represented by the nonlinear kinematic hardening model (Dunne and Petrinic, 2005) [10].....	38
Figure 2. 11: Generic representation of the stress–strain curve by means of the Ramberg–Osgood equation... [15]. .....	43
Figure 2. 12: Ramberg-Osgood Steel Material -- Hysteretic Behavior of Model [15]. .....	43
Figure 2. 13: Strain-life curves also called low cycle fatigue [16].....	44
Figure 2. 14: Schematic low cycle fatigue curve showing the transition fatigue life [9].....	46
Figure 3. 2: Coupon dimensions.....	51
Figure 3. 3: Monotonic Tensile load history .....	53
Figure 3. 4: Variable Strain Amplitude load history .....	53
Figure 3. 5: Constant Strain Amplitude load history.....	53
Table 3. 3: Coupons grouping for the testing .....	54
Figure 4. 1: Stress-Strain from Monotonic Tensile Tests for all Steel Grades Considered .....	57
Figure 4. 2: Stress-Strain from Variable Strain Amplitude Tests for the steels .....	59
Figure 4. 3: Stress-Strain Response of S275 Coupons at 1%, 3%, 5% and 7% Strain Amplitudes .....	62
Figure 4. 4: Stress-Strain Response of S355 Coupons at 1%, 3%, 5% and 7% Strain Amplitudes .....	63
Figure 4. 5: Stress-Strain Response of S460 Coupons at 1%, 3%, 5% and 7% Strain Amplitudes .....	64
Figure 4. 6: Stress-Strain Response of S690 Coupons at 1%, 3%, 5% and 7% Strain Amplitudes .....	65
Figure 4. 8: Cyclic and Monotonic Stress-Strain Curves Comparison for S355.....	67
Figure 4. 9: Cyclic and Monotonic Stress-Strain Curves Comparison for S460.....	67
Figure 4. 10: Cyclic and Monotonic Stress-Strain Curves Comparison for S690.....	68
Figure 4. 11: Representation of the V-notch according to ISO 148-1 : 2009 (E) .....	71
Figure 4. 12: Details of V-notch considered for the specimens .....	71
Figure 4. 13: Energy absorption capacity of the steel materials at 20°C and -20 °C .....	75
Figure 5. 1: Reversals to failure of all coupons tested for the steels at 1% strain amplitude .....	77
Figure 5. 2: Reversals to failure of all coupons tested for the steels at 3% strain amplitude .....	78
Figure 5. 3: Reversals to failure of all coupons tested for the steels at 5% strain amplitude .....	78



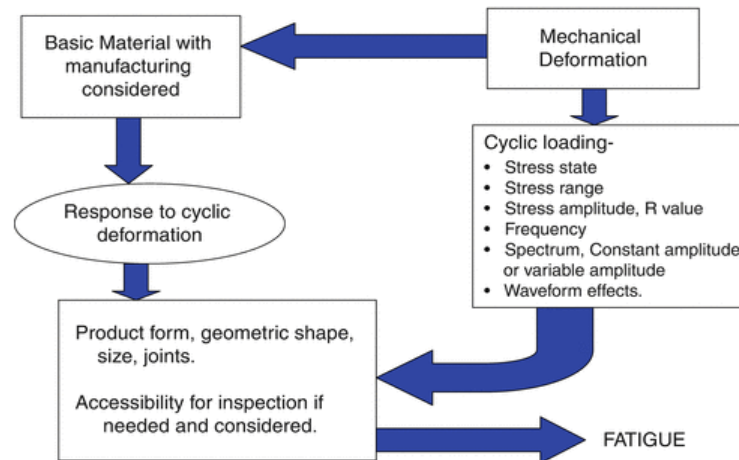
Figure 5. 4: Reversals to failure of all coupons tested for the steels at 7% strain amplitude .....	79
Figure 5. 7: Fatigue Strain-Life of S460.....	81
Figure 5. 9: Fatigue Strain-Life Comparison of all the Considered Steels.....	82
Figure 5. 10: Fatigue Strain-Life Comparison of all the Considered Steels from Literature [16] .....	83
Figure 5. 11: Hysteresis loop showing how to compute parameters [9] .....	84
Figure 6. 1: Schematic description of the Specimen .....	88
Figure 6. 2: Drawing of the specimen in Abaqus .....	89
Figure 6. 3: Material behaviors definition in Abaqus.....	90
Figure 6. 4: Step definition in Abaqus.....	90
Figure 6.5: Assigned boundary conditions .....	91
Figure 6. 6: Mesh definition and model meshing .....	92
Figure 6. 7: Deformation, von Mises stresses and stress-strain curves comparison of S275 and S355 .....	93
Figure 6. 8: Deformation, von Mises stresses and stress-strain curves comparison of S460 and S690.....	94
Figure 6. 9: Parts drawing in Abaqus for the materials calibration .....	95
Figure 6. 11: Steps to input parameters in Abaqus for Isotropic Hardening .....	98
Figure 6. 13: Steps to input parameters in Abaqus for Kinematic Hardening.....	100
Figure 6. 14: Material behaviors for cyclic tests .....	100
Figure 6. 15: Isotropic hardening parameters for S275 .....	100
Figure 6. 16: Kinematic hardening parameters for S275.....	101
Figure 6. 17: Step definition for cyclic materials modeling .....	101
Figure 6. 18: Loading protocol for L2C3-2.....	101
Figure 6. 19: Loading protocol for L2V3 .....	102
Figure 6. 20: mesh definition for cyclic materials.....	102
Figure 6. 21: Stress-Strain response comparison of L2C3-2 for the cube.....	104
Figure 6. 22: Stress-Strain response comparison of L2C3-2 for the cylinder .....	104
Figure 6. 23: Stress-Strain response comparison of L2V3 for the cube.....	105
Figure 6. 24: Stress-Strain response comparison of L2V3 for the cylinder .....	105
Figure 6. 25: Stress-Strain response comparison of L3C3-3 for the cube.....	106
Figure 6. 26: Stress-Strain response comparison of L3C3-3 for the cylinder .....	106
Figure 6. 27: Stress-Strain response comparison of L3V2 for the cylinder .....	107

# SECTION 1

## INTRODUCTION

### 1.1 Cyclic Loading and Low Cycle Fatigue

Cyclic loading can be defined as the application of repeated or fluctuating stresses, strains, or stress intensities to locations on structural components. The degradation that may occur at the location is referred as fatigue degradation. During service, structural components can either be subjected to stress that remains in the elastic range or exceeds the elastic limit. As a result, fatigue design requires a special attention for the assessment of stress and strain fields in the critical areas. For a better understanding, Figure 1.1 shows the systems view of basic fatigue considerations (Hoepfner, 1971).



**Figure 1. 1: Systems view of fatigue [1]**

An important aspect of the fatigue process is plastic deformation because fatigue cracks usually nucleate from plastic straining in localized regions. In the low cycle fatigue region and in notched members, instead of using cyclic-stress controlled tests, strain-controlled tests are preferred to better characterize fatigue behavior of a material.

Components when subjected to relatively high stress, fails at low numbers of cycles and the component is subject to low cycle fatigue (LCF) as shown in Figure 1.2. The structural components used at high temperature shows LCF failure as a predominant failure mode.

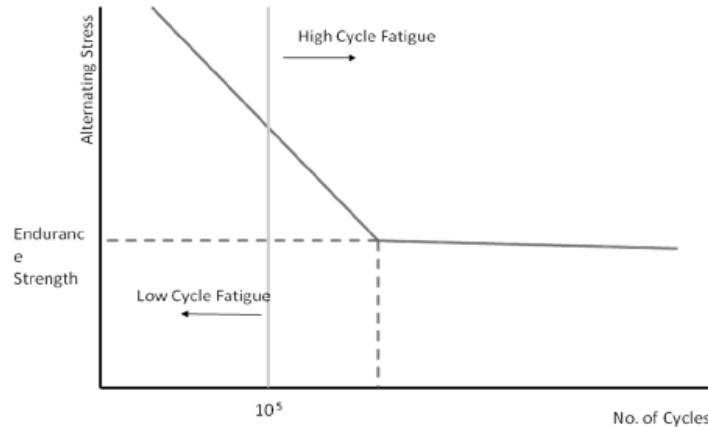


Figure 1. 2: Low and High Cycle Fatigue [2]

### 1.1.1 Notable Low Cycle Fatigue Failures

One notable event in which the failure was a result of Low Cycle Fatigue (LCF) was the Northridge Earthquake of 1994. Many buildings and bridges collapsed, and as a result over 9,000 people were injured [3]. Researchers at the University of Southern California analyzed the main areas of a ten-story building that were subjected to low-cycle fatigue. Unfortunately, there was limited experimental data available to directly construct a S-N curve for low-cycle fatigue, so most of the analysis consisted of plotting the high-cycle fatigue behavior on a S-N curve and extending the line for that graph to create the portion of the low-cycle fatigue curve using the Palmgren-Miner method. Ultimately, this data was used to more accurately predict and analyze similar types of damage that the ten-story steel building in Northridge faced [4].



Figure 1. 3: Building collapsed during the earthquake as a result of LCF [3, 4]



Figure 1. 4: Bridge collapsed during the earthquake as a result of LCF [3, 4]

It is then extremely important to understand how materials behave under cyclic loading because in designing engineered structures such as buildings, bridges, dams, tunnels etc..., the impact of not understanding the strength of materials used can be fatal. In this section are presented the objectives of the study, an introduction to the mechanical properties of steel, some applications of steel, the research framework, and the thesis outline.

## 1.2 Objectives

Compared to the monotonic tensile loading, there is a lack of experimental and numerical data on the cyclic stress-strain response and low cycle fatigue (LCF) characteristics of the European mild carbon steel. Cyclic testing is crucial in engineering since it provides information pertaining to the suitability of materials for earthquake engineering applications. Therefore, the purpose of the study is twofold:

- (a) To investigate experimentally the stress-strain behaviour of four European mild carbon steels subjected to repeated cyclic plastic deformations. Specific interests include investigation of the resistance to deformation of the steel grades (cyclic hardening or softening) and finding important parameters such as cyclic yield strength ( $S'_y$ ), cyclic strength exponent ( $K'$ ), cyclic strain hardening exponent ( $n'$ ), maximum stress ( $\sigma_{max}$ ) and strain ( $\varepsilon_{max}$ ) and number of cycles to failure ( $N_f$ ) for a material model in Abaqus.

(b) To characterize their low-cycle fatigue response. Low cycle fatigue characteristics are mainly focused on determining the Strain-Life Fatigue properties of the steel grades including fatigue strength coefficient( $\sigma'_f$ ), fatigue strength exponent (b), fatigue ductility coefficient( $\epsilon'_f$ ), and fatigue ductility exponent (c) to compare their fatigue life.

In figure 1.5, a flow chart describing the scope of the study is presented.

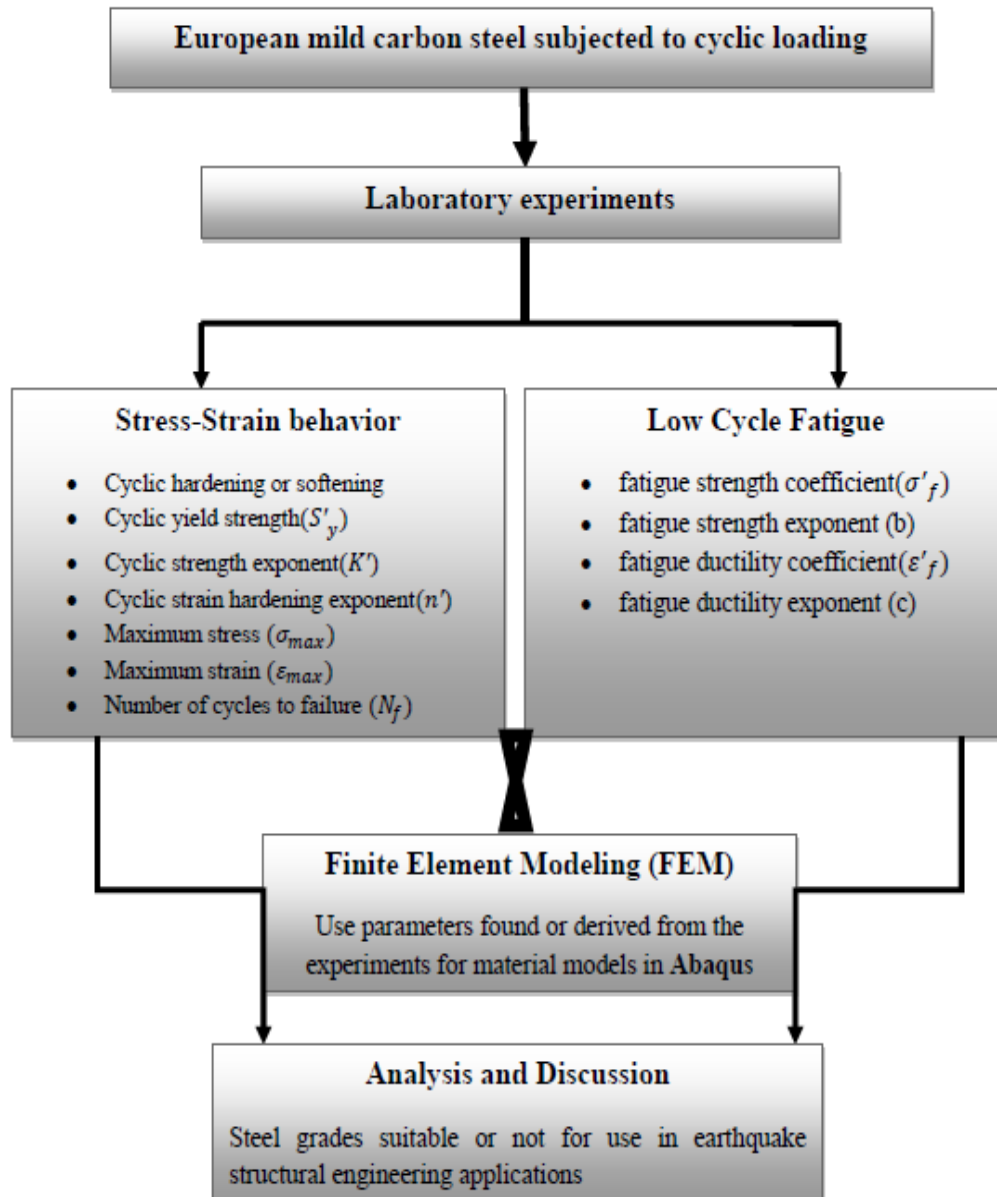


Figure 1. 5: Flowchart describing the aim of the study

## 1.3 Introduction to the Mechanical Properties of Steel

The study presents the key mechanical properties that are of interest to designer including strength, ductility, toughness, weldability, and others including modulus of elasticity, shear modulus, Poisson's ratio and coefficient of thermal expansion.

### 1.3.1 Yield Strength

Defined as the stress at which a material starts to deform inelastically, the Yield Strength, also known as yield point, is the most important property of steel. In the CEN product standards [5] the first designation relates to the yield strength for a material up to 16mm thick. For instance, the minimum yield strength ( $R_{eH}$ ) for the structural steel S355 is 355 N/mm<sup>2</sup> (MPa). While the plate or section thickness increases, the yield strength reduces. Tables 1.1 and 1.2 show the change of the minimum yield strength ( $R_{eH}$ ) and tensile strength ( $R_m$ ) of the common steels with thickness according to EN 10025-1 [5].

**Table 1. 1: Variation of the minimum yield strength (MPa or N/mm<sup>2</sup>) at ambient temperature [5]**

Steel grade	Nominal thickness (mm)					
	≤ 16	>16 ≤ 40	>40 ≤ 63	>63 ≤ 80	>80 ≤ 100	>100 ≤ 120
<b>S275</b>	275	265	255	245	245	240
<b>S355</b>	355	345	335	325	325	320
<b>S420</b>	420	400	390	380	370	365
<b>S460</b>	460	440	430	410	400	385

**Table 1. 2: Variation of the tensile strength (MPa or N/mm<sup>2</sup>) at ambient temperature [5]**

Steel grade	Nominal thickness (mm)				
	≤ 40	>40	>63	>80	>100
		≤ 63	≤ 80	≤ 100	≤ 120
S275	370 to 530	360 to 520	350 to 510	350 to 510	350 to 510
S355	470 to 630	450 to 610	440 to 600	440 to 600	430 to 590
S420	520 to 680	500 to 660	480 to 640	470 to 630	460 to 620
S460	540 to 720	530 to 710	510 to 690	500 to 680	490 to 660

### 1.3.2 Ductility

Ductility is also important to all steels in structural applications. It can be defined as a measure of the degree to which a material can elongate between the onset of yield and eventual fracture under tensile loading. Ductility is particularly important for the redistribution of stress at the ultimate limit state, bolt group design, minimize risk of fatigue crack propagation and in the fabrication processes of welding, bending and straightening. Ductility tends to decrease with increasing yield strength. Nonetheless, this effect is not significant enough to affect the design of the majority of engineering structures especially bridges. To keep away from brittle failure of structural elements, ductility is required. For steels, a minimum ductility is required that should be expressed in terms of limits for:

- The elongation at failure on a gauge length of  $5.65\sqrt{A_0}$  where  $A_0$  is the original cross-sectional area; Eurocode recommends an elongation at failure not less than 15% [5].
- The ratio  $\frac{f_u}{f_y}$  of the specified minimum ultimate tensile strength  $f_u$  to the specified minimum yield strength  $f_y$ ; Eurocode recommends a minimum value of  $\frac{f_u}{f_y} \geq 1.10$  [5].
- As illustrated in Figure 1.6, the higher the yield strength, the lower elongation will be present at failure.

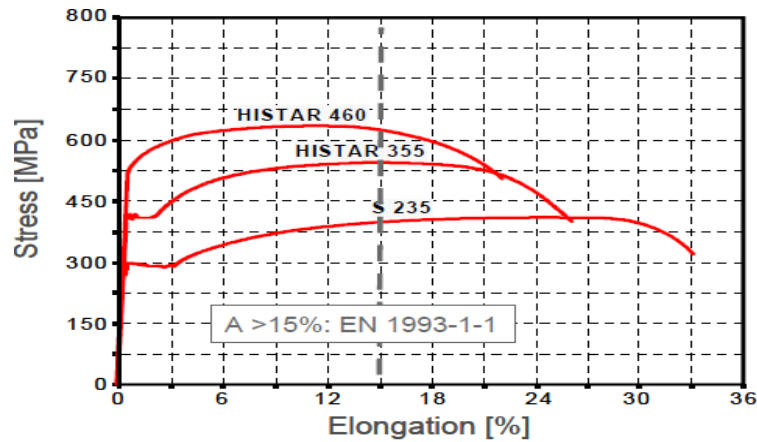


Figure 1. 6: Stress-strain curves comparison for S235, S355, and S460 [5]

### 1.3.3 Toughness

Toughness is the resistance of a material to brittle fracture when stressed. It can be defined as the amount of energy per volume that a material can absorb before rupturing. The material toughness depends on:

- Temperature: With reducing temperature, materials lose their crack resistance capacity.
- Influence of loading speed: The higher the loading speed, the lower the toughness
- Grain size: Fine grained steels are more resistant to brittle failure because whenever the crack tip reaches the grain boundary, the crack would subsequently change his growth direction and thus dissipated energy.
- Cold forming: The yield strength increases with decreasing ductility when the cold forming increases.
- Material thickness: Thinner plates with a higher share of material in the two-dimensional stress state do have more ductility than thicker plates

The toughness of steel and its ability to resist brittle fracture are dependent on a number of factors that should be considered at the specification stage. A convenient measure of toughness is the Charpy V-notch impact test. The Charpy impact test, also known as the Charpy V-notch test, is a standardized high strain-rate test which determines the amount of energy absorbed by a material during fracture.



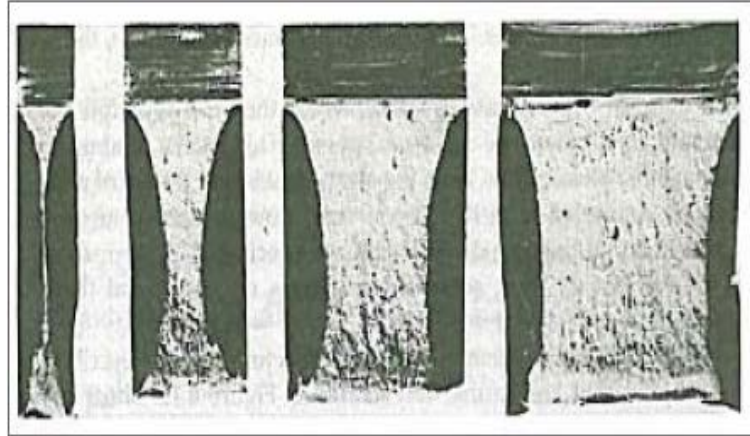


Figure 1. 7: Fracture surfaces of Charpy impact tests for plates with different material thickness [6]

### 1.3.4 Weldability

The weldability of steels highly depends on the hardenability of the steel, which is an indication of the propensity to form martensite during cooling after heating [7]. All structural steels are essentially weldable. And the hardening of steels depends on its chemical composition. With greater quantities of carbon and other alloying elements resulting in a higher hardenability and thus a lower weldability. Welding involves locally melting the steel, which subsequently cools.

In order to be able to compare alloys made up of distinct materials, a measure known as the equivalent carbon content (CEV) is used to estimate the relative weldability of different alloys. The weldability of the steel reduces with the increasing of the equivalent carbon content [7]

The trade-off between material strength and weldability is explained by the fact that low alloy steels are characterized by a reduced resistance and higher alloying contents by a poor weldability. However, with the thermomechanical rolling process, high strength steel can be produced without substantial increase in the carbon equivalent and hence, keeping an excellent weldability even for thick products [7].



Figure 1. 8: Welding stiffeners onto a large fabricated beam [7]

### 1.3.5 Other Mechanical Properties

Other mechanical properties of paramount importance to the designer include:

- Modulus of elasticity,  $E=210,000 \text{ N/mm}^2$
- Shear modulus,  $G = \frac{E}{2(1+\nu)}$ , often taken as  $81,000 \text{ N/mm}^2$
- Poisson's ratio,  $\nu = 0.3$
- Coefficient of thermal expansion,  $\alpha = 12 * 10^{-6} / ^\circ\text{C}$  (in the ambient temperature range)

## 1.4 Some Applications of Steel

Currently, Steel is been used for several structural purposes. Its application can be summarized as follows:

S275 steel is often used for railway bridges, where stiffness rather than strength governs the design, or where fatigue is the critical design case [8]. S355 steel is predominantly used in highway bridge applications, as it is readily available, and normally gives the best balance between stiffness and strength. S420 and S460 steels can offer advantages where self-weight is critical or the designer needs to reduce plate thicknesses [8]. However, the use of such steels confers no benefits in applications where fatigue, stiffness or the instability of extremely slender members is the overriding design consideration.

S690 steels are used in a variety of sectors including heavy transportation, machine building, steel constructions and lifting equipment. Their applications in many civil infrastructures are shown from Figure 1.9 to Figure 1.13.



**Figure 1. 9: Use of S275 and S355 steels in typical railway and highway bridges [8]**



**Figure 1. 10: Structural steel plates applications in bridges and buildings [8]**



**Figure 1. 11: Structural steel plates applications in ships and offshore structures [8]**



**Figure 1. 12: Structural steel plates applications in hydro power stations and boilers and pressure vessels [8]**



**Figure 1. 13: Structural steel plates applications in storage tank and machinery [8]**

## **1.5 Research Framework (RFSR-CT-2013-00021 EQUAL JOINT)**

The dissertation was conducted as one part of task 4 of the European Research Framework EQUAL JOINTS projects. Task 4 of the project is divided into six (6) parts and the current work is categorized as task 4.6 aiming at characterizing the cyclic response of European Mild Carbon Steel and was conducted at Universitatea Politehnica Din Timisoara (UPT) in Romania.

EQUAL JOINTS projects are carried out in collaboration with the following universities and companies:

- 1) UNIVERSITY OF NAPLES FEDERICO II (UNINA, Italy)
- 2) ARCELORMITTAL BELVAL & DIFFERDANGE SA (AM, Luxemburg)
- 3) UNIVERSITE DE LIEGE (ULG, Belgium)
- 4) UNIVERSITATEA POLITEHNICA DIN TIMISOARA (UPT, Romania)
- 5) IMPERIAL COLLEGE OF SCIENCE, TECHNOLOGY AND MEDICINE (England)
- 6) UNIVERSIDADE DE COIMBRA (UC, Portugal)

- 7) EUROPEAN CONVENTION FOR CONSTRUCTIONAL STEELWORK VERENIGING  
8) CORDIOLI & C.S.P.A. (Italy)

The research activities of the task 4 of the project are divided as follows:

- Task 4.1: Design of test setup  
(UNINA, UPT, ULG and AM)
- Task 4.2: Manufacturing of joint specimens  
(AM and CORDIOLI)
- Task 4.3: Experimental tests performed on the set of joints (UNINA, ULG and UPT)
- Task 4.4: cancelled
- Task 4.5: Tests on base material  
(UNINA, UPT, ULG and AM)
- **Task 4.6: Characterization of cyclic response of European mild carbon steel (UPT)**

## 1.6 Thesis Outline

Section 2 presents the review of literature which includes a review of analytical models for cyclic behavior as well as some previous works done on both cyclic and low cycle fatigue behavior.

The experimental tests for cyclic response assessment are described in Section 3. The details of the materials used, the geometry of the specimens and the implemented loading in the testing programmes, strain amplitude, and strain rate are presented.

In Section 4, the cyclic stress-strain behavior of the steel grades is analyzed. The analysis includes experimental results from monotonic tensile tests, results from variable strain amplitude tests, results from constant strain amplitude tests, results from Charpy Impact tests as well as determination of important parameters such as cyclic hardening or softening, cyclic yield strength ( $S'_y$ ), cyclic strength exponent ( $K'$ ), cyclic strain hardening exponent ( $n'$ ), maximum stress ( $\sigma_{max}$ ) and strain ( $\varepsilon_{max}$ ) and number of cycles to failure ( $N_f$ ). The results of the present work are compared with results from previous works.



In Section 5, the low cycle fatigue (LCF) behavior of the steel grades is analyzed. The analysis includes experimental results from constant strain amplitude tests as well as determination of the Strain-Life Fatigue properties of the steel grades including fatigue strength coefficient ( $\sigma'_f$ ), fatigue strength exponent (b), fatigue ductility coefficient ( $\epsilon'_f$ ), and fatigue ductility exponent (c). The transition fatigue life is also computed to verify that plastic strains dominate the low cycle fatigue behavior. The results of the present work are compared with results from previous works.

In Section 6, finite element modelling (FEM) of the tests using parameters found or derived from laboratory experiments is conducted using commercial finite element software, ABAQUS, to validate the results of the experiments.

Section 7 presents the overall research conclusions and comments. The references related to the study can be found in Section 8. Finally, an appendix is prepared containing detailed results. The idea is to provide necessary information for future work on steels subjected to cyclic loading.

## 1.7 Limitations of Tests and Numerical Results

In the study, the results obtained for the stress-strain and low cycle fatigue behavior of the four steel grades have the following restrictions:

- The study was performed on specimens machined from plates of 30mm with standard shapes. Therefore, the results obtained for the study might be different when using other steel sections.
- For all the considered steels, all the tests were performed under axial strains only. The stress-strain and low cycle fatigue behavior under multi-axial strains could be different.
- The strain rate effect on the stress-strain response was not considered in the study. The stress-strain behavior of the coupons could not be the same for different strain rate.
- The fatigue strain-life obtained for the considered steel grades is limited to 1%, 3%, 5% and 7% constant strain amplitudes.
- To obtain accurate cyclic hardening data, the calibration experiment should be performed at the same strain range anticipated in the analysis because the material does not predict different isotropic hardening behavior at different strain ranges [22].
- The results are valid for 20°C. The toughness might influence the results.

## SECTION 2

### REVIEW OF LITERATURE

#### 2.1 Review of Analytical Models for Cyclic Behavior

To investigate the behavior of steel materials under cyclic loading, several analytical relationships have been proposed including inelastic stress-strain and fatigue life relationships.

##### 2.1.1 Engineering and True Stress and Strain

Monotonic tension stress-strain properties are used in several specifications. The monotonic behavior is obtained from a tension test where a specimen with circular or rectangular cross section within the uniform gage length is subjected to a monotonically rising force until it fractures. Monotonic uniaxial stress-strain behavior can be based on engineering or nominal stress-strain or true stress-strain relationships. The difference is in using original versus instantaneous gage section dimensions.

###### 2.1.1.1 Engineering and True Stress

The nominal engineering stress ( $\sigma$ ), knowing the axial force (P) and the original cross sectional area ( $A_0$ ), is given by:

$$\sigma = \frac{P}{A_0} \quad (2.1)$$

The true stress ( $\sigma_{true}$ ), knowing the instantaneous cross sectional area (A), is given by:

$$\sigma_{true} = \frac{P}{A} \quad (2.2)$$

Because the cross sectional area decreases during loading, the engineering stress is smaller than the true stress in tension.

### 2.1.1.2 Engineering and True Strain

The engineering strain ( $\epsilon$ ) is calculated based on the original gage length ( $l$ ), the instantaneous gage length ( $l_0$ ), and the variation in length ( $\Delta l$ ) of the original gage length.

$$\epsilon = \frac{(l - l_0)}{l_0} = \frac{\Delta l}{l_0} \tag{2.3}$$

The true or natural strain ( $\epsilon_{true}$ ) is evaluated based on the instantaneous gage length as:

$$d\epsilon_{true} = \frac{dl}{l} \text{ or } \epsilon_{true} = \int \frac{1}{l} dl = \ln \left( \frac{l}{l_0} \right) \tag{2.4}$$

As shown in Figure 2.1, for very small strains, less than about 2 percent, the engineering and true stress are roughly equal and it is the same case for the engineering and true strain. Therefore, there is no distinction between engineering and true components. However, for larger strains, the differences are appreciable.

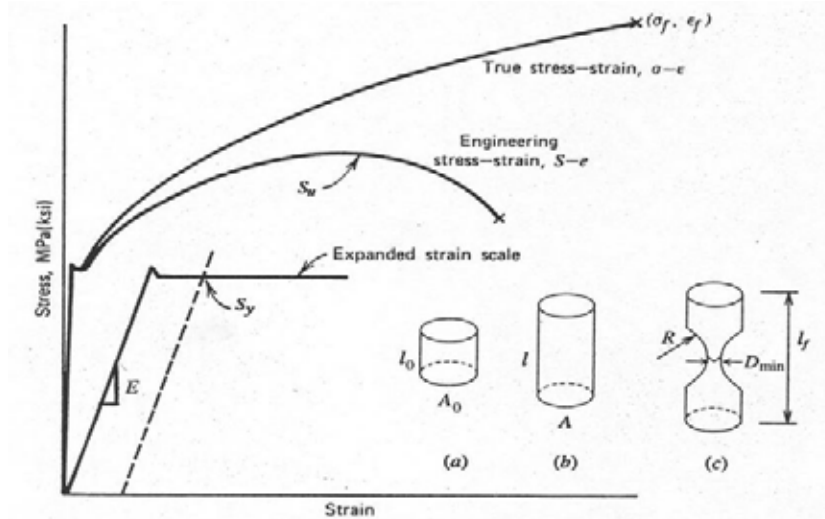


Figure 2. 1: Engineering and true stress versus engineering and true strain [9]



### 2.1.1.3 Relationships between Engineering and True Stress and Strain

A constant volume condition can be assumed up to necking such that  $A_0 \cdot l_0 = A \cdot l$ . Valid only up to necking which occurs when the ultimate strength is reached, the nominal (engineering) values can be related to the true stress and true strain using equations 2.5 and 2.6 [9]:

$$\sigma_{true} = \sigma(1 + \varepsilon) \quad (2.5)$$

$$\varepsilon_{true} = \ln\left(\frac{A_0}{A}\right) = \ln(1 + \varepsilon) \quad (2.6)$$

### 2.1.1.4 True Fracture Strength

The true fracture strength also known as breaking strength can be calculated as follows [9]:

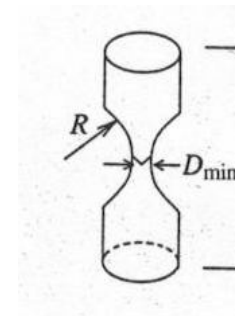
$$\sigma_f = \frac{P_f}{A_f} \quad (2.7)$$

However, correction is usually made using Bridgman correction factor for necking, which causes a biaxial state of stress at the neck surface and a triaxial state of stress at the neck interior. Equation 2.8 is not valid for brittle materials because they do not exhibit necking [9].

$$\sigma_f = \frac{\frac{P_f}{A_f}}{\left(1 + \frac{4R}{D_{min}}\right) \ln\left(1 + \frac{D_{min}}{4R}\right)} \quad (2.8)$$

R= radius of curvature of the neck

$D_{min}$ = diameter of the cross-section in the thinnest part of the neck



## 2.1.2 Elastic and Plastic Deformation

A deformation will occur in either elastic or elastic-plastic conditions, which depends on the magnitude of the applied load when a load is applied to a body. On the one hand, in the elastic deformation range, the body is returned to its original shape when the load is removed. On the other hand, inelastic deformation is irreversible and occurs when the load is such that some position within the component exceeds the elastic limit. Based on the physics of the phenomena, the elastic deformation involves a variation in the interatomic distances without changes of place while plastic deformation modifies interatomic bonds caused by slip movement in the microstructure of the material (Lemaitre and Chaboche, 1994). Figure 2.2 summarizes the difference between elastic and plastic deformation.

### 2.1.2.1 Elastic Deformation

As reported by Timoshenko (1953), Robert Hooke studied the elasticity phenomenon by measuring how far a wire string, of around 30 feet (1ft=30.48cm) in length deformed under an applied load. In the test, the magnitude of the extension was found to be proportional to the applied weight. Thus, the deformation of an elastic spring is generally described mathematically by the following equation [10]:

$$F = kx \quad (2.9)$$

Where: F= applied force; x=associated displacement and k= proportionality factor commonly referred as spring constant.

Based on equation 2.9, the force and the displacement characteristics depend on the size of the measured body. Thus, stress,  $\sigma$ , which refers to the ratio of the applied force to the cross sectional area, and strain,  $\varepsilon$ , which refers to the ratio of the extension to the initial length, are introduced to eliminate the geometrical factors (Callister, 2000). Equation 2.9 can be rewritten as [10]:

$$\sigma = E\varepsilon \quad (2.10)$$

Where  $E$  is proportionality constant which is often referred to as the Young's modulus or the modulus of elasticity (Hertzberg, 1996) for the material. Equation 2.10 is also known as Hooke's law, which describes the linear stress-strain response of a material.

### 2.1.2.2 Plastic Deformation

Plastic deformation occurs when the applied load (or stress) exceeds a certain level of stress called the elastic limit. Above this limit, the stress is no longer proportional to strain.

However, the exact stress at which this limit occurs is difficult to determine experimentally as it depends on the accuracy of the strain measurement device used. Thus, a conventional elastic limit or a yield stress value is determined by constructing a straight line parallel to the linear elastic stress-strain curve at a specified strain offset, commonly 0.2%. The junction point between the parallel line and the experimental curve is taken as the yield stress (0.2% proof stress,  $R_{p0.2}$ ) value.

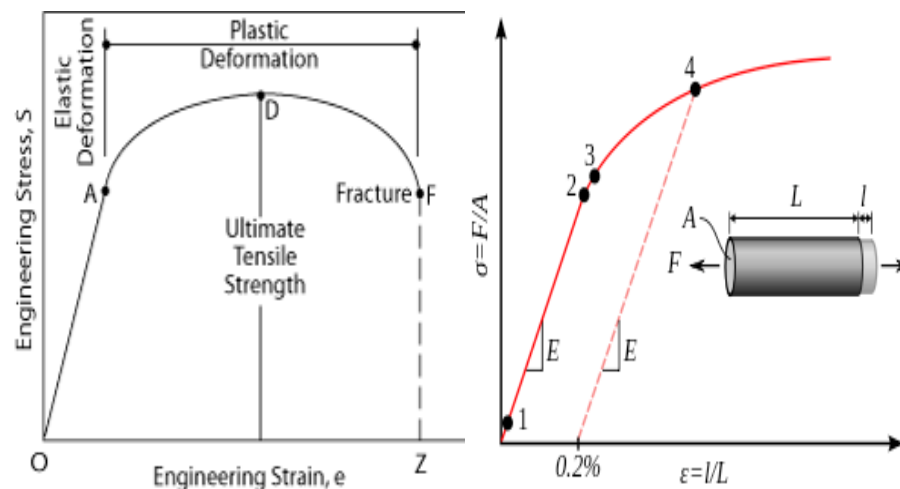


Figure 2. 2: Elastic and plastic range of the stress-strain curve (left figure). Typical stress-strain curve of a metal showing 0.002 strain offset where 1: true elastic limit; 2: Proportionality limit; 3: Elastic limit; 4: Offset yield strength (right figure) [11]

### 2.1.3 Cyclic Plasticity

When subjected to cyclic loading condition, the plastic deformations which occur in materials exhibit several phenomena such as the Bauschinger effect, cyclic hardening and softening, and material ratchetting. The cyclic loading of a material, under tension-compression conditions,

produces a hysteresis loop. The stress-strain behaviour which occurs under cyclic loading, with time independent effects are normally represented by isotropic hardening, kinematic hardening or some combination of both the isotropic and kinematic hardening models.

### 2.1.3.1 Bauschinger Effect

The stress-strain behavior obtained from a monotonic test can be totally different from that obtained under cyclic loading. This was first observed by Bauschinger. His experiments indicated the yield strength in tension or compression was reduced after applying a load of the opposite sign that caused inelastic deformation. Thus, one single reversal of inelastic strain can change the stress-strain behavior of metals. The schematic description of the Bauschinger effect is shown in Figure 2.3.

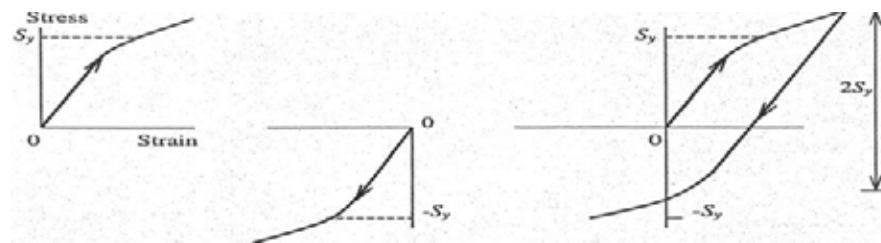


Figure 2. 3: Description of the Bauschinger effect [9]

The Bauschinger effect refers to a property of materials where the material's stress/strain characteristics varies due to the microscopic stress distribution of the material. For example, an increase in tensile yield strength occurs at the expense of compressive yield strength. The effect is named after German engineer Johann Bauschinger. The greater the tensile cold working, the lower the compressive yield strength [12].

### 2.1.3.2 Isotropic Hardening Model

Isotropic hardening relates to the variation which occurs in the equivalent stress, describing the size of the yield surface, as a function of collected plastic strain. A schematic description of the isotropic hardening model is shown in Figure 2.4.

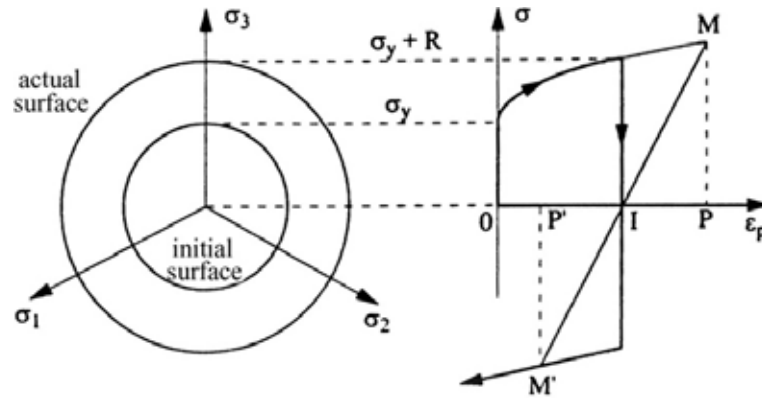


Figure 2. 4: Illustration of the isotropic hardening on the deviatoric plane and in tension-compression test conditions (Chaboche, 2008) [10]

Isotropic hardening, or possibly, the variation in the size of the yield surface is denoted by a scalar variable,  $R$ , and also known as a drag stress (Chaboche and Rousselier, 1983). The rate of evolution of isotropic hardening is represented by the following equation:

$$\dot{R} = b(Q - R)\dot{p} \tag{2.11}$$

where  $p$  is the accumulated plastic strain,  $Q$  is the asymptotic value of  $R$  and  $b$  defines the speed at which the saturation value, when variable  $R$  is constant, is approached. By integrating equation 2.11 with respect to time, the following equation is obtained:

$$R = Q(1 - e^{-bp}) \tag{2.12}$$

When the von Mises loading function is used, the yield criterion for the isotropic hardening model in the uniaxial form is expressed by the following equation [10]:

$$f = |\sigma| - R - \sigma_y = 0 \tag{2.13}$$

For which  $\sigma_y$  is the initial uniaxial yield stress in tension, or the initial elastic limit, as shown in Figure 2.4.

Subjected to cyclic loading conditions, an intact material (in which cracks do not generally influence the mechanical behaviour) exhibits an evolution of the plastic strain range as the

number of cycles increases which is called cyclic hardening or cyclic softening behavior. The cyclic hardening of a material can be defined as the decrease of the plastic strain range, corresponding with an increase of the stress amplitude with increasing number of cycles in a cyclic test. This is observed under strain-controlled test conditions. In the one hand, this behaviour has been observed in many materials such as 316 stainless steel (Hyde et al., 2010; Kim et al., 2008; Mannan and Valsan, 2006), high nickel-chromium materials (Leen et al., 2010) and nickelbased superalloys (Zhan et al, 2008; Kim et al., 2007; Yaguchi et al., 2002). On the other hand, the plastic strain range rises as cyclic loading continues in a material, exhibiting cyclic softening behaviour such as is found to occur in a 55NiCrMoV8 (Bernhart et al., 1999) and 9Cr-1Mo steel (Nagesha et al., 2002; Shankar et al., 2006; Fournier et al., 2006; Fournier et al., 2009a). The cyclic hardening phenomenon shows an increase of material's strength (Chaboche, 2008) in which the elastic strain range increases for a constant strain range. In the isotropic hardening model, this phenomenon is represented by an increase of the elastic limit ( $\sigma_Y + R$ ). For a material exhibiting cyclic softening behaviour, the constant  $Q$  is negative so that a stabilized yield surface becomes smaller than the initial one (Chaboche, 2008).

The presence of isotropic hardening can be showed by conducting biaxial tension tests such as tension-torsion tests (Lemaitre and Chaboche, 1994). For example, Murakami et al. (1989) conducted tension-torsion tests for a type 316 stainless steel and demonstrated the evolution of cyclic hardening at different temperatures. Murakami et al. (1989) also found that the temperature of the test affected the ratio of the stress amplitudes at the saturated state to that in the initial cycle; it also affected the accumulated inelastic strain required to reach cyclic stabilization.

The temperature also affects the cyclic evolution of certain materials. For example, cast iron has been shown to exhibit cyclic hardening behaviour at temperatures below 500°C, while the material has evolved in a cyclic softening condition when the test temperature is above 600°C (Constantinescu et al., 2004).

Under cyclic loading, a material, in general, shows a well balanced stage, in the middle of its lifetime. Some materials, nevertheless, such as a martensitic type steels, exhibit a primarily rapid load decrease followed by linear cyclic softening behaviour without the stabilization of the stress

amplitude for a strain-controlled test. In dealing with this behaviour, Bernhart et al. (1999) employed a two-stage isotropic hardening model, as expressed by the following equation:

$$R(p) = Q_1 p + Q_2(q)(1 - e^{-bp}) \tag{2.14}$$

Considering the stress amplitude evolution data, the constant  $Q_2$  is evaluated from the difference between the stress at first cycle and the stress approximately at the end of the primary load decrease while the constant  $Q_1$  is obtained from the slope of the secondary stage, as shown in Figure 2.5. This type of isotropic hardening model has been used for anisothermal loading conditions (Zhang et al, 2002).

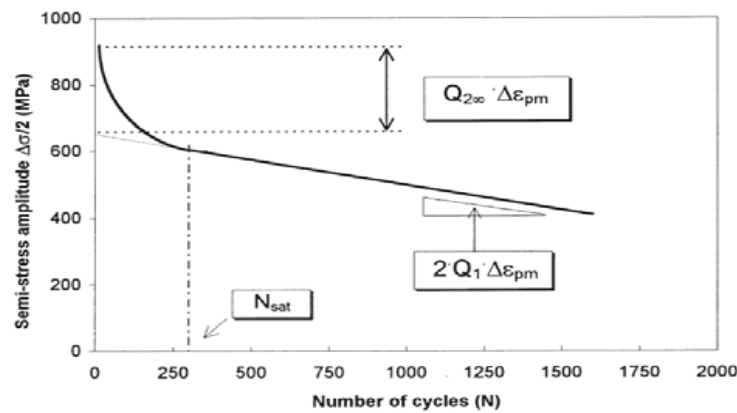


Figure 2. 5: Graphical representation of the two-stage cyclic softening model (Bernhart et al., 1999) [10]

### 2.1.3.3 Kinematic Hardening Model

Kinematic hardening model can also be used to represent the hardening of a material, which occurs because of plastic deformation. Compared to the isotropic hardening model, this model uses a different theoretical approach which can be explained by the fact that the yield surface translates in stress space, rather than expands (Dunne and Petrinic, 2005).

Also called the back stress or rest stress tensor, the kinematic hardening parameter  $\chi$  is a tensor (Chaboche and Rousselier, 1983), which defines the instantaneous position of the loading surface (Lemaitre and Chaboche, 1994). A graphic description of the kinematic hardening model in stress space and the corresponding model in a tension-compression test, in which  $k$  represents the elastic limit value is shown in Figure 2.6.

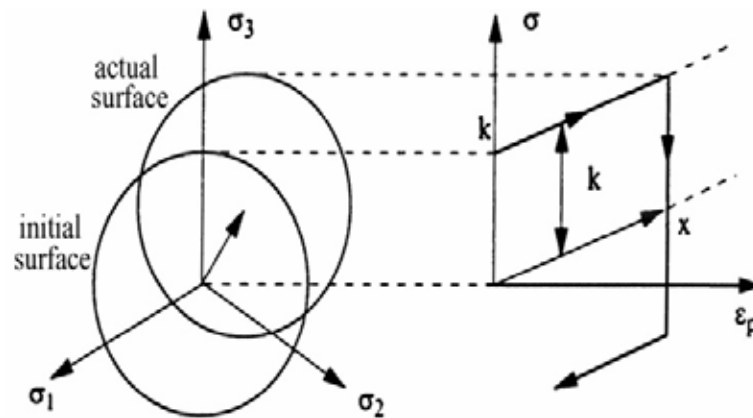


Figure 2. 6: Graphic description of the kinematic hardening in deviatoric plane and in tension-compression test (Chaboche, 2008) [10]

It is commonly found that, in a tension-compression test, the yield stress in compression is lower than that in tension if the test was conducted in tension first. This behaviour is referred as the Bauschinger effect in which plastic deformation increases the yield strength in the direction of plastic flow and decreases it in the reverse direction (Zhang and Jiang, 2008).

The kinematic hardening model is more suitable for representing this phenomenon where the model assumes that the elastic region remains constant, both initially and during cyclic loading (Dunne and Petrinic, 2005), as shown graphically in Figure 2.6. The use of the kinematic hardening model to anticipate the Bauschinger effect can be found in Chun et al. (2002).

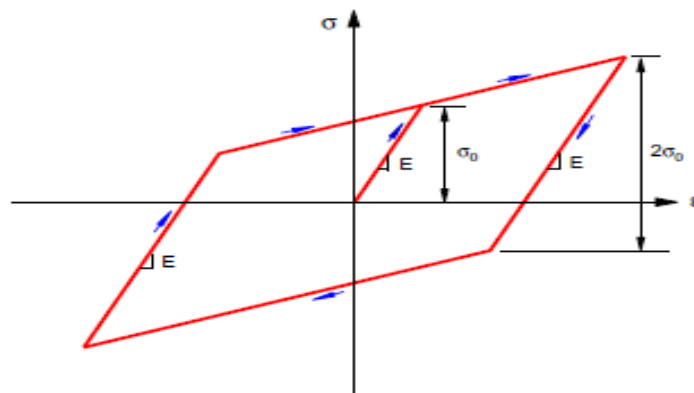


Figure 2. 7: Graphic representation of the Bauschinger effect in which the elastic limit is denoted by  $\sigma_0$  (Jiang and Zhang, 2008) [10].

In the uniaxial form, the yield criterion for the kinematic hardening model can be expressed by the following equation:



$$f = |\sigma - \chi| - k \quad (2.15)$$

For which  $k$  is the initial yield stress value. In the kinematic hardening model, the initial yield stress is also described as the initial elastic limit or the initial size of the yield surface (Chaboche, 1989; Lemaitre and Chaboche, 1994).

Prager (1949) elaborated the simplest model, called linear kinematic hardening model, to describe kinematic hardening using a linear relationship between the change in kinematic hardening and the change in plastic strain. The model is represented by equation 2.16:

$$\dot{\chi} = \frac{2}{3} c \dot{\epsilon}_p \quad (2.16)$$

Where  $c$  is the material constant corresponding to the the gradient of the linear relationship (Avanzini, 2008). In the case of uniaxial loading, equation 2.16 can be rewritten as follows:

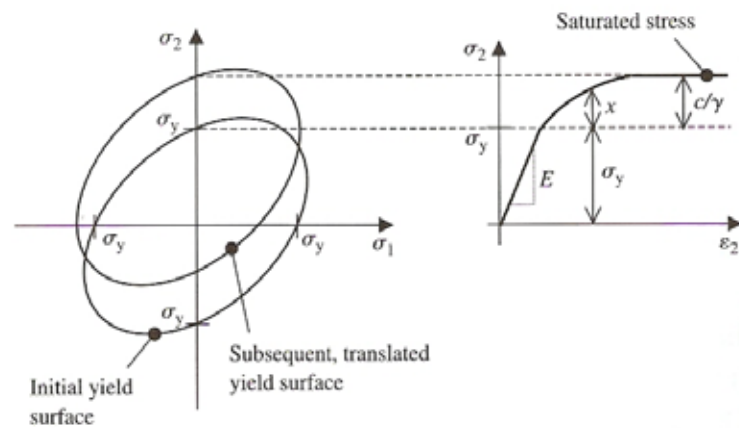
$$\dot{\chi} = c \dot{\epsilon}_p \quad (2.17)$$

Where  $\chi$  represents a scalar variable; the magnitude of  $\chi$  is 3/2 times the kinematic hardening tensor parameter (Dunne and Petrinic, 2005). Mroz (1967) proposed an improvement to the linear kinematic hardening model by introducing a multilinear model which consists of a multisurface model representing a constant work hardening modulus in stress space.

Linear strain hardening is not often observed in the actual cyclic loading tests. Generally, the stress-strain behaviour obtained from cyclic loading tests is a nonlinear relationship. The Armstrong-Frederick type kinematic hardening model, originally developed in 1966, has been used widely to represent this nonlinear stress-strain relationship. The model introduces a recall term, called dynamic recovery, into the linear model (Frederick and Armstrong, 2007) which is described by equation 2.18:

$$\dot{\chi} = \frac{2}{3} c \dot{\epsilon}_p - \gamma \chi \dot{p} \quad (2.18)$$

Where  $\gamma$  is a material constant. The recall term incorporates a fading memory effect of the strain path and causes a nonlinear response for the stress-strain behaviour. (Bari and Hassan, 2000). For the nonlinear kinematic hardening model of the time independent plasticity behaviour, the value of  $\frac{c}{\gamma}$  determines the saturation of stress value in the plastic region and its combination with the  $k$  value represents the maximum stress for the plasticity test (Dunne and Petrinic, 2005). Figure 2.8 shows a description of the saturated stress.



**Figure 2. 8: Graphic representation of the saturated stress represented by the nonlinear kinematic hardening model (Dunne and Petrinic, 2005) [10]**

The constants in the nonlinear kinematic hardening model are described by a different equation than that in equation 2.18 , as for instance, found in Chaboche and Rousselier (1983), Zhan and Tong (2007) and Gong et al. (2010). The equation is given as follows:

$$\dot{\chi} = C\left(\frac{2}{3}\alpha\dot{\epsilon}_p - \chi\dot{p}\right) \tag{2.19}$$

Where  $\alpha$  is the saturation of the stress value in the plastic region, which is identical to the value of  $\frac{c}{\gamma}$  , and  $C$  represents the speed to reach the saturation value, which is equal to  $\gamma$ . Hence, both the nonlinear kinematic hardening equations 2.18 and 2.19 are identical, except for the fact that the constants are different in definition.

The Armstrong-Frederick hardening relation has been adjusted by decomposing the total backstress into a number of additive parts (Jiang and Kurath, 1996). The reason for the superposition of the kinematic hardening model is to extend the validity of the kinematic hardening model to a larger domain in stress and strain (Chaboche and Rousselier, 1983). The model is also intended to describe the ratchetting behavior better (Lemaitre and Chaboche, 1994). The total backstress  $\chi$  is therefore given by the following equation:

$$\chi = \sum_{i=1}^M \chi_i \tag{2.20}$$

For which  $\chi_i$  is a part of the total backstress,  $i = 1, 2, \dots, M$  and  $M$  is the number of the additive components of the kinematic hardening. The model is usually divided into two or three kinematic variables. However, more variables are sometimes employed in certain cases, for example, in the study of the ratchetting effect (Bari and Hassan, 2000), in order to get a better agreement with experimental data. It is suggested by Chaboche (1986) that the first rule ( $\chi_1$ ) should start hardening with a very large modulus so that it can stabilize quickly. Figure 2.9 shows a good example of the superposition of three kinematic hardening variables.

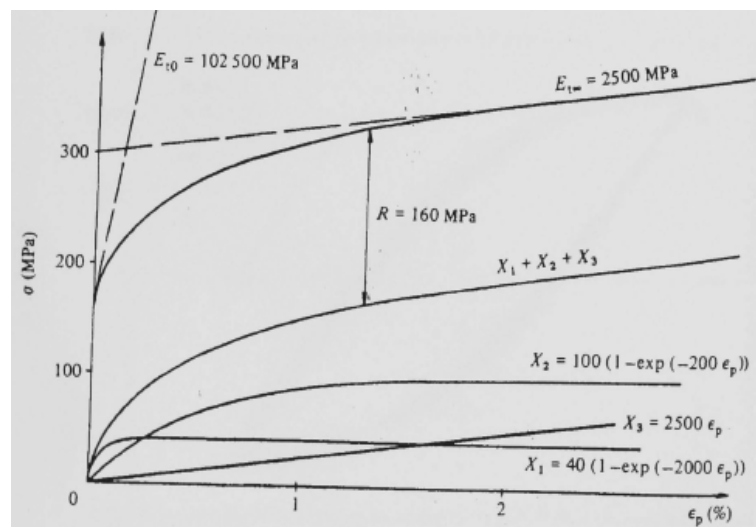


Figure 2. 9: Schematic representation of the stress-strain curve obtained from the superposition of three kinematic hardening variables (Lemaitre and Chaboche, 1994) [10]

### 2.1.3.4 Combined Isotropic-Kinematic Hardening Model

In the recent years, the literature on the mixed isotropic and kinematic hardening rules is so abundant that a complete listing of all references would be not only difficult, but also entirely redundant.

In a previous work by Tarigopula et al. (2008) on dual-phase steel DP800, the classical cyclic hardening model of Chaboche, which combines the Voce law for isotropic hardening and the Armstrong–Frederick law for kinematic hardening, was shown to give satisfactory results for simple deformation modes such as the uniaxial tensile non-proportional loading. However, in the practical forming of components, the deformation modes are quite complicated [13].

Both the cyclic hardening and softening and Bauschinger phenomena are normally observed in tests of the real material. This observation specifies the requirement to combine both isotropic and kinematic hardening rules in order to anticipate the strain hardening and the cyclic hardening/softening of engineering materials. In the uniaxial form, the yield criterion of the combined isotropic and kinematic hardening models can be expressed by the following formula [13]:

$$f = |\sigma - \chi| - k - R \quad (2.21)$$

The behavior of the material in theory with a combined isotropic and kinematic hardening model will include both the translation and the expansion/contraction of the yield surface in stress space. An example of the implementation of this combined model can be found in Zhao et al. (2001).

D.L. Henann et al. (2008) developed a large deformation viscoplasticity theory with mixed isotropic and kinematic hardening according to the dual decompositions. They concluded that the simple theory with combined isotropic and kinematic hardening developed was only foundational in nature, and there are numerous specialized enhancements/ modifications to the theory that need to be incorporated in order to match actual experimental data for different metals [14]. Figure 2.10 presents a schematic representation of their work comparing axial stress versus

axial strain for distinct types of hardening in strain-cycle simulation in straightforward tension and compression.

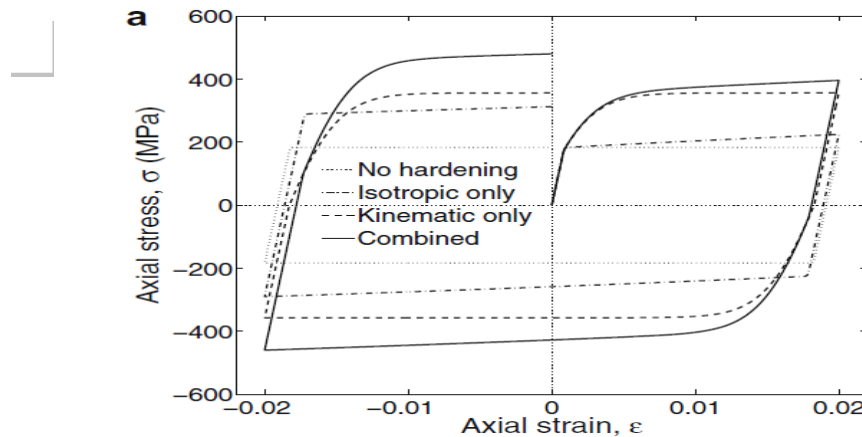


Figure 2. 10: Comparison of axial stress versus axial strain for various types hardening in a symmetric strain-cycle simulation in simple tension and compression (Henann et al. 2008) [14]

### 2.1.4 Ramberg-Osgood Relationship

The Ramberg–Osgood equation was elaborated to relate the non linear relationship between stress and strain—that is, the stress–strain curve—in materials near their yield points. It is especially useful for metals that harden with plastic deformation showing a flat elastic-plastic transition. In earthquake engineering, Ramberg–Osgood functions are often used to model the behavior of structural steel materials and components. The Ramberg-Osgood function is expressed as [15]:

$$\epsilon = \frac{\sigma}{E} + K\left(\frac{\sigma}{E}\right)^n \tag{2.22}$$

Where:

$\epsilon$  is strain,  $\sigma$  is stress,

$E$  is Young modulus, and

$K$  and  $n$  are constants that depend on the material being considered

On the right side, the first term,  $\frac{\sigma}{E}$  is equal to the elastic part of the strain, while the second term,  $K\left(\frac{\sigma}{E}\right)^n$ , accounts for the plastic part, the parameters **K and n** (cyclic strain coefficient and cyclic strain hardening exponent) describing the hardening behavior of the material. Introducing the yield strength of the material,  $\sigma_0$ , and defining a new parameter,  $\alpha$ , related to **K** as:  $\alpha = K\left(\frac{\sigma_0}{E}\right)^{n-1}$ , the Ramberg-Osgood equation can be rewritten as [15]:

$$\varepsilon = \frac{\sigma}{E} + \alpha \frac{\sigma}{E} \left(\frac{\sigma}{\sigma_0}\right)^{n-1} \quad (2.23)$$

The value  $\alpha \frac{\sigma_0}{E}$  for which  $\sigma = \sigma_0$  can be seen as yield offset as shown in Figure 2.11. Commonly used values for **n** range from 0.2 to 0.5, although more precise values are usually obtained by fitting of tensile (or compressive) experimental data. Values for  $\alpha$  can also be found by means of calibration of experimental data, although for some materials, it can be fitted in order to have the yield offset equal to the accepted value of strain of 0.2%, which means:  $\alpha \frac{\sigma_0}{E} = 0.002$ .

Due to the power-law relationship between stress and plastic strain, the Ramberg–Osgood model implies that inelastic strain is present even for extremely low levels of stress. For cyclically loaded metals (Bannantine et al. 1990), a log-log plot of true stress versus true plastic strain has generally been approximated by a straight line resulting in the power law function shown in equation 2.24 as the basis for the cyclic stress-strain curve.

$$\varepsilon = \frac{\sigma}{E} + \left(\frac{\sigma}{K}\right)^{\frac{1}{n}} \quad (2.24)$$

$$\frac{\sigma}{E} = \varepsilon_e; \text{ elastic strain}$$

$$\left(\frac{\sigma}{K}\right)^{\frac{1}{n}} = \varepsilon_p; \text{ plastic strain}$$

The strain hardening coefficient and exponent can be obtained from regression of experimental stress versus plastic strain data using a power equation. For a complete hysteresis loop, the stress

and strain values can be doubled based on Massing’s hypothesis (Massing 1926). For any arbitrary start point, equation 2.25 becomes applicable and describes the stress-strain relationship over the strain range.

$$\Delta\varepsilon = \frac{\Delta\sigma}{E} + 2\left(\frac{\Delta\sigma}{2K}\right)^{\frac{1}{n}} \tag{2.25}$$

Where:

$\Delta\varepsilon$  is strain range, and

$\Delta\sigma$  is stress range

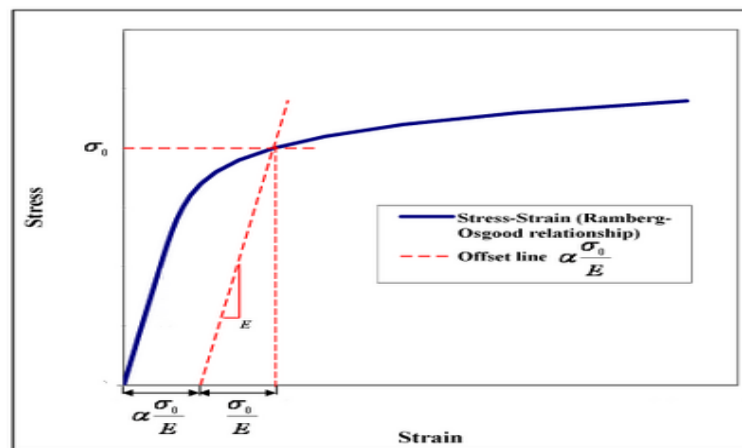


Figure 2. 11: Generic representation of the stress–strain curve by means of the Ramberg–Osgood equation. Strain corresponding to the yield point is the sum of the elastic and plastic components [15].

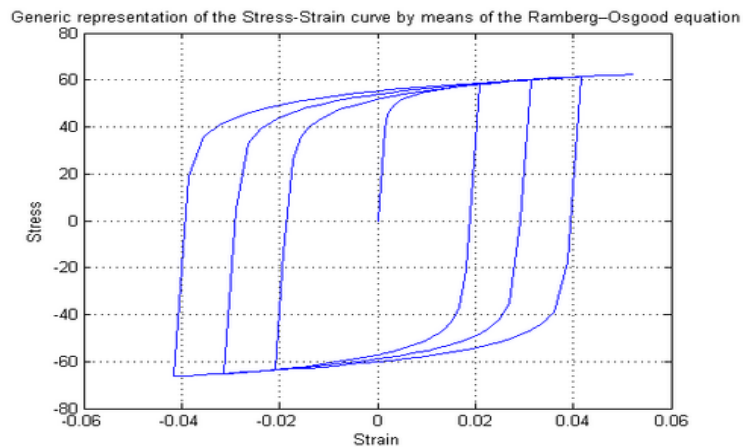


Figure 2. 12: Ramberg-Osgood Steel Material -- Hysteretic Behavior of Model [15].

### 2.1.5 Fatigue Strain-Life Relationship

Generally, to estimate the fatigue life in structural design, the stress-life approach is most often used. The stress-life approach is applicable for situations involving primarily elastic deformation. Under these conditions the component is predicted to have an extensive lifetime. However, for situations involving high stresses, high temperatures, or stress concentrations such as notches, where significant plasticity can be involved; the approach is not appropriate. In other words, stress life methods are most useful at high cycle fatigue, where the applied stresses are elastic, and plastic strain occurs only at the tips of fatigue cracks.

To deal with low cycle fatigue, the suitable approach of modeling fatigue behavior is the strain-life or local strain, which is able to account directly for the plastic strains often present at stress concentration.

Rather than the stress amplitude  $\sigma_a$ , the loading is characterized by the plastic strain amplitude  $\frac{\Delta \epsilon_p}{2}$ . Under these conditions, if a plot is made of  $\log(\frac{\Delta \epsilon_p}{2})$  versus  $\log(2N_f)$ , the following linear behavior is generally observed as shown in Figure 2.13:

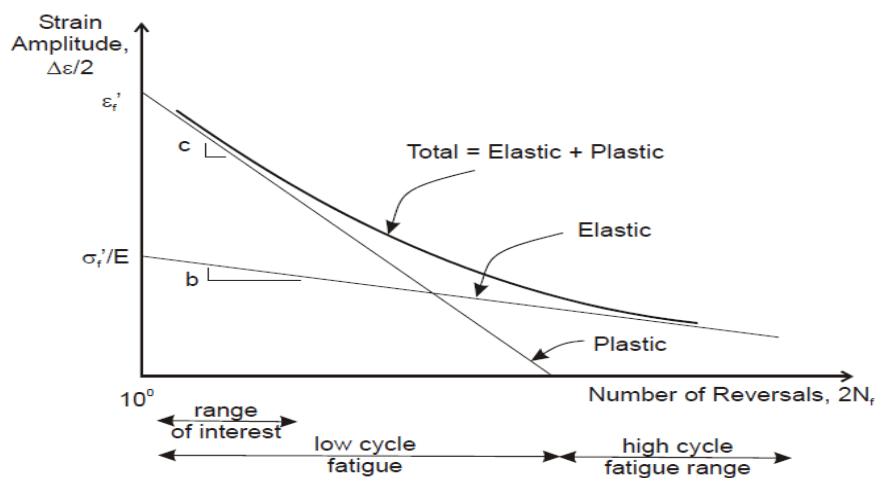


Figure 2. 13: Strain-life curves also called low cycle fatigue [16]



- The straight line elastic behavior can be transformed to Basquin's equation (stress-life approach) [9]:

$$\frac{\Delta\sigma}{2} = \sigma_a = \sigma'_f(2N_f)^b \quad (2.26)$$

- The relation between plastic strain and fatigue life is given by the Coffin-Manson law (Manson 1953, Coffin 1954):

$$\frac{\Delta\varepsilon_p}{2} = \varepsilon'_f(2N_f)^c \quad (2.27)$$

- The intercepts of the two straight lines are  $\frac{\sigma'_f}{E}$  for the elastic component and  $\varepsilon'_f$  for the plastic component.
- The slopes of the elastic and plastic lines are **b** and **c**, respectively.
- Therefore, the total strain amplitude is given by [9]:

$$\frac{\Delta\varepsilon}{2} = \varepsilon_a = \frac{\Delta\varepsilon_e}{2} + \frac{\Delta\varepsilon_p}{2} = \frac{\sigma'_f}{E}(2N_f)^b + \varepsilon'_f(2N_f)^c \quad (2.28)$$

Where:

$$\frac{\Delta\varepsilon}{2} = \varepsilon_a = \text{total strain amplitude}$$

$$\frac{\Delta\varepsilon_e}{2} = \text{elastic strain amplitude} = \frac{\Delta\sigma}{2E} = \frac{\sigma_a}{E}$$

$$\frac{\Delta\varepsilon_p}{2} = \text{plastic strain amplitude}$$

$\sigma'_f$  = fatigue strength coefficient

**b** = fatigue strength exponent

$2N_f$  = reversals to failure

$\varepsilon'_f$  = fatigue ductility coefficient

**c** = fatigue ductility exponent

**E** = modulus of elasticity

$$\frac{\Delta\sigma}{E} = \sigma_a = \text{stress amplitude}$$

- The coefficients and exponents can be obtained from regression of experimental data fatigue to individual relationships of elastic and plastic parts of the strain-life equation.
- At large strains or short lives, the plastic strain component is predominant, and at small strains or longer lives the elastic strain component is predominant.
- The transition life (at  $2N_t$ ) is found by setting the plastic strain amplitude equal to the elastic strain amplitude. In other words, the life where elastic and plastic components of strain are equal is called the transition fatigue life and is computed using the following equation:

$$2N_t = \left( \frac{\epsilon'_f E}{\sigma'_f} \right)^{\frac{1}{b-c}} \tag{2.29}$$

- For lives less than  $2N_t$  the deformation is mainly plastic, whereas for lives greater than  $2N_t$  the deformation is mainly elastic.

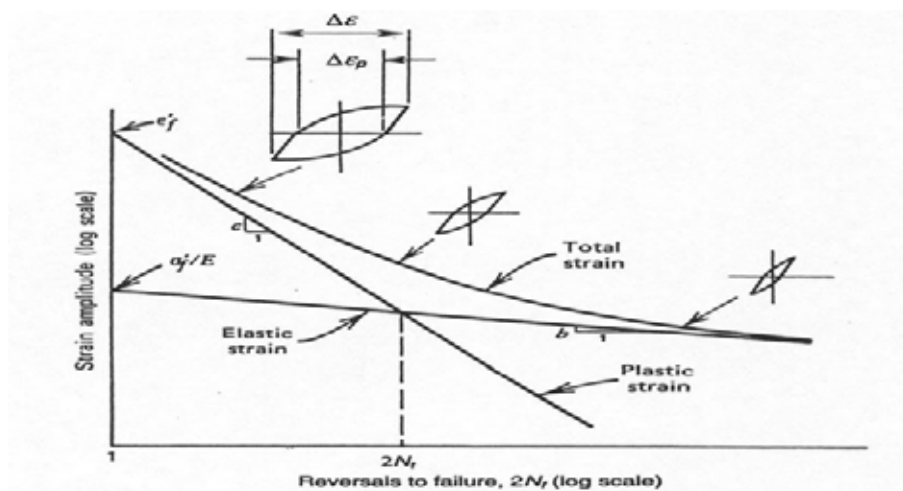


Figure 2. 14: Schematic low cycle fatigue curve showing the transition fatigue life [9]

## 2.2 Summary of the Low Cycle Fatigue Steel Research

A shortage of both experimental and numerical data can be observed on the cyclic behavior of European mild carbon steel. Generally, only few studies have been conducted on the low cycle fatigue of the European mild carbon steel.

Alternatively, most earthquake related research focused on the behavior of structural components or entire assemblies under cyclic loading but not on the evaluation of structural material itself. One of the first researchers to conduct an investigation on the effects of plastic strains on beam behavior were Bertero and Popov (1965). Their study aimed to investigate early buckling of flanges, but strains were also monitored and recorded to be up to 2.5%. Their study has given birth to several researches concentrated on the structural component behavior with a majority of experiments on beam-column joints. After the observed damage following the 1994 Northridge earthquake (Malley 1998), this type of research focused basically on welded steel moment frame joints. Bending tests were also carried out on machine cone shaped steel cantilever studs done on purpose to be used as structural earthquake energy dissipators (Buckle & King 1988). The recorded strains attained up to 10%, nonetheless similar to the beam-column experiments these maximum strains were only located in the outer fibers of the components due to the bending action [16].

No data on the characterization of cyclic response of European mild carbon steel was available for the common steels. The most relevant data was presented on a comparison of the fatigue behavior between S355 and S690 steel grades [17]. These steel grades were specified according to the EN 10025 standard. Minimum yield stresses of 355 and 690 MPa were specified, respectively, for the S355 and S690 steel grades, for thicknesses below 16 mm. The S355 steel grade exhibited a tensile strength within the range of 470 and 630 MPa and the S690 steel grade presented a tensile strength between 770 and 940 MPa, also for thicknesses below 16 mm.

In order to verify the actual static strength properties of the two steel grades used for the experiment, quasi-static monotonic tensile tests were carried out, covering both steel grades. Average yield stresses of 419 MPa and 765.7 MPa were measured, respectively for the S355 and

S690 steel grades. Average tensile strengths of 732 MPa and 823 MPa were obtained, respectively, for the S355 and S690 steel grades.

In general, these strength properties satisfy the limits specified in the EN 10025 standard. However, the sample of the S355 steel grade used in the study exhibited a tensile strength above the range specified in the standard. The tensile tests were instrumented with strain gauges which allowed the evaluation of the modulus of elasticity. Average values of 210.5 and 209.4 GPa were measured, respectively, for the S355 and S690 steel grades. The study concluded that the fatigue tests on smooth specimens showed that the S690 high strength steel grade exhibited a lower fatigue resistance than the S355 steel, for strain amplitudes higher than 0.33% or fatigue lives below 6720 cycles, which represents the low cycle fatigue regime. In the high cycle fatigue regime, the S690 steel has shown a higher fatigue resistance than the S355 steel. This superior fatigue resistance, based on smooth specimen test data, corresponds to a higher resistance to fatigue crack initiation [17].

To effectively investigate material characteristics, the cross section should be under uniform strain distribution as in the case of axial loading. Limited data regarding steel low cycle fatigue is accessible from foreign research. New Zealand reinforcing steel, which was produced according to New Zealand Standard NZS 6402-1989 in Grade 300N/mm<sup>2</sup> and 430N/mm<sup>2</sup>, was studied for plastic stress-strain behavior using coupons machined from rebar (Dodd, 1992). Nonetheless, the cycles were not fully reversed as the compression deformations were not equally reached when compared to the tension deformations because of test setup restrictions and specimen buckling issues.

In addition, Japanese researchers carried out low cycle fatigue coupon experiments on low yield point steels for potential use as energy dissipation mechanism in base isolation or for unbonded braces (Eiichiro et al., 1998). The study selected 44 coupons tested with constant strain amplitudes ranging between 0.15% and 1.5%, but only included two specimens at 1.5% strain with the rest all less than 1% amplitude strain. The strain in structural components that are plastically resisting earthquake loads can be considerably higher [16].

Moreover, in US researchers conducted a comprehensive study on the stress-strain and low cycle fatigue properties of plate steels subjected to repeated cyclic plastic deformations (Peter Dusicka et al., 2006). The steel grades considered were GR345, HPS485, HT440, LYP100 and LYP225. Of specific interest was the cyclic stress as measured relative to the yield strength and the variability of the achieved stresses across different steel grades. Low cycle fatigue characteristics were also desired to compare the fatigue life.

The overall experimental results showed that the cyclic stress for structural grade steels stabilized to a constant within the first two cycles, but for low yield point steels the stress did not stabilize and the fatigue life of all the steels was similar within 1% and 7% strain amplitudes and at constant strain rate of 0.1%/sec [16].

Obviously, it can be clearly seen that there is a lack of both experimental and numerical data on the cyclic response and low cycle fatigue characteristics of European mild carbon steel. Based on the previous works presented here, the comprehensive study on the stress-strain and low cycle fatigue properties of plate steels subjected to repeated cyclic plastic deformations conducted by Peter Dusicka et al. (2006) is quite similar to this study. Then, the results from cyclic behavior and low cycle fatigue behavior of this study will be compared with those found by Peter Dusicka et al.(2006).

In fact, this research will be able to provide both experimental and numerical data which could use for the establishment of design criteria of European mild carbon steel under cyclic loading.

## SECTION 3

### EXPERIMENTAL TESTS FOR CYCLIC RESPONSE ASSESSMENT

#### 3.1 Equipment

The majority of the experiments were performed on steel coupons subjected to cyclic strains at room temperature. A UTS load frame from the Department of Steel Structures and Structural Mechanics at the Faculty of Civil Engineering of Politehnica University of Timisoara (Romania) was used to subject the steel specimens to axial deformations. In Figure 3.1 is shown one specimen during testing.

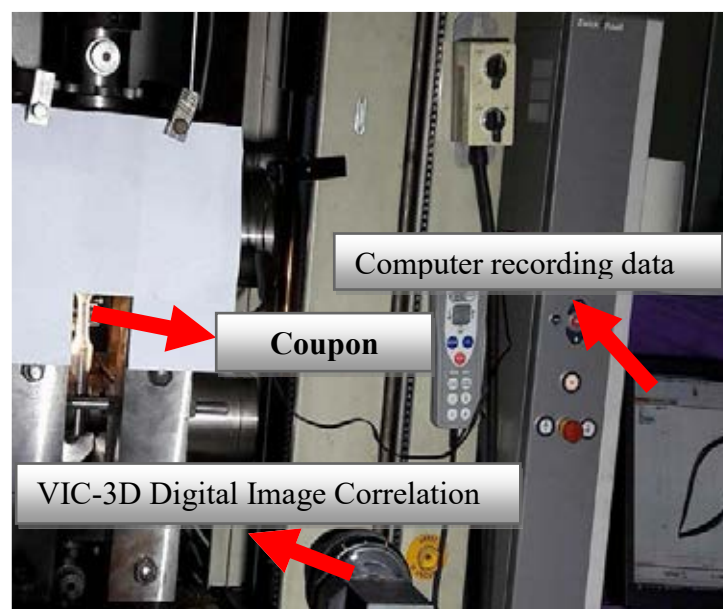


Figure 3. 1: Photograph of the UTS for testing of the specimens

#### 3.2 Test Coupons Arrangement and Dimensions

The test specimens had a cylindrical shape. All the tests were performed according to the ASTM E606/E606M – 12 which is the Standard Test Method for Strain-Controlled Fatigue Testing.

To minimize surface roughness effects, finely polished surfaces have been used. And to prevent buckling of the specimens, following arrangement have been adopted: Stocky configuration, fine alignment and restrain of lateral movement of the cross-heads.

Total length of one specimen was 290mm taken from steel plate with a thickness of 30mm. Details of the specimen dimensions are shown in Figure 3.2.

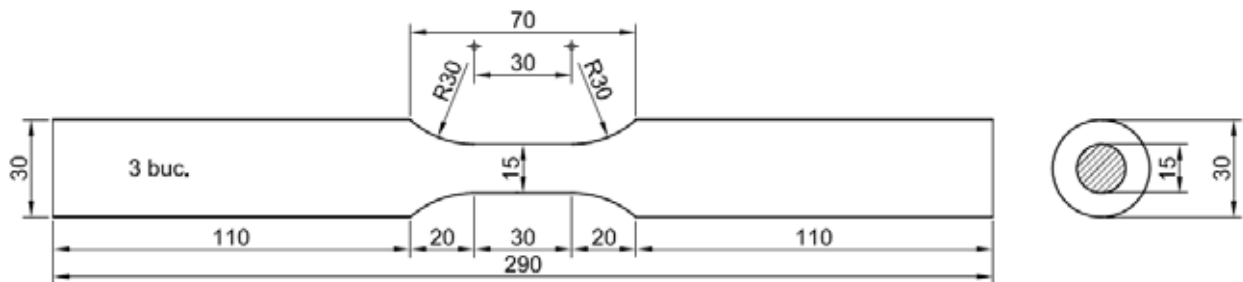


Figure 3. 2: Coupon dimensions

### 3.3 Steel Material Details

The following four steel grades have been considered for the study: S275, S355, S460 and S690. **S275** steel plate meets European structural steel standard EN 10025 : 2004. S275 structural steel plate is a common carbon structural steel with minimum yield strength of 275MPa, it bears many similarities to ASTM A36 in both chemistry and physical properties. S275 structural steel plate can be bolted, riveted and welded in a full range of construction and fabrication including bridges and other general structural projects [18].

**S355** steel plate is a high-strength low-alloy European standard structural steel covering four of the six categories within the EN 10025: 2004 standard. With minimum yield strength of 355 MPa, it meets requirements in chemistry and physical properties similar to ASTM A572 / 709. It is used particularly for structural steelworks including bridge components, components for offshore structures, power plant, mining and earth-moving equipment, load-handling equipment and wind tower components [18].

**S460** falls within the European standard structural steel of EN 10025: 2001 standard and is a specially designed steel for use in harsh environments such as offshore structures. With minimum yield strength of 460 MPa, typical applications of S460 are in construction of fixed offshore structures such as oil rigs and service platforms [19].

**S690** steel plate is a high strength, quenched and tempered fine-grain structural steel. With minimum yield strength of 690 MPa, this grade is intended for structural applications where weight savings is important. It is a EN specification designed to achieve a 690 MPa minimum

yield point. The specification itself is comparable to some ASTM standards (i.e. A514), but it is not required to comply with exactly the same tolerances. The tolerances for S690 plates can be found in EN10029 and EN10064 [18].

**Table 3. 1: Some Properties of the Steel Grades Used**

Property	Steel			
	S275	S355	S460	S690
Standard	EN 10025 : 2004	EN 10025: 2004	EN 10025: 2001	EN10029 and EN10064
Category	Mild carbon steel	Mild carbon steel	High-strength low-alloy	High strength
Nominal Yield Strength (MPa)	275	355	460	690

### 3.4 Chemical Composition of the Steels

The chemical composition of structural steel is very important and highly regulated. It is an essential factor which defines the mechanical properties of the steel material. Regulated elements include Carbon (C), Manganese (Mn), Phosphorus (P), Sulfur (S) and Silicon (Si). In Table 3.2 are displayed the maximum percentage of certain regulated elements for the steel grades considered in the present work.

**Table 3. 2: Chemical Composition of the Considered Steel Grades [Source:AZO Materials]**

Steel Grade	Max % of certain regulated elements				
	C	Mn	P	S	Si
S275	0.25	1.6	0.04	0.05	0.05
S355	0.23	1.60	0.05	0.05	0.05
S460	0.12	1.6	0.025	-	0.5
S690	0.20	1.70	0.025	0.015	0.80



### 3.5 Load History Types

Using a constant strain rate of 0.2%/sec, three loading protocols have been used for the experiments: Monotonic tensile, variable (incremental) amplitude and constant strain amplitude ranged from 1% to 7% of increment 2. They are shown from Figure 3.3 to Figure 3.5.

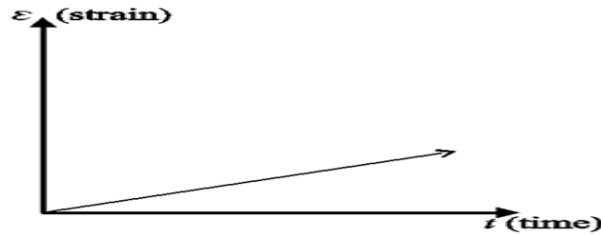


Figure 3. 3: Monotonic Tensile load history

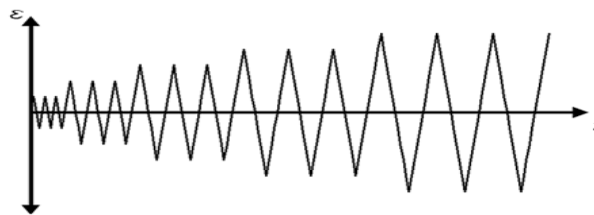


Figure 3. 4: Variable Strain Amplitude load history



Figure 3. 5: Constant Strain Amplitude load history

### 3.6 Coupons Grouping for the Testing

A total of 72 coupons have been tested for the three categories of loading protocol including monotonic tensile, variable (incremental) strain amplitude, and constant strain amplitude. To gain statistical confidence of the data, three tests were performed for each category of specimen. Table 3.3 provides details of the number of coupons tested.

The constant strain amplitudes considered were 1%, 3%, 5% and 7%. In addition, Charpy Impact tests have been conducted for all the considered steel grades. All details regarding Charpy Impact tests for the steels are presented in Section 4.6.

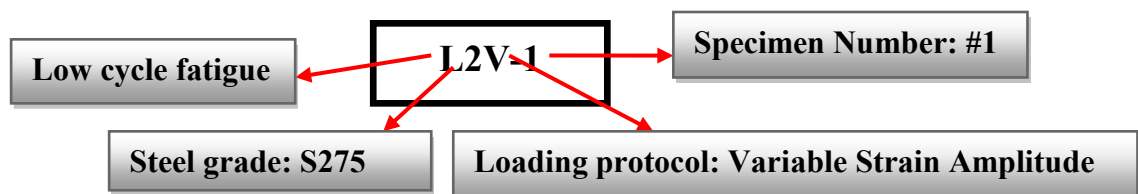
**Table 3. 3: Coupons grouping for the testing**

Steel Grade	Loading Protocol	Number of Coupons Tested
S275	Monotonic Tensile	3
	Variable Strain Amplitude	3
	Constant Strain Amplitude	12
S355	Monotonic Tensile	3
	Variable Strain Amplitude	3
	Constant Strain Amplitude	12
S460	Monotonic Tensile	3
	Variable Strain Amplitude	3
	Constant Strain Amplitude	12
S690	Monotonic Tensile	3
	Variable Strain Amplitude	3
	Constant Strain Amplitude	12
Total		72

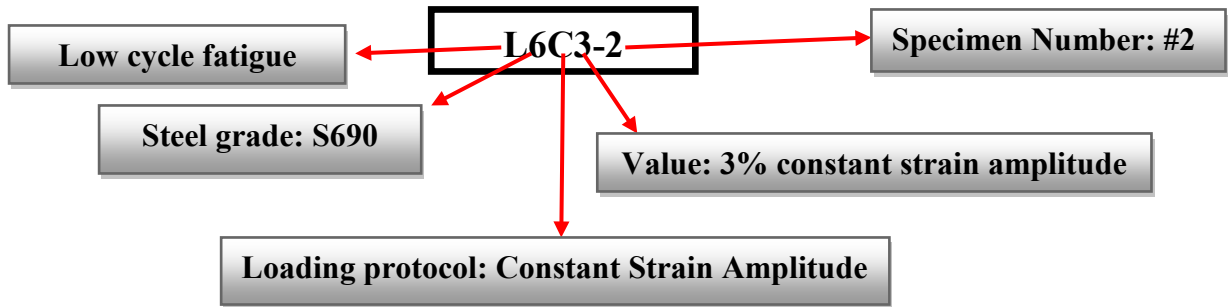
### 3.7 Specimens Nomenclature and Data Processing

Due to the amount of data, to avoid confusion, the specimens were named as follows from the left to the right:

For monotonic tensile and variable strain amplitude tests, the first letter stands for low cycle fatigue because the key purpose of the study was low cycle fatigue behavior investigation, the first digit represents the steel grade, and the second letter represents the loading protocol and the second digit for the specimen number.



For constant strain amplitude tests, the first letter stands for low cycle fatigue, the first digit represents the steel grade, and the second letter represents the loading protocol, the second digit for constant strain amplitude value and the last digit for the specimen number.



At the completion of the tests, all the needed data were imported to Excel and saved as Comma-Separated Values (CSV) files for quick processing in MATLAB. To avoid error, first one Matlab script was created to read all the data (72 specimens) in form of tables. And then other scripts were created to plot the curves needed. For instance, one script was created to plot the curves for the 72 specimens simultaneously with chart title, axes titles, and saved automatically with specific sizes in a specific folder as Enhanced Metafile (EMF). However, some plots were also processed in Excel.

## SECTION 4

### CYCLIC STRESS-STRAIN BEHAVIOR

#### 4.1 Results from Monotonic Tensile Tests

In total, twelve (12) specimens were tested under monotonic tensile load history. To be more precise, three (3) specimens for each steel grade. However, after the testing of two specimens for each steel grade, if the results were similar or nearly similar, the third experiment was not performed considering that the two coupons tested already gave excellent results. All the coupons tested for the steel grades provided excellent statistical confidence for the first two specimens except for S690 for which all the three tests were performed.

All the tests were conducted up to fracture. For each category of specimen, the detailed results consisting of stress-strain curves, coupons, observations made, if the specimen exhibited buckling or not and failure mode are presented in the appendix. The results for the selected specimens are presented in Figure 4.1 which combines the stress-strain obtained from monotonic tensile tests for all steel grades. It can be clearly seen that as expected the lower the steel grade, the higher the ductility. Also, the higher the steel grade, the higher the yield strength and the ultimate tensile strength. Overall, while the strength increases, the ductility of the material reduces.

In Table 4.1 are presented the recorded mechanical properties obtained from monotonic tensile tests such as modulus of elasticity, yield strength, offset yield strength or proof stress, ultimate tensile strength, largest strain amplitude recorded, true fracture strength and true fracture strain or ductility. The true fracture strength and true fracture strain or ductility are calculated according to equations 2.5 and 2.6 respectively.

Mechanical properties such as yield strength, proof stress, ultimate tensile strength and true fracture strength increased from S275 to S690 while the Young's modulus, strain amplitude and ductility decreased.

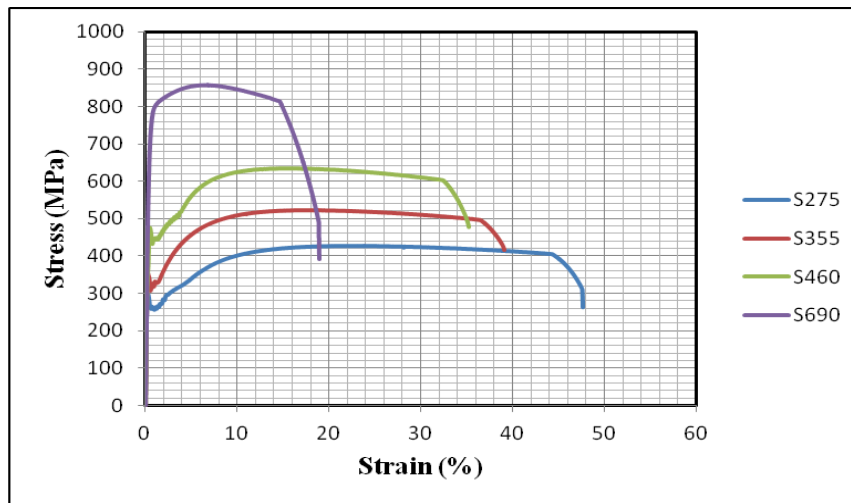


Figure 4. 1: Stress-Strain from Monotonic Tensile Tests for all Steel Grades Considered

Table 4. 1: Recorded Mechanical properties of the Steel Grades Considered from Monotonic Tensile Tests

Property	Steel			
	S275	S355	S460	S690
Modulus of elasticity, $E$ ( GPa )	214	208	205	202
Yield strength $f_y$ ( MPa )	311	357	487	800
Proof stress $f_{p0.2}$ ( MPa )	293	346	482	772
Ultimate tensile strength, $f_u$ ( MPa )	426	523	634	860
True fracture strength, $\sigma_f$ ( MPa )	630	727	856	1023
Largest strain amplitude, $\epsilon_{max}$ (%)	48	39	35	19
Ductility, $\epsilon_f$ (%)	39	33	30	17

## 4.2 Results from Variable Strain Amplitude Tests

Twelve (12) specimens were tested under variable strain amplitude load history in total. The detailed results of all the specimens in this category consisting of number of cycles-strain curves, number of cycles-stress curves, stress-strain curves, coupons, observations made, if the specimen exhibited buckling or not and failure mode are presented in the appendix.

The stress-strain results obtained for each steel grade from variable strain amplitude tests for the selected specimens are presented in Figure 4.2. Some results showed some inaccuracy due to buckling which was most likely caused by specimen misalignment. For instance, for the high strength steel (S690), specimen L6V1 was stopped due to excessive buckling. However, although the recorded maximum stresses relatively differed when compared with specimens L6V2 and L6V3, the other results obtained in terms of number cycles to failure and recorded maximum strain only slightly differed. More details are provided in the appendix.

Cyclic hardening which is characterized by stress increase from one cycle to the next was evident in both the steels S275 and S355 whereas, S460 and the high strength steel (S690) exhibit a combination of cyclic hardening and cyclic softening. However, cyclic softening was observed when the corresponding coupons were about to fracture.

In Table 4.2 are presented the recorded mechanical properties obtained from variable strain amplitude tests including number of cycles to failure, maximum stress, maximum strain, and the normalized maximum stress ratio. The normalized maximum stress ratio was computed to indicate the achieved resistance of each steel grade.

The normalized maximum stress ratio is given by:

$\sigma_{\max}/f_y$  where  $f_y$  is taken from Table 4.1 for the corresponding steel grade.

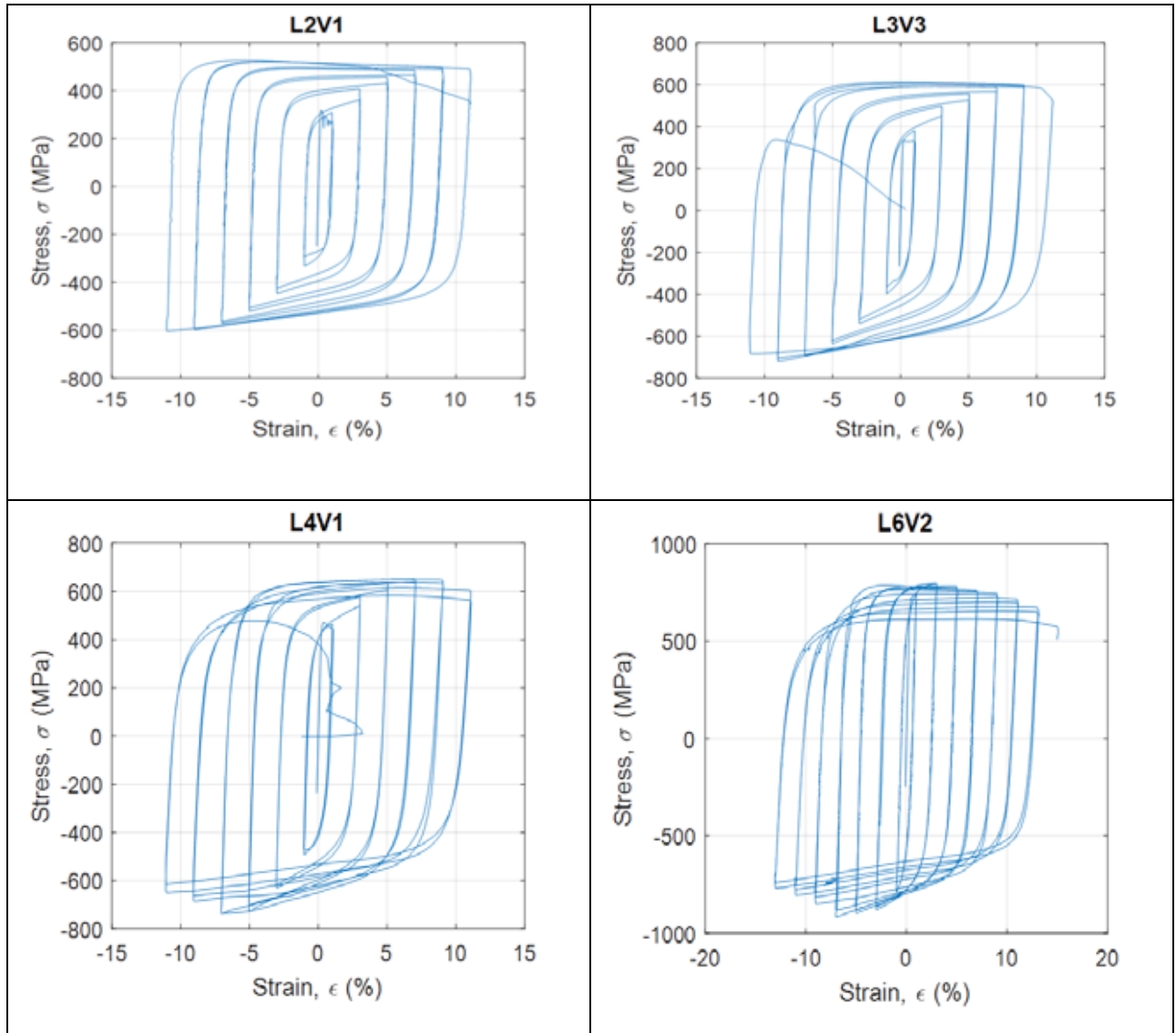


Figure 4. 2: Stress-Strain from Variable Strain Amplitude Tests for the steels

**Table 4. 2: Mechanical Properties of the Steel Grades Considered from Variable Strain Amplitude Tests**

Property	Steel			
	S275	S355	S460	S690
Number of cycles to failure, $2N_f$	32	32	36	30
Maximum stress, $\sigma_{max} (MPa)$	541	609	690	857
Maximum strain, $\varepsilon_{max} (%)$	10	11	12	9
Normalized maximum stress ratio, $\sigma_{max} / f_y$	1.7	1.7	1.4	1.1

#### 4.2.1 Results Comparison with Literature

**Table 4. 3: Normalized Maximum Stress Ratio of the Steel Grades Considered Tests from Literature [16]**

Property	Steel				
	GR345	HPS485	HT440	LYP100	LYP225
Normalized Max. Stress Ratio $\sigma_{max} / f_{ya}$	2.1	1.5	1.5	5.3	2.0

Overall, the highest numbers of cycles to failure as well as the largest strain amplitude were achieved by S460. Whereas, the lowest number of cycles to failure and the lowest strain amplitude were recorded for S690. S690 also achieved the lowest normalized maximum stress ratio magnitude. This was the same from Literature for which the high performance steel (HPS485) achieved the lowest normalized maximum stress ratio magnitude. Both S275 and S355 exhibited equal normalized maximum stress ratio magnitudes and reversals. Using constant strain amplitudes ranged between 1% and 7%, a further study was conducted for all the steel grades considered.



### 4.3 Results from Constant Strain Amplitude Tests

A total of 48 specimens were tested under constant strain amplitude load history. For each steel grade, experiments were performed on twelve (12) coupons which represented three (3) coupons for each targeted constant strain amplitude being  $\pm 1\%$ ,  $\pm 3\%$ ,  $\pm 5\%$  and  $\pm 7\%$ .

All the tests ended with different types of failure i.e. fracture, buckling or bulging. The detailed results of all the specimens in this category consisting of number of cycles-strain curves, number of cycles-stress curves, stress-strain curves, coupons, observations made, if the specimen exhibited buckling or not and failure mode can be found in the appendix.

The stress-strain responses obtained from constant strain amplitude tests are shown for each steel grade per constant strain amplitude from Figure 4.3 to Figure 4.6. After processing all the data, the results were analyzed and the cyclic stress-strain curves for which fracture did not occur between the sensors were considered as not usable for the cyclic response but usable for the low cycle fatigue response. In the appendix all the curves are presented to guide future research work on cyclic loading.

The maximum number of tests, three (3), performed for each targeted strain amplitude per category of steel grade was not always similar or nearly similar. Note that an important consideration in axial fatigue testing is uniformity of stress and strains in the specimen gage section. A major source of non-uniformity of gage section stress and strains is bending moment.

Overall, all the steel grades exhibited transient behavior meaning that changes in cyclic deformation behavior were more pronounced at the beginning of each cyclic loading, but the materials gradually stabilized with continued cycling (steady-state). For each steel grade, the number of cycles to failure decreased with increasing constant strain amplitude.

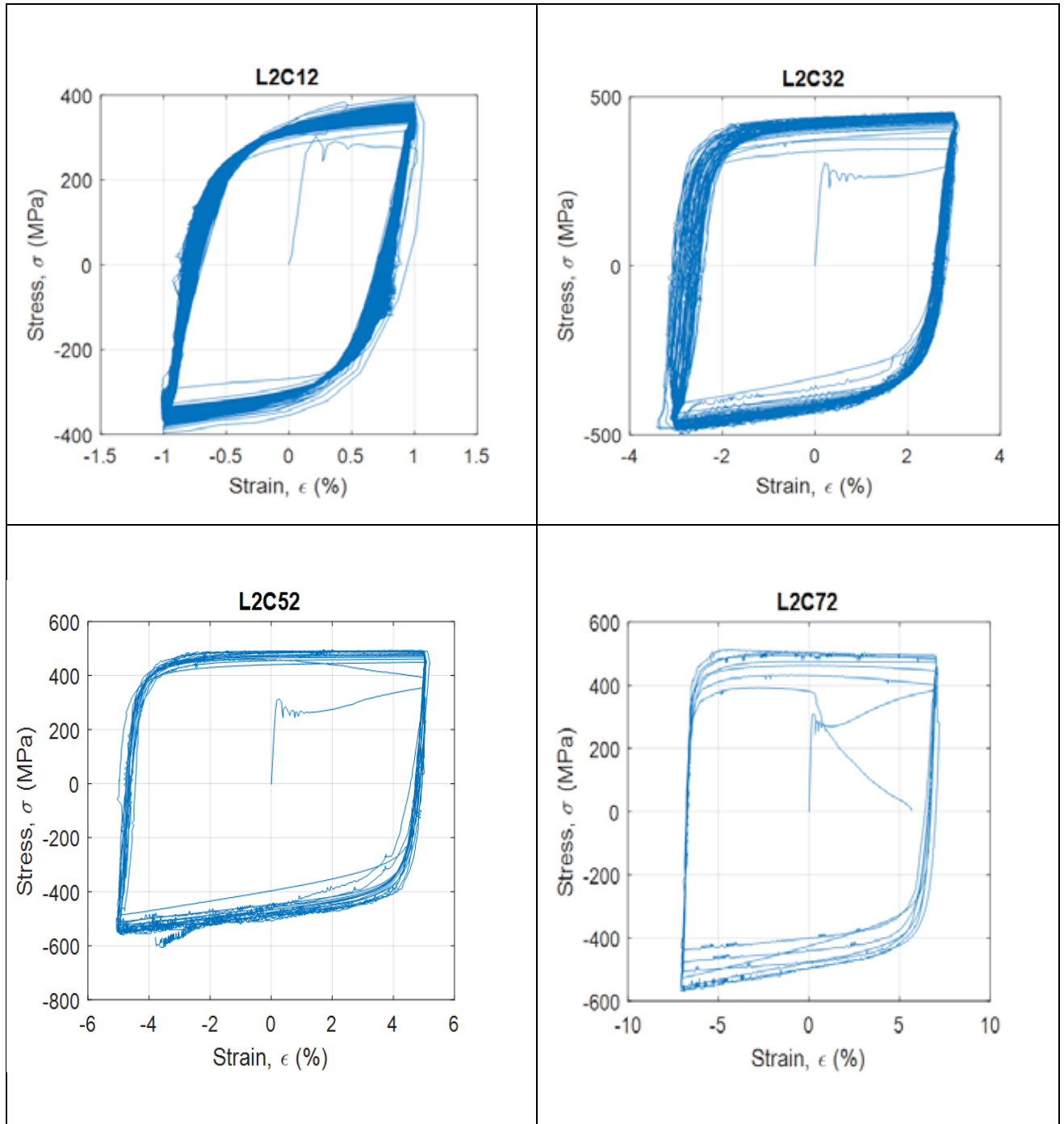


Figure 4. 3: Stress-Strain Response of S275 Coupons at 1%, 3%, 5% and 7% Strain Amplitudes

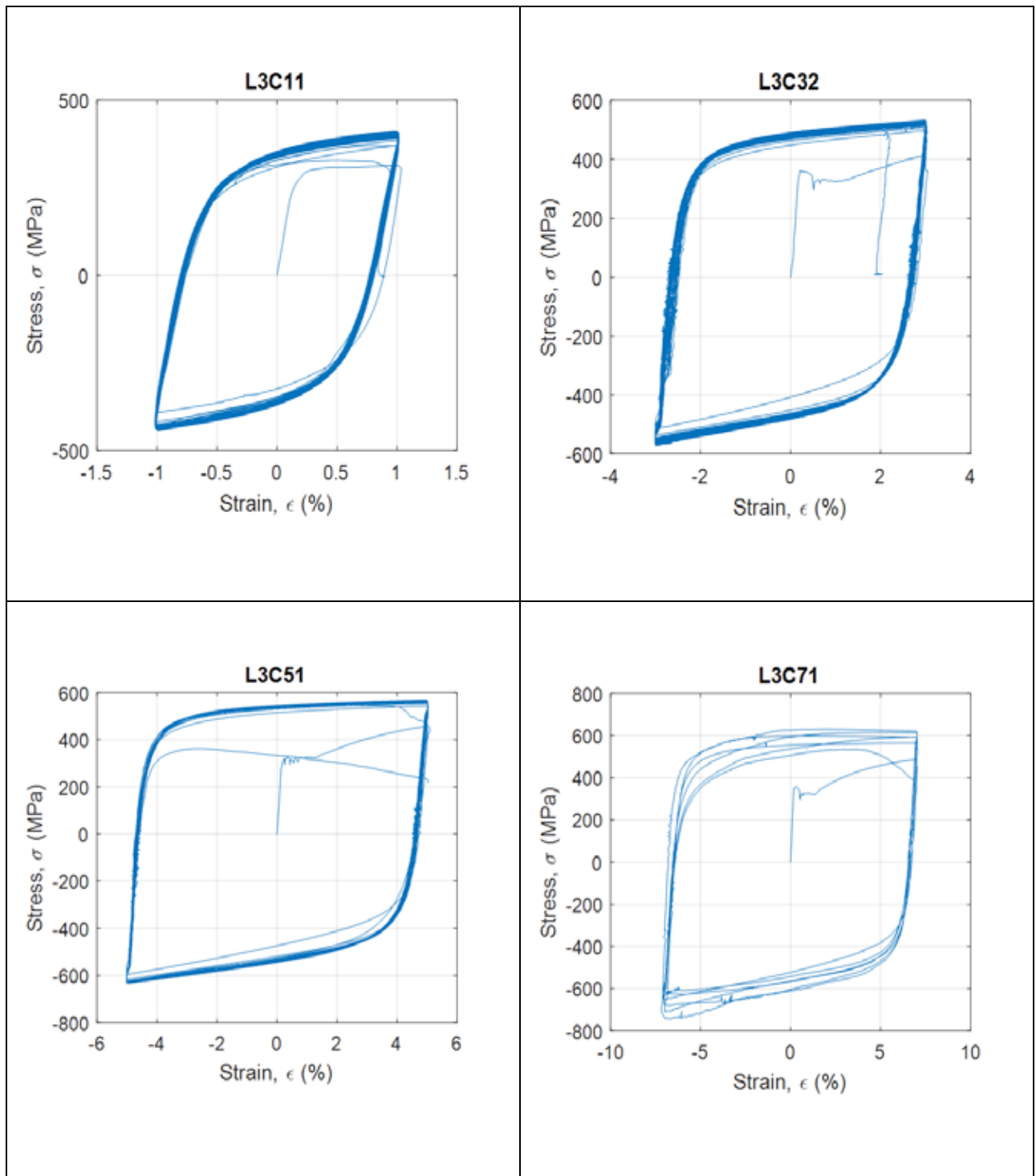


Figure 4. 4: Stress-Strain Response of S355 Coupons at 1%, 3%, 5% and 7% Strain Amplitudes

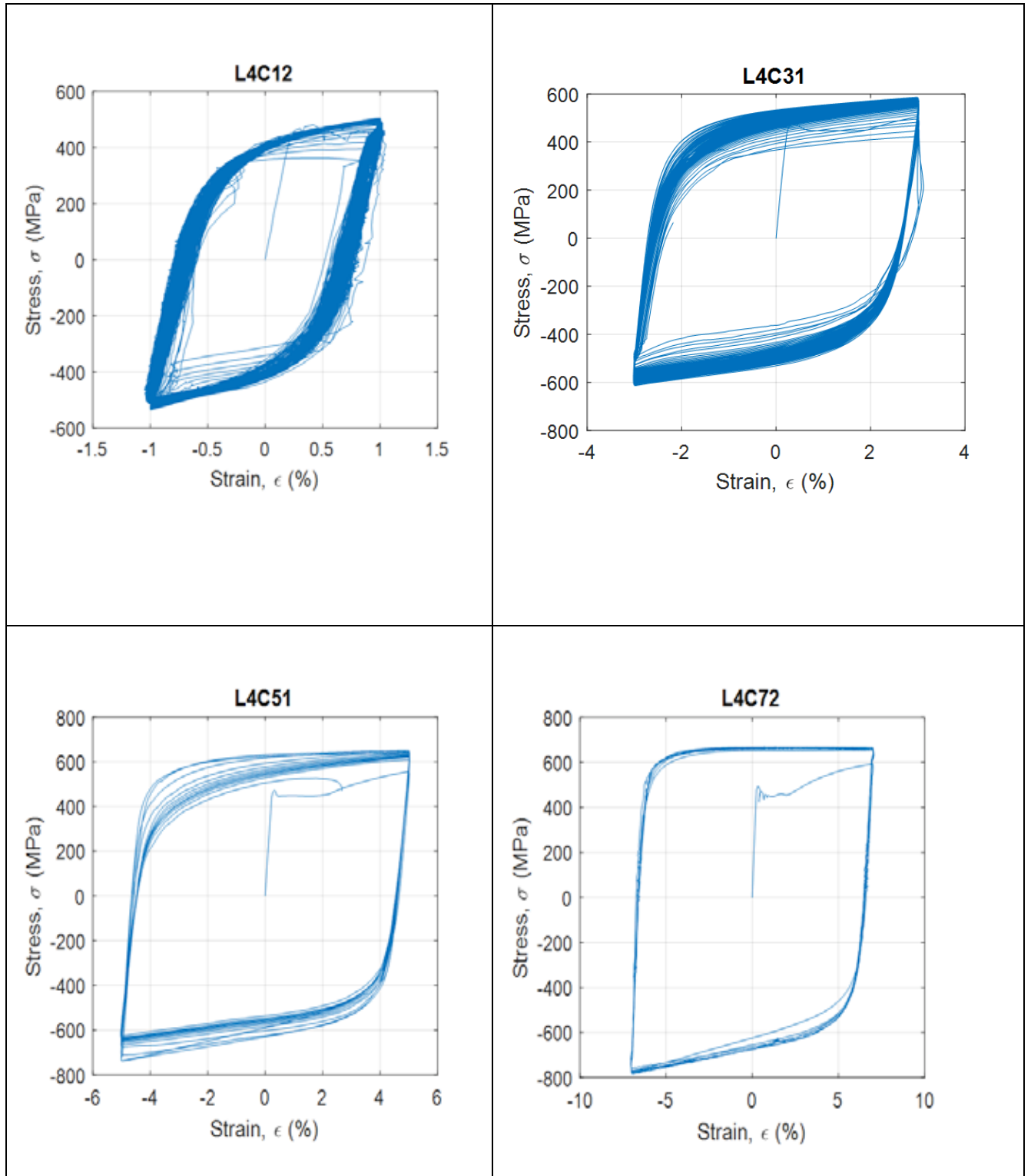


Figure 4. 5: Stress-Strain Response of S460 Coupons at 1%, 3%, 5% and 7% Strain Amplitudes

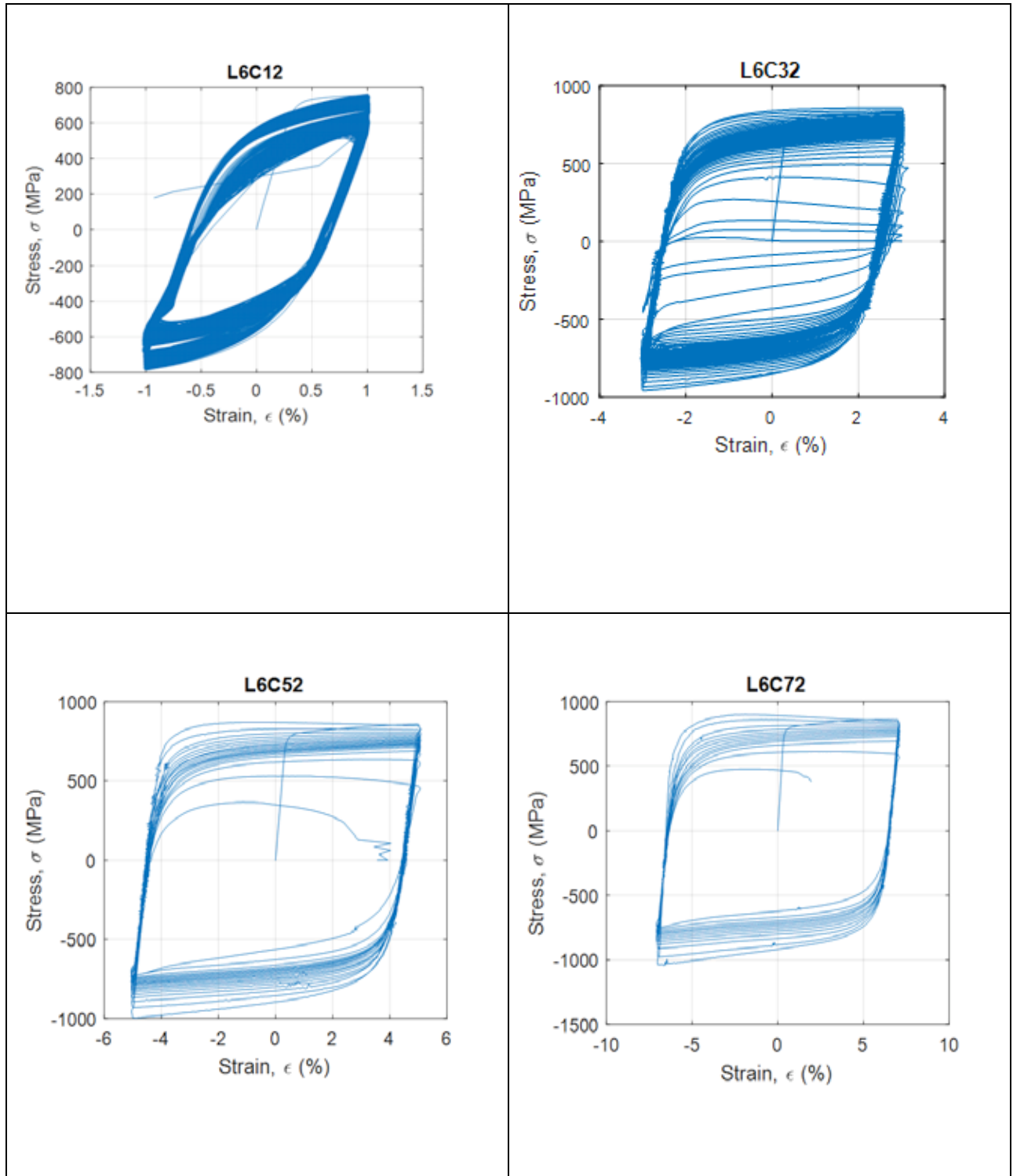


Figure 4. 6: Stress-Strain Response of S690 Coupons at 1%, 3%, 5% and 7% Strain Amplitudes

## 4.4 Cyclic and Monotonic Stress-Strain Curves Comparison

In order to investigate the behavior of the four steel grades in terms of increased or decreased resistance deformation referred as cyclic hardening or cyclic softening, the cyclic responses from variable strain amplitude tests were compared with the monotonic responses from Figure 4.7 to Figure 4.10.

Comparing the monotonic with the cyclic curves, cyclic hardening exists when the cyclic curve (peak tensile stresses) lies above the monotonic curve. Whereas, cyclic softening is present when the cyclic curve is below the monotonic curve.

Overall, from the first to the last cycle, cyclic hardening was evident in both S275 and S355. In contrast, cyclic softening was evident from the first to the last cycle in the high strength steel, S690. However, S460 exhibited a combination of cyclic softening within the first cycle followed by cyclic hardening within the remaining cycles. Note that the hardening was also influenced by the strain amplitude.

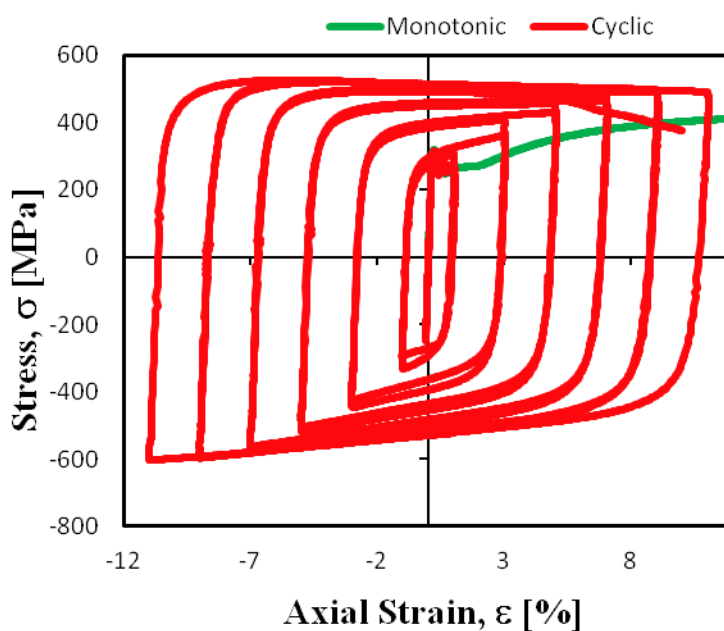


Figure 4. 7: Cyclic and Monotonic Stress-Strain Curves Comparison for S275

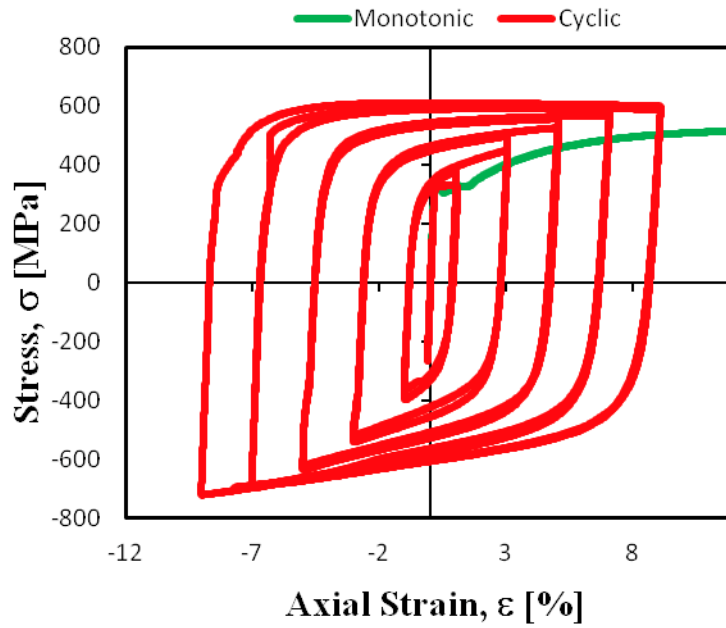


Figure 4. 8: Cyclic and Monotonic Stress-Strain Curves Comparison for S355

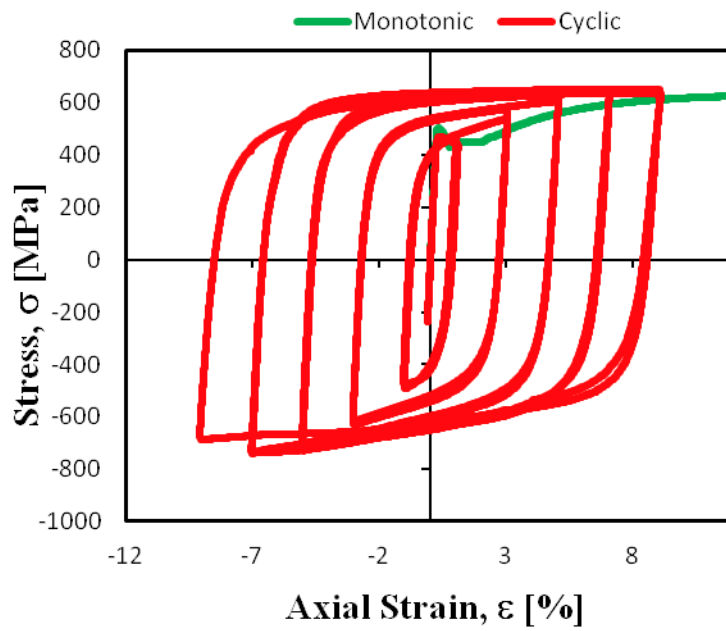


Figure 4. 9: Cyclic and Monotonic Stress-Strain Curves Comparison for S460

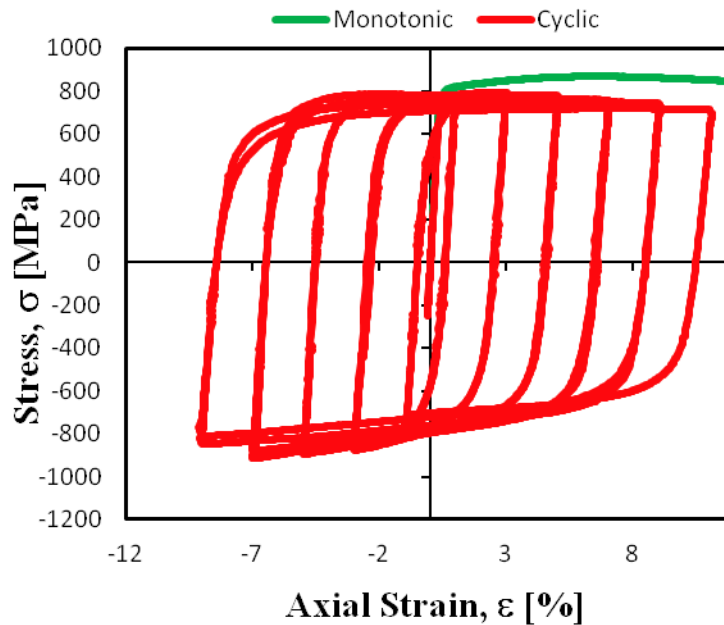


Figure 4. 10: Cyclic and Monotonic Stress-Strain Curves Comparison for S690

#### 4.5 Recorded Properties from Constant Strain Amplitude Tests

In addition to investigation conducted on cyclic hardening, cyclic softening or combination of both for the constant strain amplitude tests, the key mechanical properties recorded were maximum stress for the coupons tested for targeted strain amplitude, cyclic strain hardening exponent, cyclic strength coefficient and cyclic yield strength for each steel grade.

The maximum stress was obtained directly from the data recorded during the experiments. The cyclic strength coefficient ( $K'$ ) and the cyclic strain hardening exponent ( $n'$ ) were calculated based on rough estimations derived from the low cycle fatigue properties and are given by [9]:

$$K' = \frac{\sigma'_f}{(\epsilon'_f)^{n'}} \tag{4.1}$$

$$n' = \frac{b}{c} \tag{4.2}$$

Where:

$K'$  → cyclic strength coefficient



$\sigma'_f \rightarrow$  fatigue strength coefficient (MPa)

$\varepsilon'_f \rightarrow$  fatigue ductility coefficient (%)

$n' \rightarrow$  cyclic strain hardening exponent

$b \rightarrow$  fatigue strength exponent

$c \rightarrow$  fatigue ductility exponent

Parameters such as fatigue strength coefficient ( $\sigma'_f$ ), fatigue ductility coefficient ( $\varepsilon'_f$ ), fatigue strength exponent ( $b$ ) and fatigue ductility exponent ( $c$ ) are taken from the calculated low cycle fatigue (LCF) properties. The previous properties have been defined particularly to determine the cyclic yield strength. Yield strength is an important material characteristic in designing structural components. The cyclic yield strength ( $f'_y$ ) is defined at 0.2% strain offset corresponding to a plastic strain of 0.002 on the cyclic stress-strain curve. It was estimated using equation 4.3 [9]:

$$f'_y = (0.002)^{n'} * K' \quad (4.3)$$

The recorded maximum stresses for each coupon tested at the corresponding strain amplitude are presented in Table 4.4 and other parameters such as cyclic strain hardening exponent, cyclic strength coefficient and cyclic yield strength are given in Table 4.5.

Table 4. 4: Maximum recorded stress for each coupon [ $\sigma_{max}$  (MPa)]

Loading Protocol	$\varepsilon_t$	Steel			
		S275	S355	S460	S690
Constant Strain Amplitude	1%	365	413	500	842
	3%	475	473	586	858
	5%	513	617	695	870
	7%	548	631	671	901

From Table 4.4, it can be concluded that each steel grade exhibited increasing maximum stress for 1%, 3% and 7% constant strain amplitudes. However, a variation was shown in the maximum stress at 5% strain amplitude. Overall, as expected the highest maximum stress was achieved by the high strength steel, S690, at 7 % constant strain amplitude while the lowest by S275 at 1% constant strain amplitude.

**Table 4. 5: Recorded Properties from Constant Strain Amplitude Tests**

Property	Steel			
	S275	S355	S460	S690
Cyclic strain hardening exponent $n'$	0.076	0.082	0.077	0.088
Cyclic strength coefficient $K'$ (MPa)	784	888	1009	1507
Cyclic yield strength $f'_y$ (MPa)	489	533	625	872
Highest maximum stress, $\sigma_{max}$ (MPa)	548	631	695	901

A close correlation was observed among all the steel grades considering their cyclic strain hardening exponent. A close correlation was also observed for the cyclic strength coefficient and cyclic yield strength being 1.72 for S690, 1.61 for S460, 1.67 for S355 and 1.6 for S275.

Also, the cyclic yield strength and the highest maximum stress obtained for each steel grade have shown concordance.

## 4.6 Results from Charpy Impact Tests

The toughness of steel and its ability to resist brittle fracture are dependent on a number of factors that should be considered at the specification stage. A convenient measure of toughness is the Charpy V-notch impact test. The Charpy impact test, also known as the Charpy V-notch test, is a standardized high strain-rate test which determines the amount of energy absorbed by a material during fracture.

Charpy Impact tests have been conducted for the considered steel grades aiming at verifying whether during breakage they satisfy the minimum absorbed required energy.

### 4.6.1 Standard, Methodology and Specimens

The Charpy Impact tests were performed according to the International Standard ISO 148-1 : 2009 (E) which is for Metallic Materials-Charpy Pendulum Impact test.

The energy absorbed by the steels during impact were determined based on V-notch test methodology. In Figures 4. 11 and 4.13 as well as Tables 4.7 and 4.8 are presented the V-notch graphical geometry considered for the testing, tolerances and permissible values for test piece dimensions.

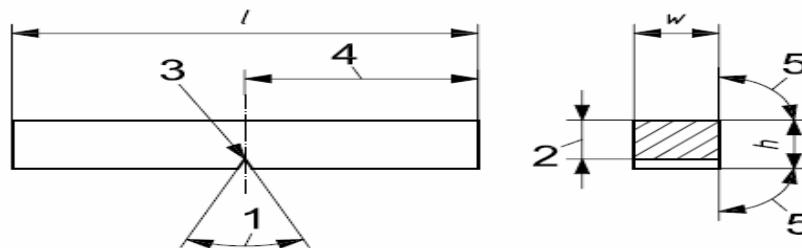


Figure 4. 11: Representation of the V-notch according to ISO 148-1 : 2009 (E)

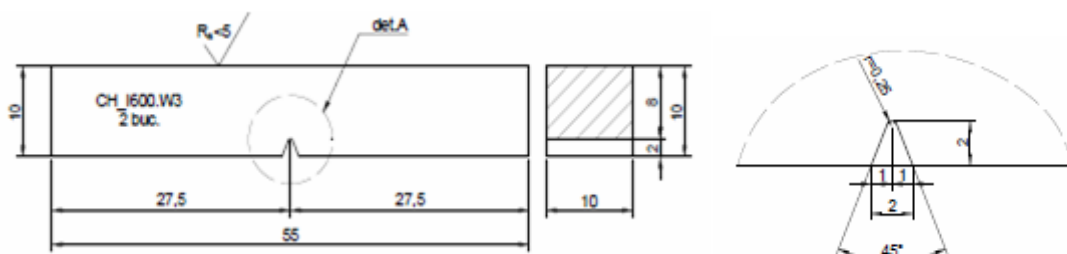


Figure 4. 12: Details of V-notch considered for the specimens

Table 4. 6: Tolerances on specified test piece dimensions [ISO 148-1 : 2009 (E)]

Designation	Symbol and No.	V-notch test piece		
		Nominal dimension	Machining tolerance	Tolerance class <sup>a</sup>
Length	<i>l</i>	55 mm	± 0,60 mm	js15
Height <sup>b</sup>	<i>h</i>	10 mm	± 0,075 mm	js12
Width <sup>b</sup> :	<i>w</i>			
— standard test piece		10 mm	± 0,11 mm	js13
— reduced-section test piece		7,5 mm	± 0,11 mm	js13
— reduced-section test piece		5 mm	± 0,06 mm	js12
— reduced-section test piece		2,5 mm	± 0,05 mm	js12
Angle of notch	1	45°	± 2°	—

Table 4. 7: Maximum permissible values of element thickness *t* in mm [EN 1993-1-10 : 2005 (E)]

Steel grade	Sub-grade	Charpy energy CVN		$\sigma_{Ed} = 0,75 f_y(t)$						
		at T [°C]	$J_{min}$	10	0	-10	-20	-30	-40	-50
S235	JR	20	27	60	50	40	35	30	25	20
	J0	0	27	90	75	60	50	40	35	30
	J2	-20	27	125	105	90	75	60	50	40
S275	JR	20	27	55	45	35	30	25	20	15
	J0	0	27	75	65	55	45	35	30	25
	J2	-20	27	110	95	75	65	55	45	35
	M,N	-20	40	135	110	95	75	65	55	45
	ML,NL	-50	27	185	160	135	110	95	75	65
S355	JR	20	27	40	35	25	20	15	15	10
	J0	0	27	60	50	40	35	25	20	15
	J2	-20	27	90	75	60	50	40	35	25
	K2,M,N	-20	40	110	90	75	60	50	40	35
	ML,NL	-50	27	155	130	110	90	75	60	50
S420	M,N	-20	40	95	80	65	55	45	35	30
	ML,NL	-50	27	135	115	95	80	65	55	45
S460	Q	-20	30	70	60	50	40	30	25	20
	M,N	-20	40	90	70	60	50	40	30	25
	QL	-40	30	105	90	70	60	50	40	30
	ML,NL	-50	27	125	105	90	70	60	50	40
	QL1	-60	30	150	125	105	90	70	60	50
S690	Q	0	40	40	30	25	20	15	10	10
	Q	-20	30	50	40	30	25	20	15	10
	QL	-20	40	60	50	40	30	25	20	15
	QL	-40	30	75	60	50	40	30	25	20
	QL1	-40	40	90	75	60	50	40	30	25
	QL1	-60	30	110	90	75	60	50	40	30

## 4.6.2 Tests Temperature and Materials details

Based on temperature, two (2) categories of tests were performed: One category at 20°C and the other one at -20°C. In Tables 4.9 and 4.10 are displayed dimensions of the coupons for each steel grade for each targeted temperature.

Table 4. 8: Materials dimension at 20°C

Temperature	Material	Dimensions (mm)			
		Width (w)	Thickness	Length (l)	Notch Width
20°C	S275 J2	9.9	9.9	50	7.98
	S355 J2	9.98	10	50	7.96
	S460 N	9.92	9.95	50	7.97
	S690 Q	9.89	9.82	50	8.02

Table 4. 9: Materials dimension at -20°C

Temperature	Material	Dimensions (mm)			
		Width (w)	Thickness	Length (l)	Notch Width
-20°C	S275 J2	10	10.01	50	8
	S355 J2	10.01	10	50	8
	S460 N	9.88	9.88	50	8
	S690 Q	10	10.01	50	8

## 4.6.3 Energy Absorption Capacity

The results for the two aforementioned categories of coupons are summarized in Tables 4.11 and 4.12. A histogram plot using steel materials versus the energy absorbed at breakage is shown in Figure 4.13. Firstly, all the impact tests were classified as OK because for all the considered steels, the energy absorbed at fracture exceeded significantly the minimum energy required for traverse orientation at both 20°C and -20°C.

Secondly, for the two categories of tests more energy was needed to fracture the high strength steel (S690) which represented more than twice and almost twice the energy needed to break

S460 respectively at 20 and -20°C. Whereas, less energy was needed to fracture S355 at 20°C and S460 at -20°C. S275 absorbed the second highest amount of energy before rupturing at 20°C but the amount was reduced with reducing temperature.

Interestingly, for the reduced temperature (-20°C), S355J2 did require more energy to fracture than at 20°C. In general, with increasing temperature, materials require more energy to break.

Partial breakage was observed in all the steel materials with 100% shear fracture at 20°C except for the high strength steel. However, at -20°C the high strength steel exhibited 100% shear fracture.

Overall, the ability of all the steel materials to resist brittle fracture was considered as excellent. They exhibited high tensile toughness with good ductility.

**Table 4. 10: Energy absorption capacity of the steel materials at 20 °C**

20°C	Material	Absorbed energy (J)	Minimum required energy (J)	Breakage	Shear fracture (%)	Status
Temperature	S275 J2	184.7	27	Partial	100	OK
	S355 J2	100.3	27	Partial	100	OK
	S460 N	133.3	40	Partial	100	OK
	S690 Q	232	30	Partial	90	OK

**Table 4. 11: Energy absorption capacity of the steel materials at -20 °C**

-20°C	Material	Absorbed energy (J)	Minimum required energy (J)	Breakage	Shear fracture (%)	Status
Temperature	S275 J2	143.5	27	Partial	70	OK
	S355 J2	152.5	27	Partial	90	OK
	S460 N	102	40	Partial	55	OK
	S690 Q	200	30	Partial	100	OK

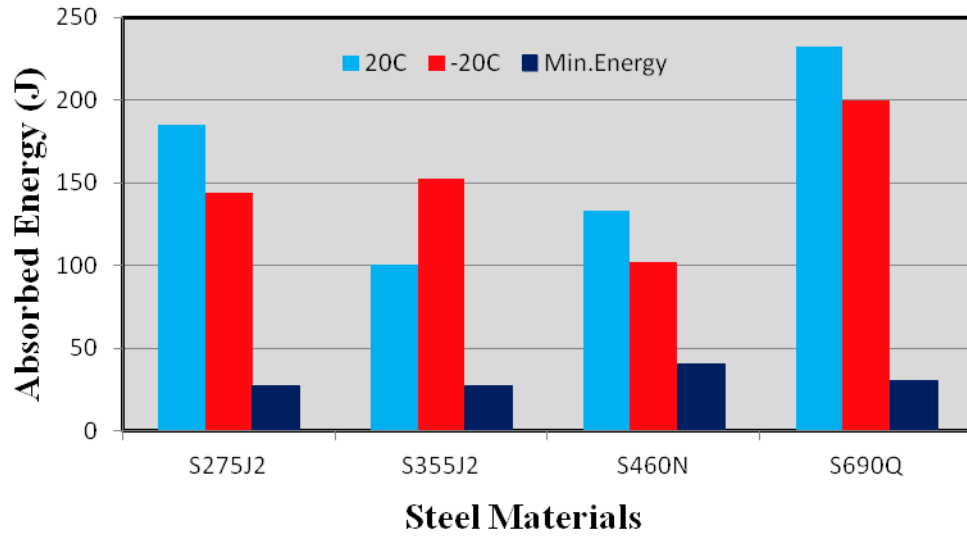


Figure 4. 13: Energy absorption capacity of the steel materials at 20°C and -20 °C

## SECTION 5

### LOW CYCLE FATIGUE (LCF) BEHAVIOR

#### 5.1 Recorded Fatigue Life

The low cycle fatigue (LCF) data was presented for constant strain amplitude cyclic coupon tests. The recorded fatigue life is summarized in Table 5.1. The values in Table 5.1 were recorded as the average of two or three coupons tested for each category of specimens in terms of the achieved number of reversals to failure for the four considered steel grades at the considered constant strain amplitudes. Note that average was taken only for values showing close correlation. Otherwise, the value showing consistence when compared to other steel grades at the same strain amplitude was considered. For instance, for S690 at 1% strain amplitude, two tests were performed with recorded data 261 and 976 number of cycles to failure. The number of cycles to failure 976 was considered because it was consistent when compared with the values recorded for the other steel grades at 1% strain amplitude (see the table).

**Table 5. 1: Reversals to Failure ( $2N_f$ )**

Loading Protocol	$\epsilon_t$	Steel			
<b>Constant Strain Amplitude</b>		S275	S355	S460	S690
	1%	1216	1140	810	976
	3%	115	121	113	113
	5%	34	30	27	30
	7%	12	12	17	17



### 5.1.1 Variation of the Recorded Fatigue Life

For a better and a quick understanding of the variation among the cyclic coupon tests, histogram plots of the recorded fatigue life versus steel grades for each considered constant strain amplitude are shown from Figure 5.1 to Figure 5.4. The variation was shown for all the coupons tested. For each steel grade and each strain amplitude, three (3 ) specimens were tested except for S690 at 1% strain amplitude for which only two results were presented.

Obviously, at 1% strain amplitude, all the steel grades exhibited higher number of cycles to failure. Whereas, the lowest numbers of cycles to failure were recorded at 7% strain amplitude for all the steels. In order words, the lower the constant strain amplitude, the higher the number of cycles to failure.

Despite some inconsistency among few results for specimens of the same category, the tests have shown credibility. Overall, based on the average values, for each strain amplitude, the recorded reversals have shown both increase and decrease, and vice-versa.

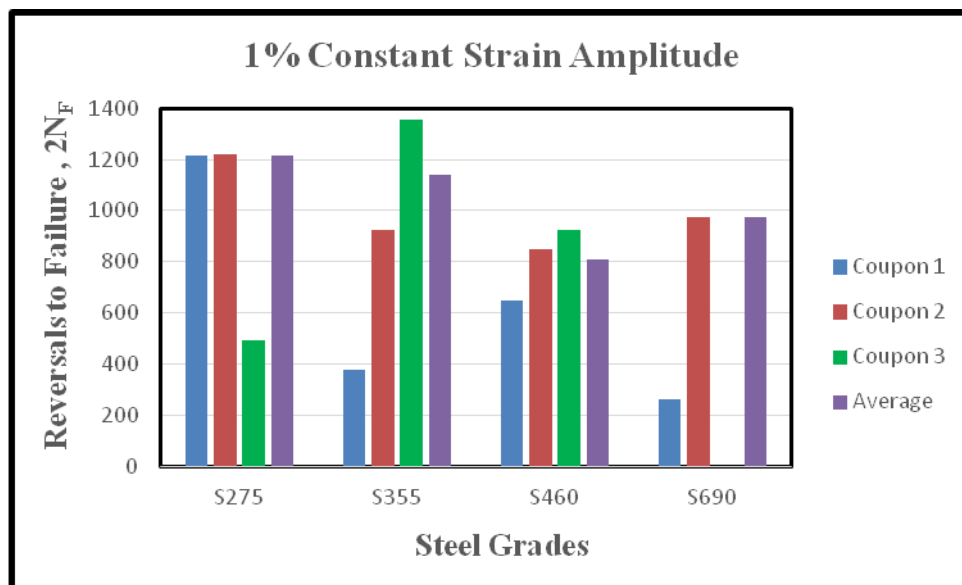


Figure 5. 1: Reversals to failure of all coupons tested for the steels at 1% strain amplitude

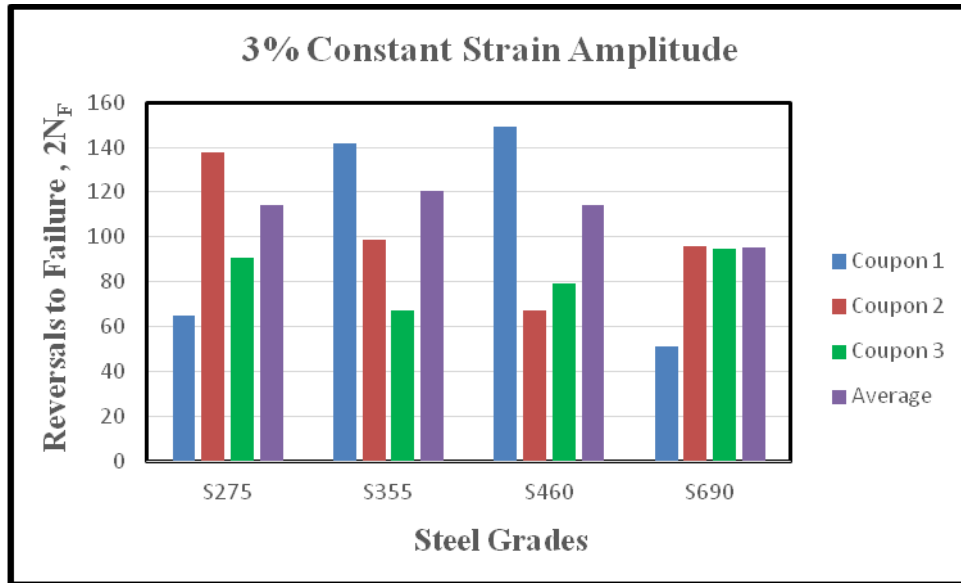


Figure 5. 2: Reversals to failure of all coupons tested for the steels at 3% strain amplitude

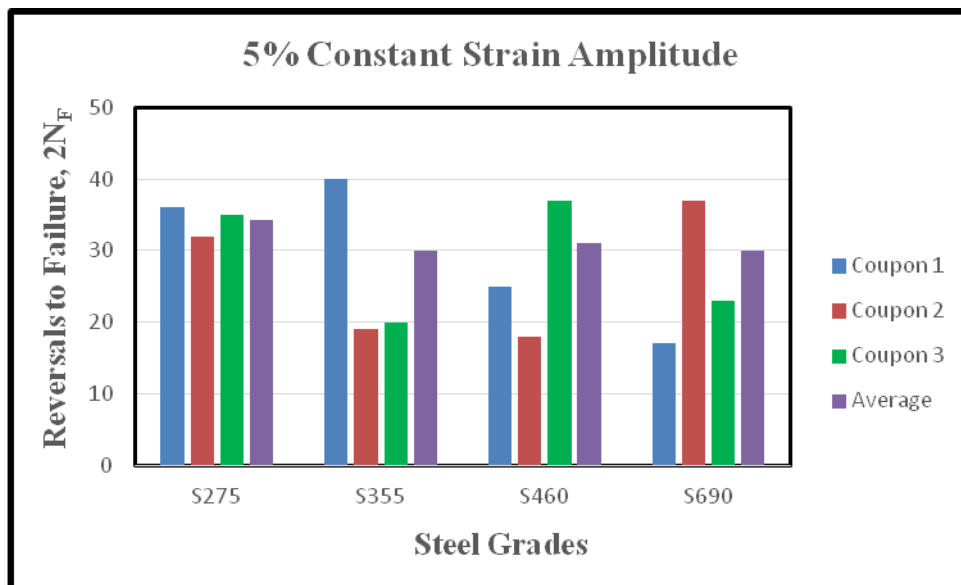


Figure 5. 3: Reversals to failure of all coupons tested for the steels at 5% strain amplitude

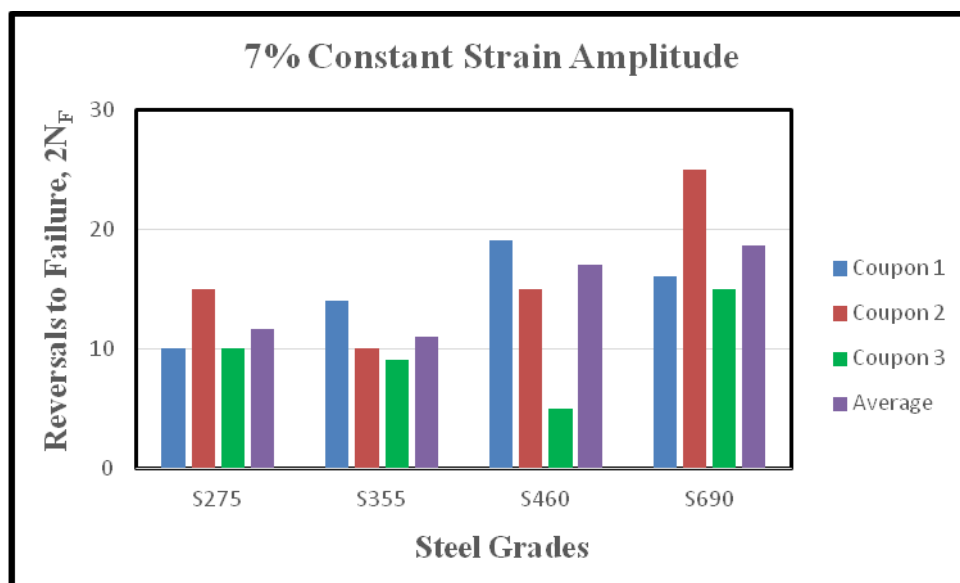


Figure 5. 4: Reversals to failure of all coupons tested for the steels at 7% strain amplitude

## 5.2 Low Cycle Fatigue of the Steel Grades

### 5.2.1 For Each Steel Grade

From Figure 5.5 to Figure 5.8 are shown the fatigue strain-life results of each steel grade. The results were obtained by data regression of reversals versus strain amplitude on log-log plots using power function. For each steel grade, the number of cycles to failure recorded for all the three coupons tested for each strain amplitude were used to obtain the low cycle fatigue curve except for S690 at 1% strain amplitude for which only one coupon was considered because the plot of the standard travel versus strain was not symmetric.

R-squared is a statistical measure of how close the data are to the fitted regression line. For each steel grade, the R-Squared value approached 1. It means that the variability of the low cycle fatigue response data fitted perfectly for each steel because the higher the R-squared, the better low cycle fatigue response fit data. The R-squared values for S275 and S355 were equal and it was the same case for S460 and S690. Globally, all the R-squared values were approximately the same.

However, despite good correlation between the results, a large scatter compared to the fitting line was observed at 1% strain amplitude for S460 which might be due to the cross-head displacement during testing contributing to shorten the fatigue life relatively.

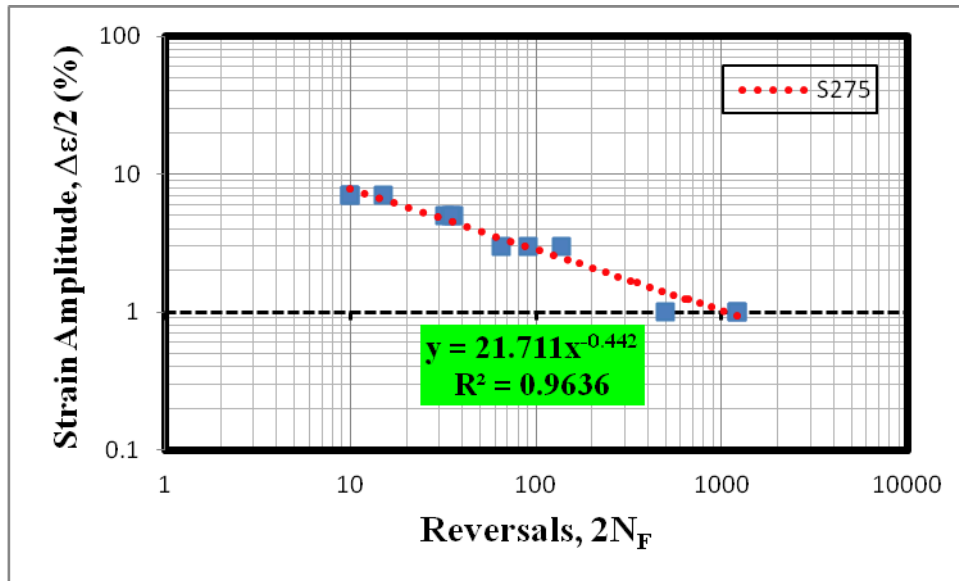


Figure 5. 5: Fatigue Strain-Life of S275

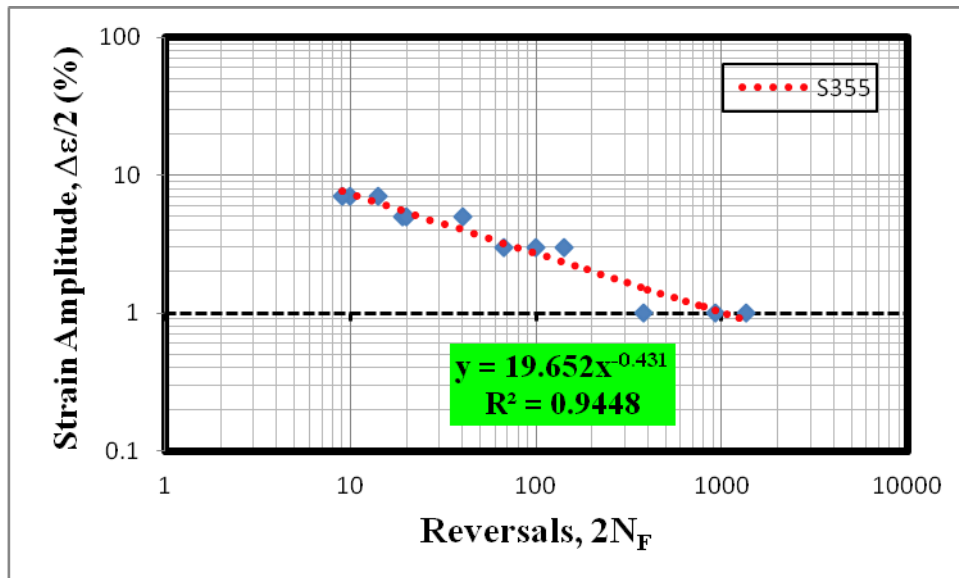


Figure 5. 6: Fatigue Strain-Life of S355

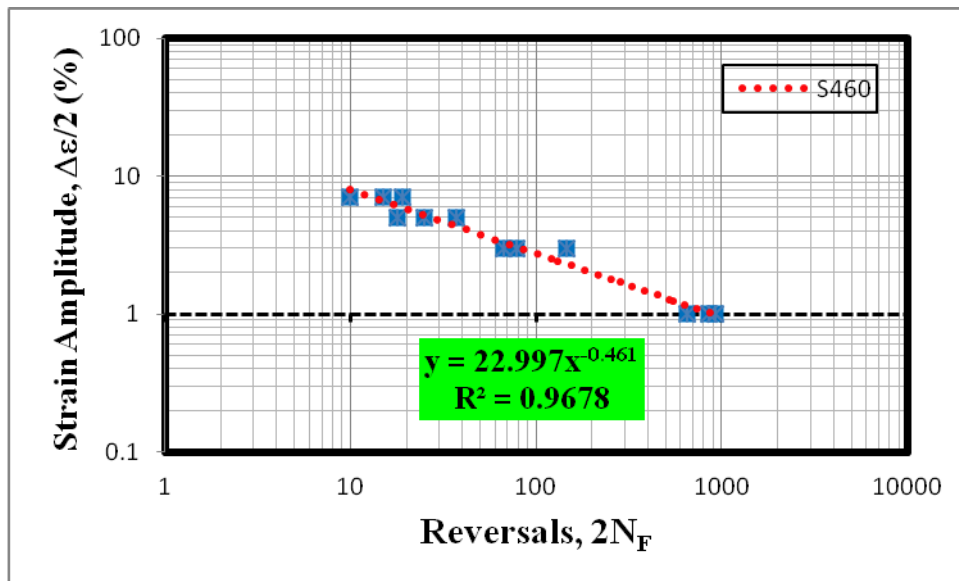


Figure 5. 7: Fatigue Strain-Life of S460

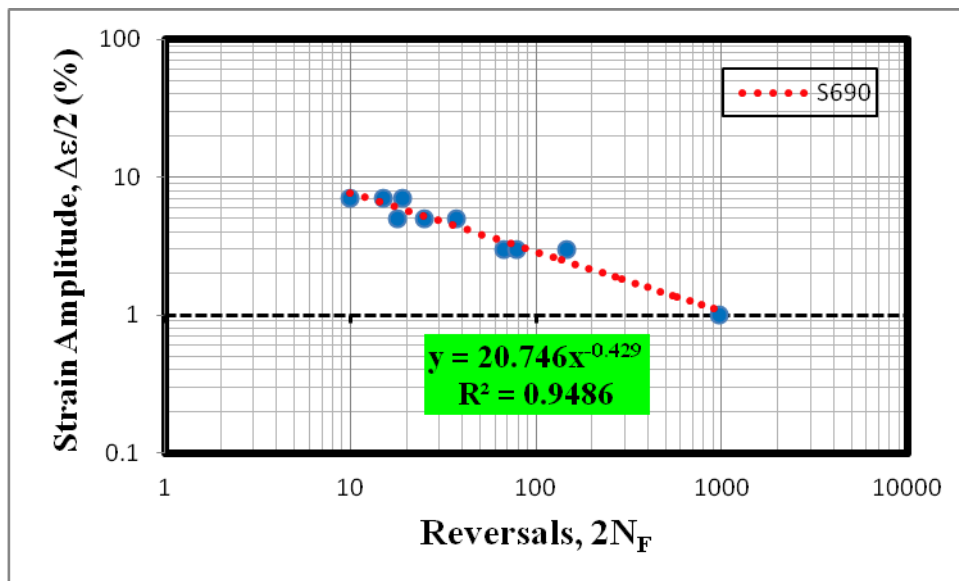


Figure 5. 8: Fatigue Strain-Life of S690

### 5.2.2 For all the Considered Steel Grades

In Figure 5.9 is compared the fatigue strain-life of all the considered steel grades. A close correlation between the fatigue life and the recorded data has been shown among the strain amplitudes considered. Globally, S355 exhibited higher fatigue life than all the other steel grades considered. The second highest fatigue life was exhibited by S275 while the lowest by

S460. Overall, even though the fatigue strain-life of the steels changed but they exhibited approximately similar behavior.

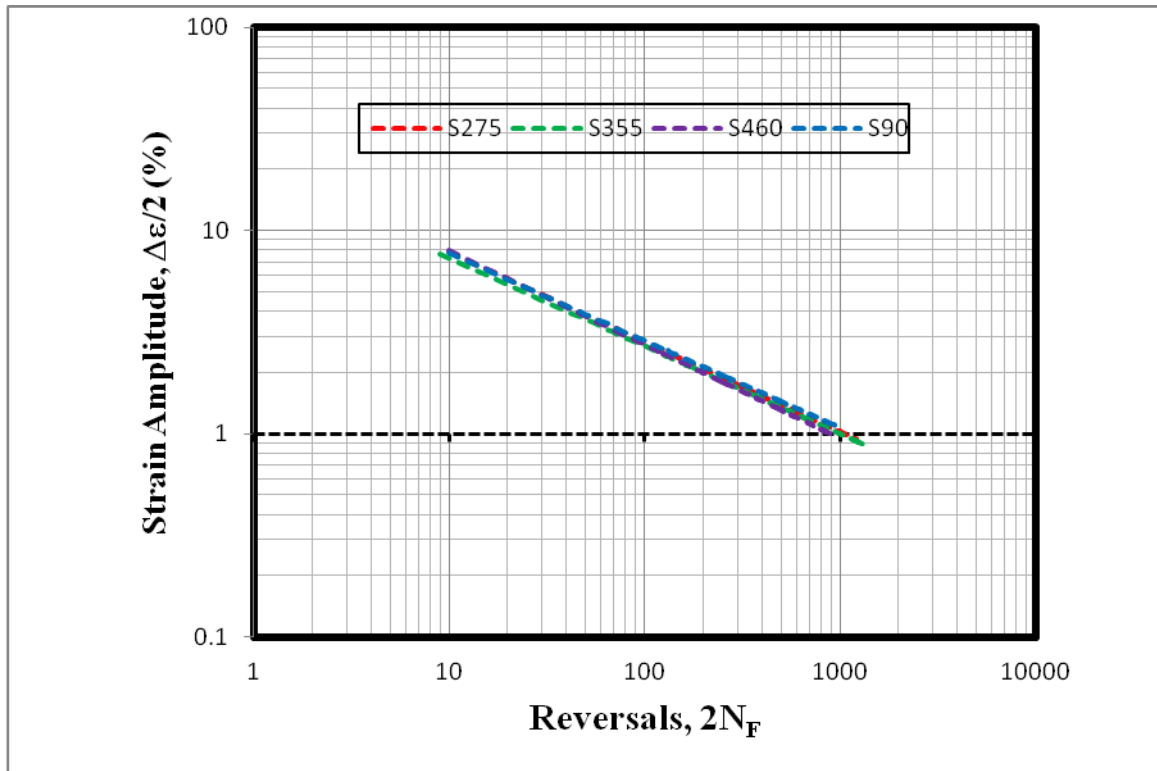


Figure 5. 9: Fatigue Strain-Life Comparison of all the Considered Steels

### 5.2.3 Comparison and Summary of the Results

From the literature (Peter Dusicka et. al, 2006), an experimental evaluation of the low cycle fatigue was conducted on five grades of plate steel. The coupons were tested to failure using complete reverse cyclic axial of constant strain amplitudes ranged from 1% to 7% and at constant strain rate of 0.1%/sec.

As shown in Figure 5.10, they concluded that the low cycle fatigue life of the different steels did vary, but overall the fatigue life was almost similar for all steel grades except for LYP225 due to limited data available.

For the present work, an experimental evaluation of the low cycle fatigue was conducted on four grades European mild carbon steel. The coupons were tested to failure using complete reverse

cyclic axial of constant strain amplitudes ranged from 1% to 7% with increment 2 and at constant strain rate of 0.2%/sec.

Compared to the literature, nearly the same trend occurred for the current work (see Figure 5.9). The low cycle fatigue life of the different steels vary, but overall the fatigue life almost lies within the same range for all steel grades.

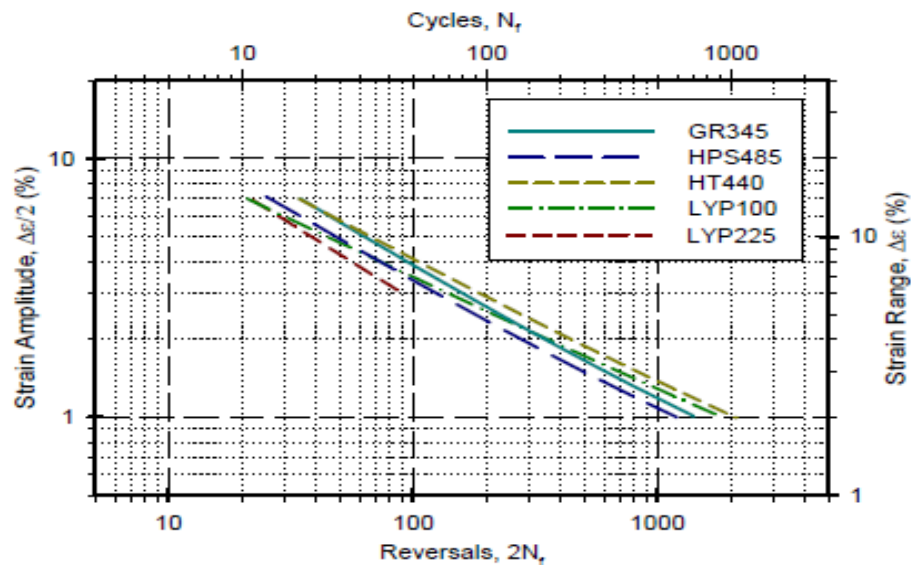


Figure 5. 10: Fatigue Strain-Life Comparison of all the Considered Steels from Literature [16]

### 5.3 Determination of the Strain-Life Fatigue Properties

The Strain-Life Fatigue properties including fatigue strength coefficient ( $\sigma'_f$ ), fatigue strength exponent (b), fatigue ductility coefficient ( $\epsilon'_f$ ), and fatigue ductility exponent (c), are obtained from regression of experimental data fatigue to individual relationships of elastic and plastic parts of the strain-life equation using linear fit plots.

The elastic line is a plot of reversals to failure ( $2N_f$ ) versus stress amplitude ( $\frac{\Delta\sigma}{2}$ ). The reversals or number of cycles were taken directly from experimental data. The stress amplitude for each coupon tested was taken as the average of maximum and minimum stress. The intercept of the

elastic line was taken as fatigue strength coefficient and its slope as the fatigue strength exponent.

The plastic line is a plot of reversals to failure ( $2N_f$ ) versus plastic strain amplitude ( $\frac{\Delta\varepsilon_p}{2}$ ). The reversals or number of cycles were taken directly from experimental data. The plastic strain amplitude for each coupon tested was derived from the following equation [9]:

$$\Delta\varepsilon = \Delta\varepsilon_p + \Delta\varepsilon_e = \Delta\varepsilon_p + \frac{\Delta\sigma}{E} \tag{5.1}$$

Where:

$\Delta\varepsilon \rightarrow$  Total strain range

$\Delta\sigma \rightarrow$  True Stress range

$E \rightarrow$  Modulus of Elasticity

$\Delta\varepsilon_e \rightarrow$  True elastic strain range

$\Delta\varepsilon_p \rightarrow$  True plastic strain range

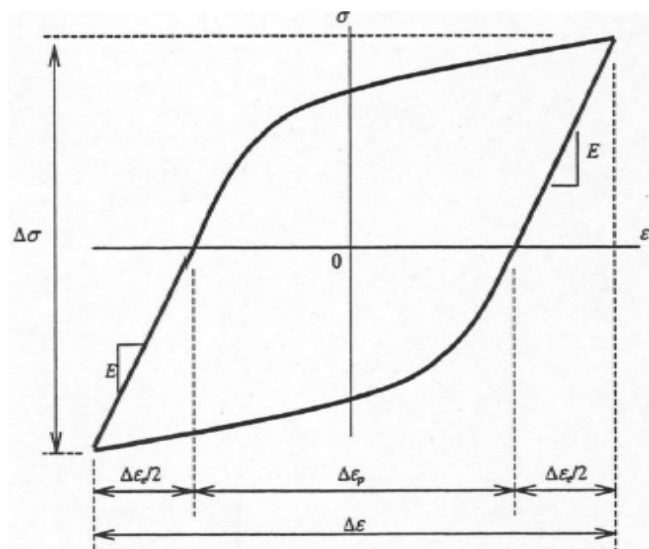


Figure 5. 11: Hysteresis loop showing how to compute parameters [9]

The intercept of the plastic line was taken as fatigue ductility coefficient and its slope as the fatigue ductility exponent. Figure 5.11 is presented in order to provide a better understanding on how the stress amplitude and the plastic strain amplitude have been calculated.

### 5.3.1 Results and Comparison with Literature



The Strain-Life Fatigue properties of the steel grades including fatigue strength coefficient ( $\sigma'_f$ ), fatigue strength exponent ( $b$ ), fatigue ductility coefficient ( $\epsilon'_f$ ), and fatigue ductility exponent ( $c$ ) are presented in Table 5.3. A close correlation can be observed from the fatigue life relationship

and the recorded data. The high strength steel (S690) exhibits higher fatigue strength coefficient and exponent but lower fatigue ductility exponent.

Overall, the fatigue strength exponent,  $b$ , ranged from -0.051 to -0.059 and the fatigue ductility exponent,  $c$ , ranged from -0.670 to -0.675. The fatigue strength coefficient, ( $\sigma'_f$ ), ranged from 739 MPa to 1364 MPa and the fatigue ductility coefficient ( $\epsilon'_f$ ) ranged from 0.456 to 0.5. The results were compared with the results obtained from literature, Table 5.2, and shown almost the same trends

**Table 5. 2: Fatigue Life Coefficients from Literature [16]**

Coefficient	Steel				
	GR345	HPS485	HT440	LYP100	LYP225
Fatigue Strength Coefficient, $\sigma'_f$ MPa (ksi)	894 (130)	886 (129)	1000 (145)	475 (68.8)	507 (73.6)
Fatigue Strength Exponent, $b$	-0.082	-0.072	-0.101	-0.081	-0.063
Fatigue Ductility Coefficient, $\epsilon'_f$	0.535	0.432	0.422	0.275	0.446
Fatigue Ductility Exponent, $c$	-0.590	-0.575	-0.524	-0.459	-0.612

**Table 5. 3: Fatigue Life Coefficients of the Considered Steel Grades**

Coefficient	Steel			
	S275	S355	S460	S690
Fatigue strength coefficient, $\sigma'_f$ (MPa)	739	824	946	1364
Fatigue strength exponent, b	-0.051	-0.055	-0.052	-0.059
Fatigue ductility coefficient, $\varepsilon'_f$	0.456	0.404	0.434	0.5
fatigue ductility exponent, c	-0.675	-0.672	-0.674	-0.670

## 5.5 Transition Fatigue Life

In general, plastic strains dominate low cycle fatigue behavior and elastic strains dominate high cycle fatigue behavior [9]. Since the study was on low cycle fatigue behavior, the transition fatigue life was calculated to verify if plastic strains dominated. Plastic strains dominate if the transition fatigue life ( $2N_t$ ) is greater than the number of cycles to failure or reversals ( $2N_f$ ). If the reversals are greater than the transition fatigue life, then elastic strains dominate [9].

The transition fatigue life ( $2N_t$ ) of each steel grade was calculated using equation 2.29 and shown in Table 5.4. According to the results, for each steel grade, the transition fatigue life exceeded the number of cycles to failure. Therefore, plastic strains dominate.

**Table 5. 4: Comparison between Transition Fatigue Life and Reversals for the Steel Grades Considered**

<b>Property</b>	<b>Steel</b>			
	<b>S275</b>	<b>S355</b>	<b>S460</b>	<b>S690</b>
Transition Fatigue Life $2N_t$	2504	1800	1488	1147
Reversals (highest value) $2N_f$	1216	1140	870	976

## SECTION 6

### FINITE ELEMENT MODELING (FEM)

After completing the laboratory experiments, a major goal of the study was to find or derive necessary parameters from experimental results for materials modeling in Abaqus. Using material calibration, the aim was to validate the experimental results.

Numerical modeling has been conducted to validate results obtained from Monotonic tensile, Constant strain amplitude as well as Variable amplitude tests. Parameters for the modeling of variable strain amplitude coupons such as equivalent plastic true strain and true stress for the isotropic hardening components and plastic strain and yield stress for the kinematic hardening components have been derived from constant strain amplitude tests data for each corresponding steel material.

#### 6.1 FEM for Monotonic Tensile Tests

Following are details for the modeling of monotonic tensile tests:

##### 6.1.1 Part

The major difference among the specimens presented in this section is in the input parameters for each steel grade particularly for the material property. Cross section dimensions are similar for all of them. A schematic description of the specimen is shown in Figure 6.1 and the specimen geometry in Abaqus is shown in Figure 6.2. The dimensions were shown in Figure 3.2.

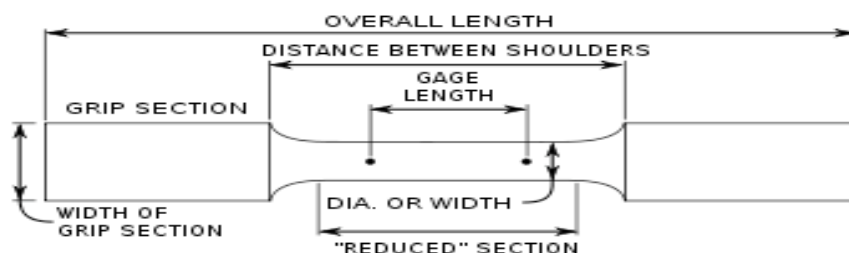


Figure 6. 1: Schematic description of the Specimen

For the Abaqus model, the distance given by the difference between “distance between shoulders” and “reduced section” as shown in Figure 6.2 was drawn as straight line for more convenience in drawing and most important because it did not affect the results. The results were not affected too much because for all the monotonic tensile tests, the failure occurred between the sensors and in Abaqus the results were taken within the gage length.



Figure 6. 2: Drawing of the specimen in Abaqus

### 6.1.2 Material Definition

As shown in Figure 6.3, the following material behaviors were used for each model: Mass density, regularization, elastic and plastic components.

- Mass density was defined for stress/displacement elements.

$$\text{Mass density: } \rho = 7850 \text{Kg/m}^3$$

- To regularize the input parameter, an error tolerance was used. Logarithmic regularization was used to provide a better match to typical strain-rate-dependent data.

$$\text{Rtol}=0.03$$

- For the elastic components, typical values have been used for the Young’s Modulus and the Poison’s ratio.

$$\text{E} = 210 \text{GPa and } \nu = 0.3$$

- For the plastic components, stress-strain curves obtained from experiments were modified using the following relationships:

$$\sigma_{\text{true}} = \sigma(1 + \epsilon)$$

$$\epsilon_{\text{true}} = \ln(1 + \epsilon)$$

Where:

$\sigma_{\text{true}}$  → True stress

$\sigma$  → Engineering stress (obtained from experiments)

$\varepsilon_{\text{true}}$  → True Strain

$\varepsilon$  → Engineering Strain (Obtained from experiments)

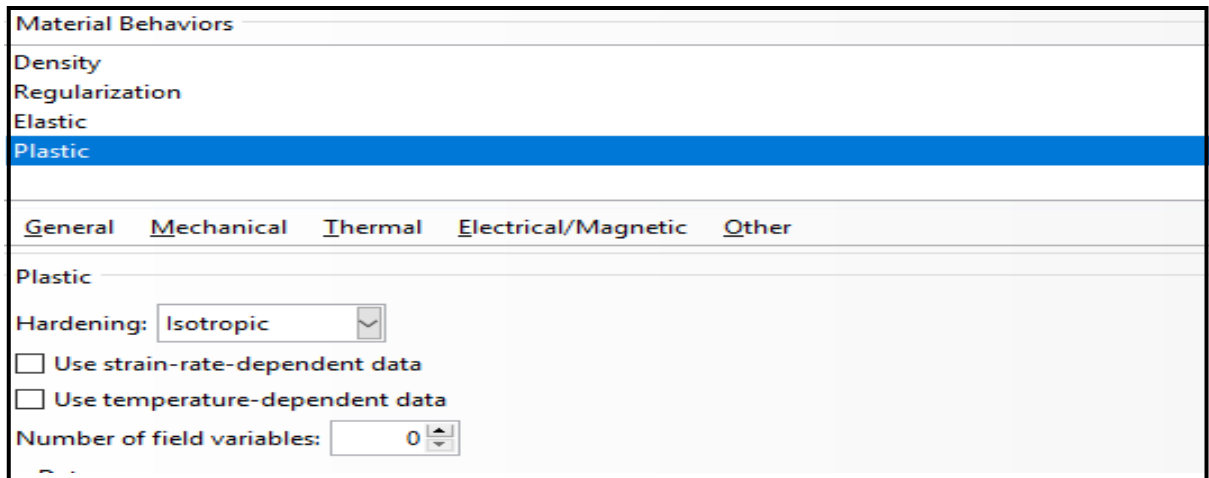


Figure 6. 3: Material behaviors definition in Abaqus

### 6.1.3 Step

Dynamic implicit analysis with quasi-static application was used because it takes initial guess, iterates to convergence and is very accurate. To reduce the running time, a time period of 1 second has been used as shown in Figure 6.4.

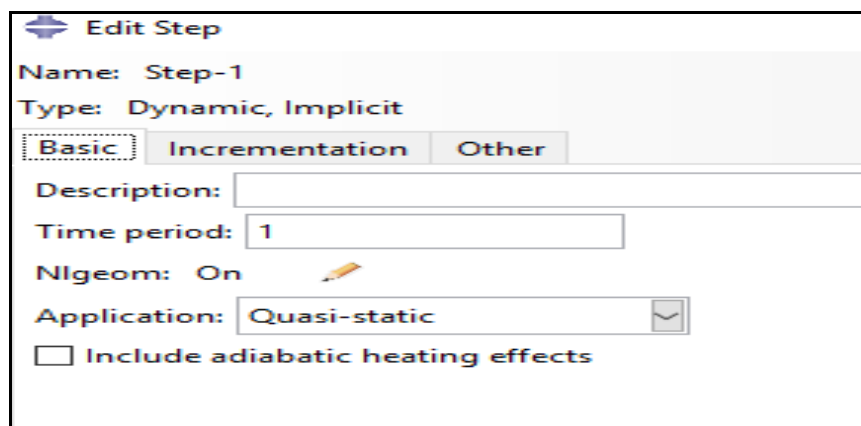


Figure 6. 4: Step definition in Abaqus

### 6.1.4 Load Definition

Two boundary conditions were applied at the reference point located at the top and bottom of the model. The one at the bottom is fixed and the one at the top is movable assuming a displacement of 1mm.

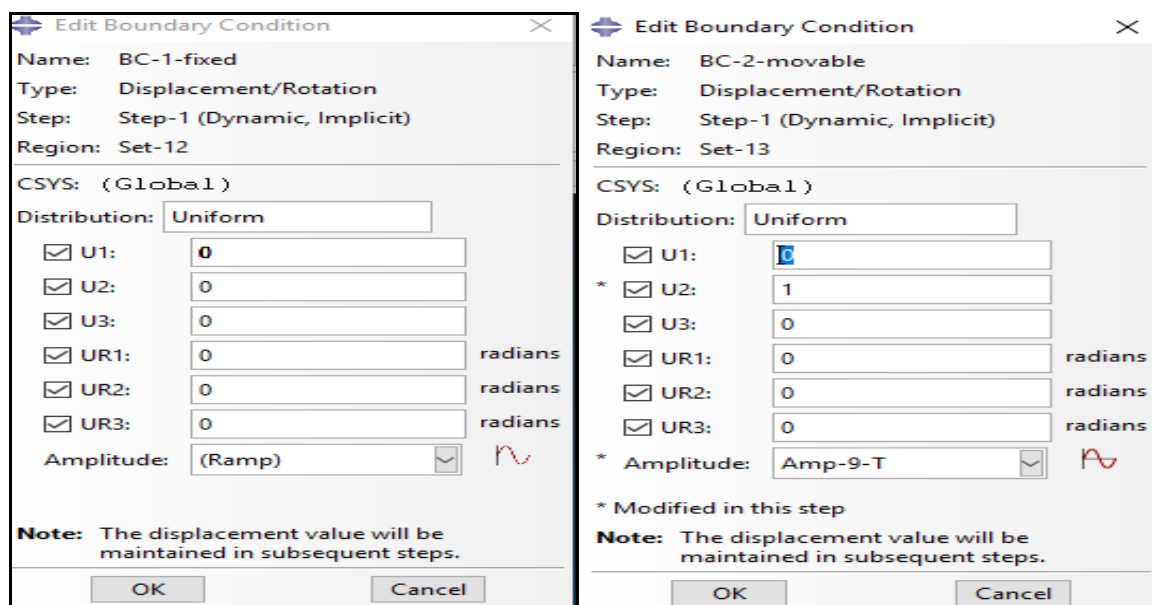
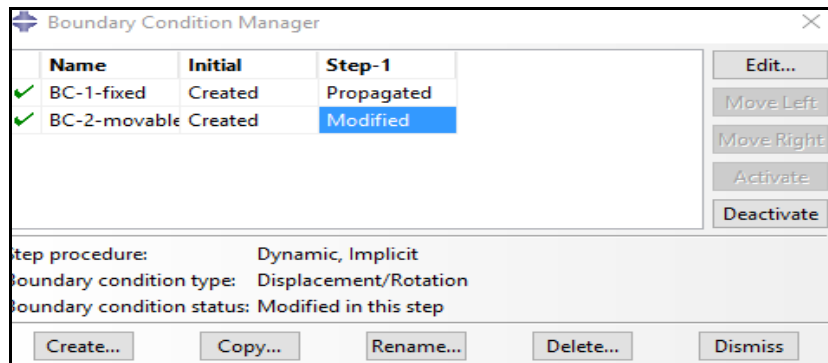


Figure 6.5: Assigned boundary conditions

### 6.1.5 Mesh Definition

Meshing plays a crucial role in the analysis of finite element modelling. To improve the quality of the mesh and get accurate results, the geometry of the model has been partitioned. Only one mesh size has been considered.

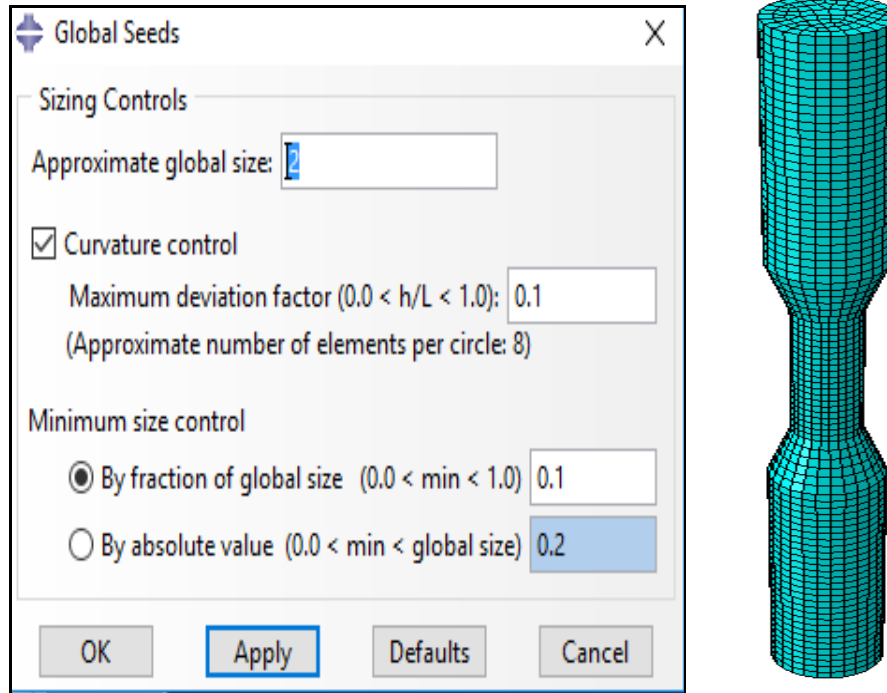


Figure 6. 6: Mesh definition and model meshing

## 6.2 Numerical Results for Monotonic Tensile Load History

In Figures 6.7 and 6.8 are displayed the deformation, the von Mises stresses and the stress-strain curves obtained from Abaqus and Experiments for each steel grade. The numerical results for all the steel materials considered revealed closed agreement with the results obtained from laboratory experiments.



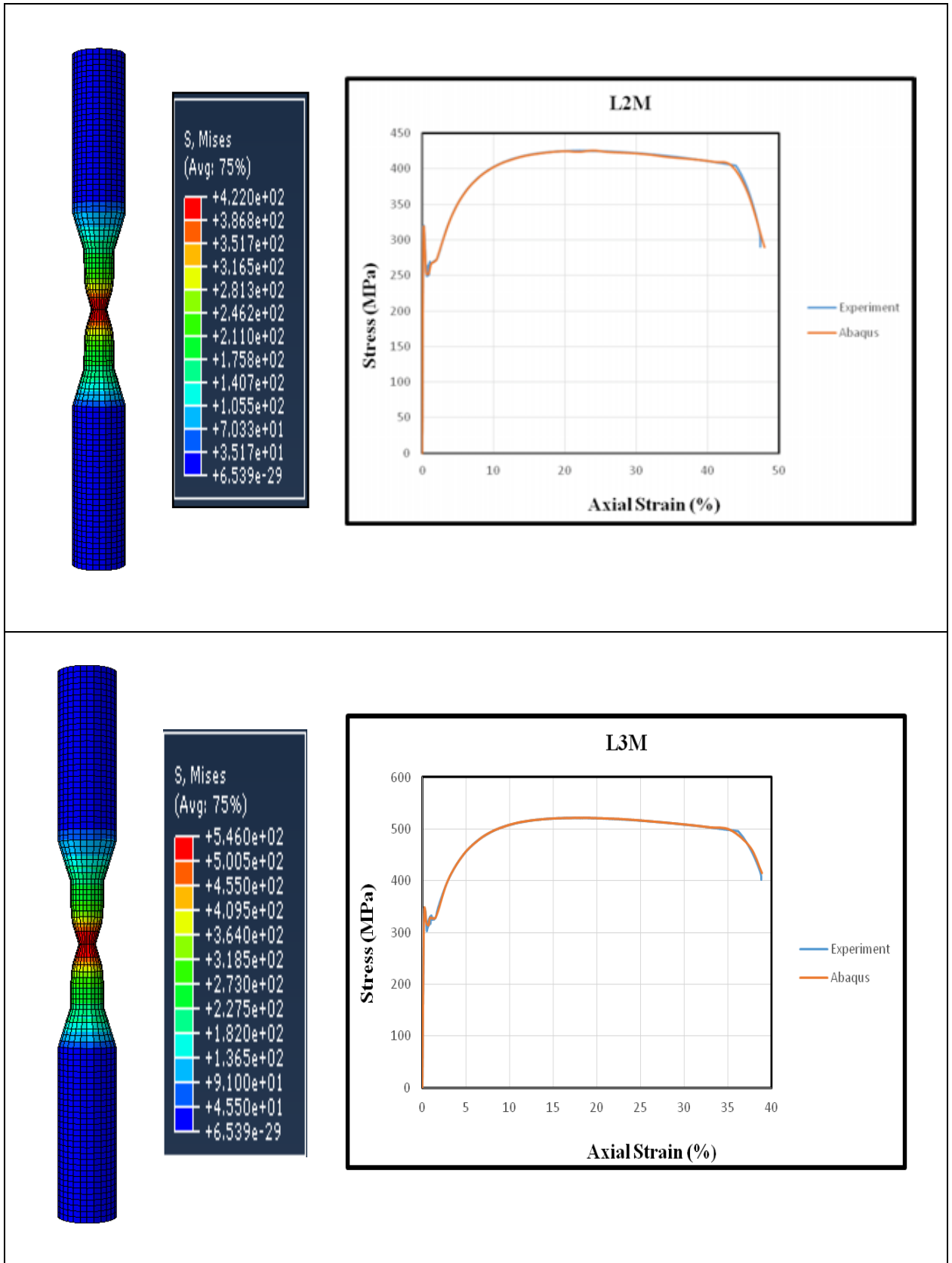


Figure 6. 7: Deformation, von Mises stresses and stress-strain curves comparison of S275 and S355

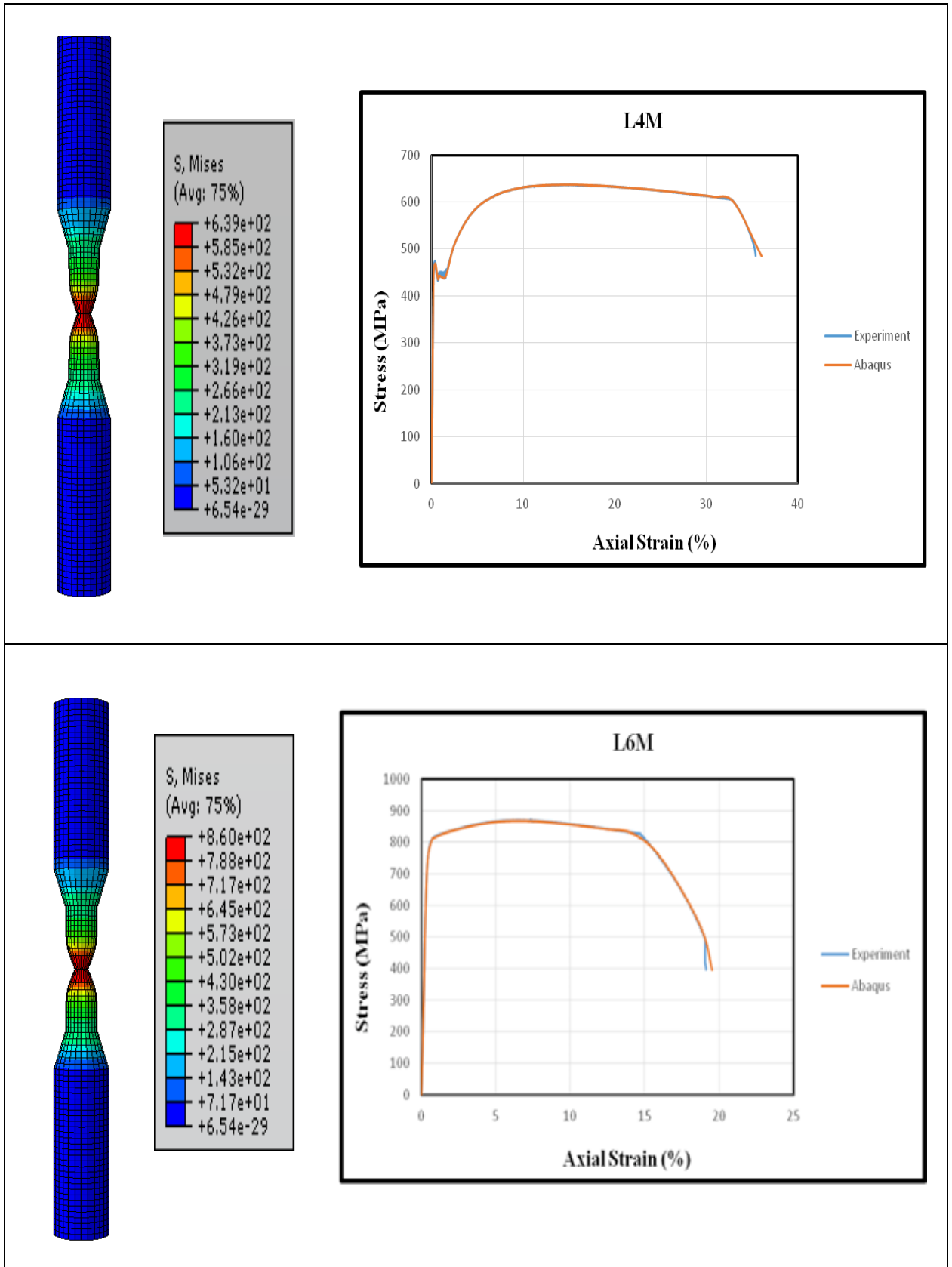


Figure 6. 8: Deformation, von Mises stresses and stress-strain curves comparison of S460 and S690

## 6.3 FEM for Cyclic Tests

For the cyclic tests, materials modelling have been done as follows:

### 6.3.1 Assumptions and Parts

To calibrate materials in Abaqus, the following assumptions have been made:

1. If materials calibration on a cube and a cylinder corresponding to the gage length geometry of the original specimen provided close results when compared with the experimental results, then no need to use the original specimen for the modeling expecting that the results for the whole specimen and cube/cylinder would be similar or nearly similar.
2. When using data from constant strain amplitude tests to find parameters for both constant and variable amplitude load history, if the numerical results for at least two out of the four considered steel materials revealed close correlation with experimental results, hence it is not necessary to model for all the four grade steels assuming that the results would display approximately the same trends.

Therefore, based on the assumptions, a cube of 1x1x1mm and a cylinder of height and diameter equal to the original specimen gage length (maximum 15mm) have been used to calibrate the steels materials.

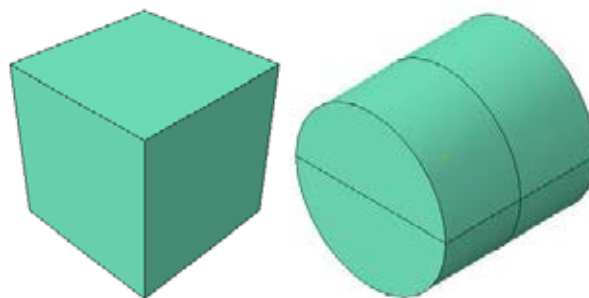


Figure 6. 9: Parts drawing in Abaqus for the materials calibration

### 6.3.2 Material Definition

For the plastic components, analysis steps of the calibration for the kinematic hardening models are taken from Abaqus Analysis User's manual (version 6.6). In Abaqus, two types of analysis

are proposed: Linear Kinematic Hardening model and Nonlinear Isotropic-Kinematic (combined) Hardening model. For the study, materials calibrations have been done using Non-Linear Isotropic-Kinematic (Combined) Hardening because generally it provides a more accurate approximation to the stress-strain relation than the linear model although it is more complex.

### 6.3.2.1 Isotropic Hardening

In Abaqus, there are three ways to calibrate material in order to find the input parameters for the isotropic hardening component [22]:

- 1) Defining the isotropic hardening component by the exponential law
- 2) Defining the isotropic hardening component by tabular data
- 3) Defining the isotropic hardening component in a user subroutine in Abaqus/Standard

To find the parameters for the isotropic hardening component, calibration has been done using tabular data. Following are the steps:

- Abaqus input parameters for the isotropic hardening component include **equivalent stress** and **equivalent plastic strain**.
- These two parameters were derived by conducting symmetric strain-controlled using cyclic stress-strain curves obtained from constant strain amplitude tests data within the considered strain range as shown in Figure 6.10.
- Starting with an initial yield stress, peak tensile stresses were obtained by selecting randomly a number of cycles which provided automatically the corresponding strains with the help of an excel sheet.
- For each peak tensile stress, a corresponding compressive stress was found.
- All the engineering stresses and strains were converted to true stresses and strains using the following relationships:

$$\sigma_{\text{true}} = \sigma(1 + \epsilon)$$

$$\epsilon_{\text{true}} = \ln(1 + \epsilon)$$

- After finding all the necessary values, the true plastic strain range has been approximated as follows:

$$\Delta \epsilon_{\text{pl}} \approx \Delta \epsilon - 2\sigma_1^t/E [22]$$

Where:

$\Delta\varepsilon_{pl}$  → true plastic strain range

$\Delta\varepsilon$  → total true strain range

$\sigma_1^t$  → first peak tensile stress

$E$  → Young's Modulus

- For each considered cycle  $i$ , the equivalent true plastic strain has been given by:

$$\overline{\Delta\varepsilon_{pl,i}} = 0.5(4i - 3) * \Delta\varepsilon_{pl}[22]$$

- The corresponding equivalent true stress has found based on the following formula:

$$\sigma_{0,i} = \sigma_{t,i} - \alpha_i [22]$$

Where for each cycle  $i$ :

$\sigma_{0,i}$  → equivalent true stress

$\sigma_{t,i}$  → peak tensile stress

$\alpha_i$  → Backstress

- For each corresponding cycle, the backstress was derived as follows:

$$\alpha_i = \frac{\sigma_{t,i} - \sigma_{c,i}}{2} [22]$$

- Finally, data pairs  $(\sigma_{0,i}, \overline{\Delta\varepsilon_{pl,i}})$  including the initial equivalent stress at zero equivalent plastic strain were used as cyclic hardening input parameters in Abaqus and specified in tabulated form.

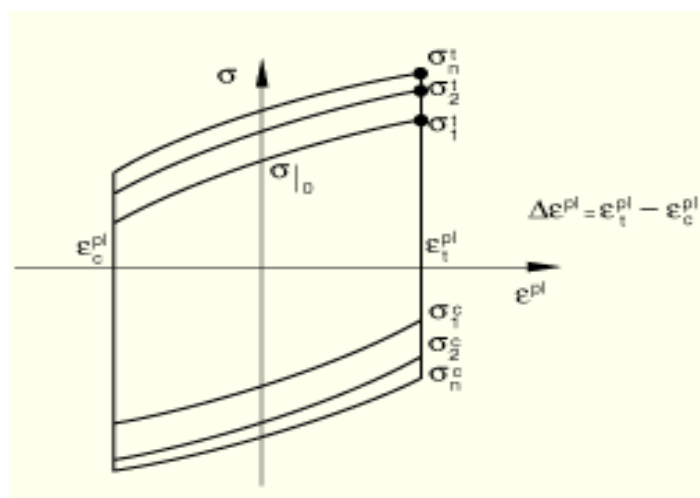


Figure 6.10: Symmetric strain cycle experiment [22]

**ABAQUS/CAE Usage:** Property module: material editor: Mechanical→Plasticity→Plastic: Hardening: Isotropic: Suboptions→Cyclic Hardening

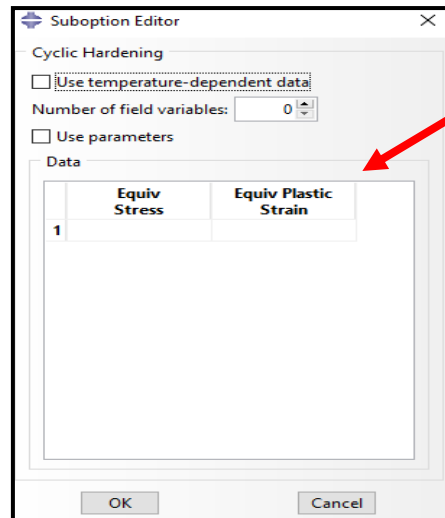


Figure 6. 11: Steps to input parameters in Abaqus for Isotropic Hardening

### 6.3.2.2 Kinematic Hardening

As for isotropic hardening, three ways are also available in Abaqus to calibrate material in order to find the input parameters for the kinematic hardening component [22]:

- 1) Defining the kinematic hardening component by specifying the material parameters directly being the kinematic hard parameter ( $C_i$ ) and the corresponding material dependent dynamic recovery term ( $\gamma_i$ ) if they are already calibrated from test data.
- 2) Defining the kinematic hardening component by specifying half-cycle test data which can be used when limited test data are available.
- 3) Defining the kinematic hardening component by specifying test data from a stabilized cycle.

To find the parameters for the kinematic hardening component, calibration has been done using test data from a stabilized cycle based on the following steps:

- Abaqus input parameters for the kinematic hardening component include **yield stress** and **plastic strain**.

- These two parameters were derived by selecting randomly a stabilized cycle from the stress-strain curves obtained from constant strain amplitude tests data for each steel grade. A cycle is said to be stabilized when the steady-state condition is reached meaning that the stress-strain curve no longer changes shape from one cycle to the next.
- As shown in Figure 6.12, from the stabilized cycle a number of engineering yield stresses were selected randomly and converted to true yield stresses for Abaqus input.
- By shifting the strain axis to  $\epsilon_{p,0}$  as displayed in Figure 6.12, the corresponding engineering plastic strain and later converted to true plastic strain for each selected yield stress has been found using the following relationship:

$$\epsilon_{pl,i} = \epsilon_i - \frac{\sigma_i}{E} - \epsilon_{p,0} \quad [22]$$

Where:

$\epsilon_{pl,i}$  → plastic strain

$\epsilon_i$  → corresponding strain to each selected yield stress (see figure 6.13)

$\sigma_i$  → selected yield stress  $i$

- Finally, data pairs  $(\sigma_i, \epsilon_{pl,i})$  were used as combined hardening input parameters in Abaqus and specified in tabulated form.

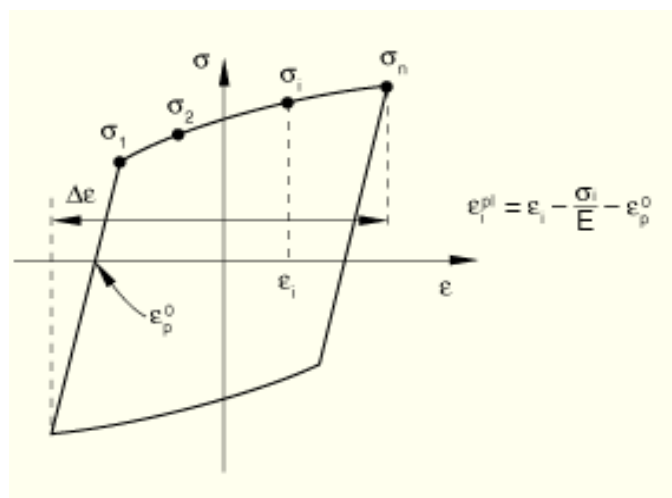


Figure 6. 12: Stress-Strain data for a stabilized cycle [22]

ABAQUS/CAE Usage: Property module: material editor: Mechanical→Plasticity→Plastic: Hardening: Combined: Data type: Stabilized

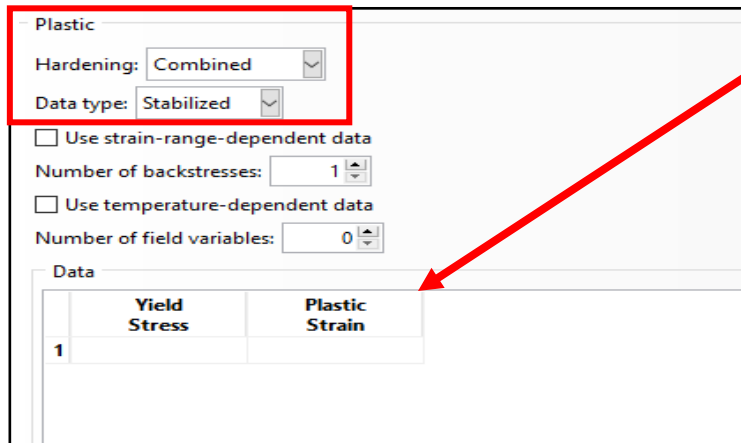


Figure 6. 13: Steps to input parameters in Abaqus for Kinematic Hardening

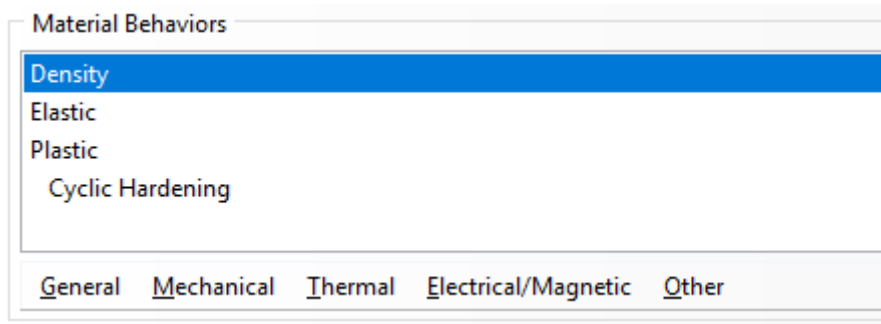


Figure 6. 14: Material behaviors for cyclic tests

The values for the density and the elastic component (Young’s modulus and Poisson’s ratio) were taken as the same as for monotonic load history. For the plastic component, following figures are parameters derived for S275.

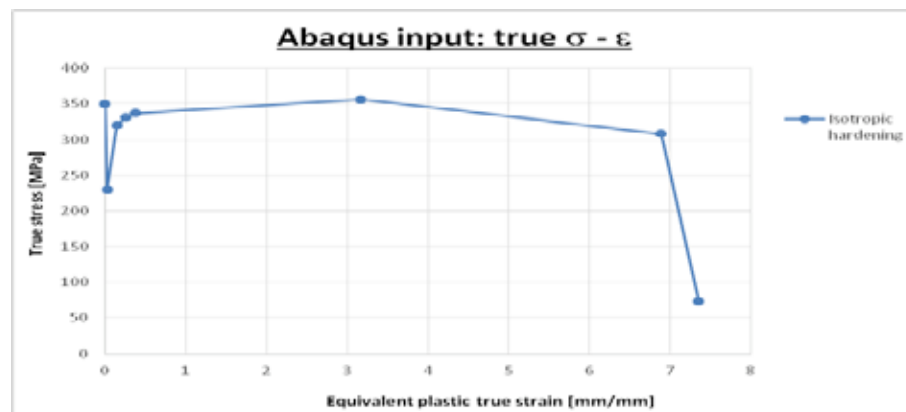


Figure 6. 15: Isotropic hardening parameters for S275



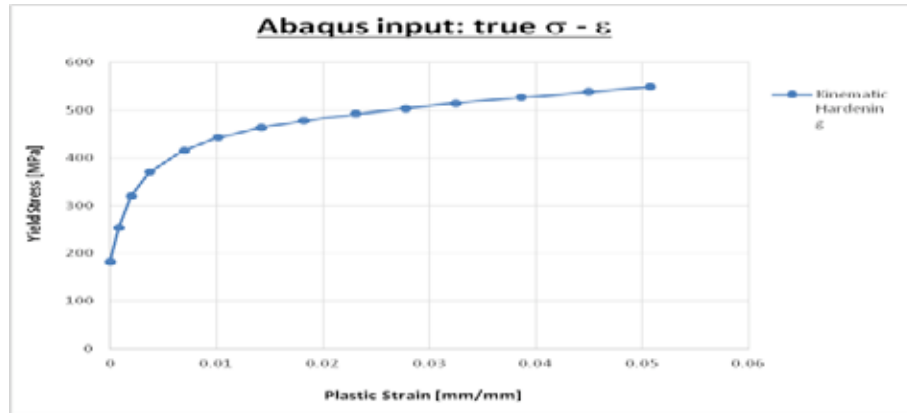


Figure 6. 16: Kinematic hardening parameters for S275

### 6.3.3 Step

Compared to the monotonic tensile load history, static general analysis with direct method equation solver and Full Newton solution technique was used to model the cyclic tests.

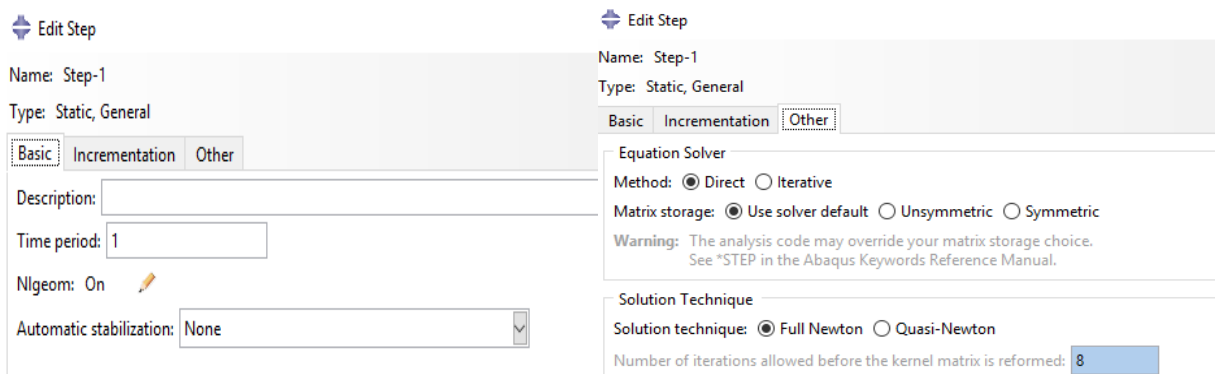


Figure 6. 17: Step definition for cyclic materials modeling

### 6.3.4 Load Definition

The boundary conditions have been set up in a similar way for the modeling of monotonic tensile tests but with different loading protocol.

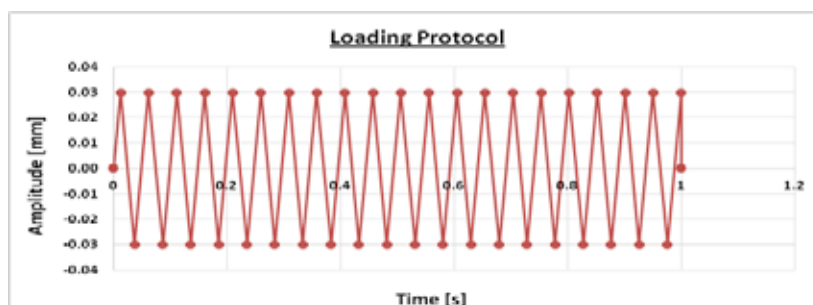


Figure 6. 18: Loading protocol for L2C3-2

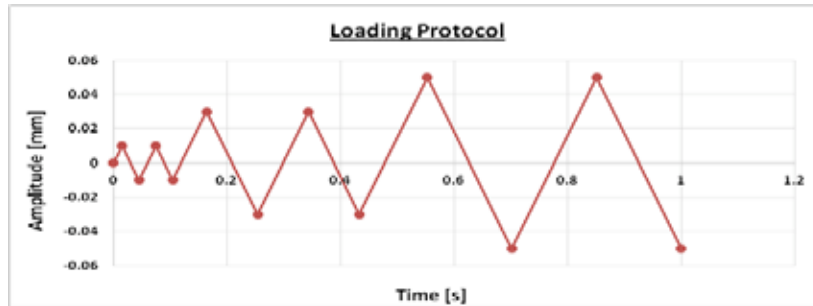


Figure 6. 19: Loading protocol for L2V3

### 6.3.5 Mesh Definition

Meshing plays a key role in finite element modeling (FEM). In one hand, even though big element size decreases the simulation time and computational cost but it also decreases the accuracy of the results. On the other hand, small element size while improving considerably the accuracy of the results also increases the simulation time and the computational cost. Therefore, it is important to carefully select the mesh density to achieve accurate results while reducing the computational effort.

For the cylinder modeling, a mesh of 2mm has been used by mean of an 8-node linear brick, incompatible modes.

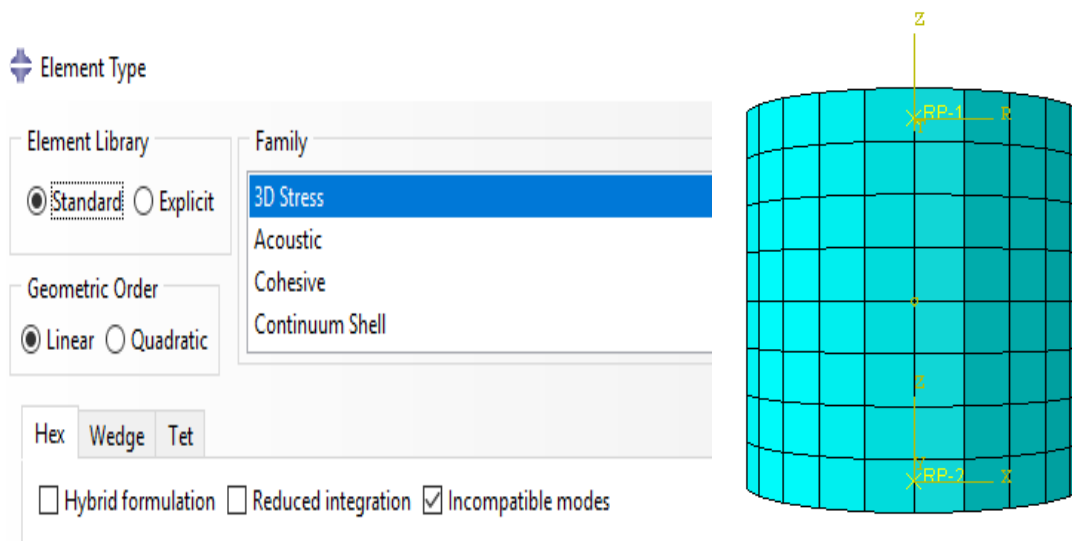


Figure 6. 20: mesh definition for cyclic materials



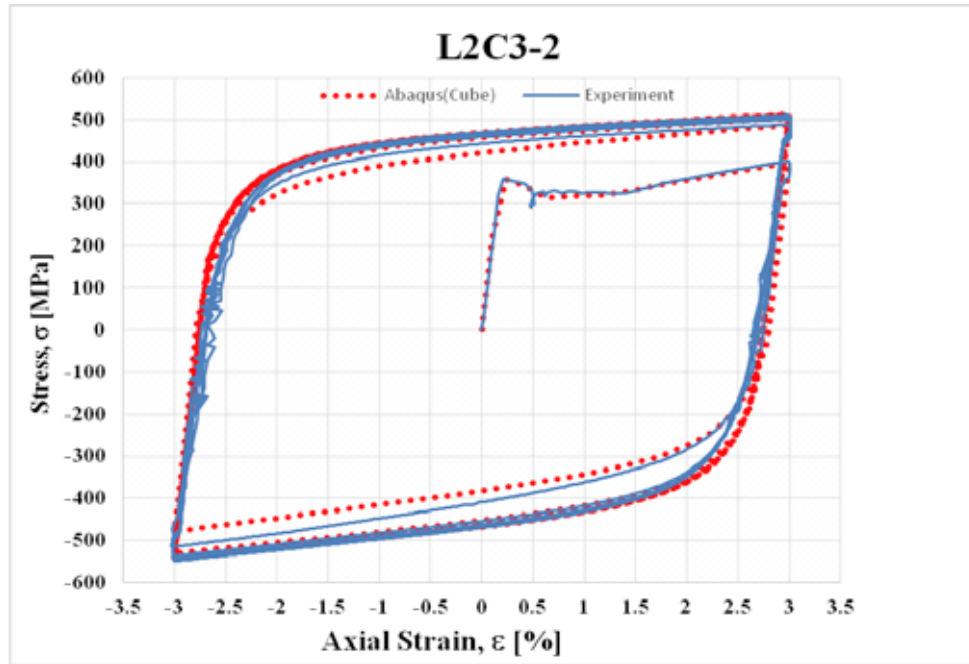


Figure 6. 22: Stress-Strain response comparison of L2C3-2 for the cube

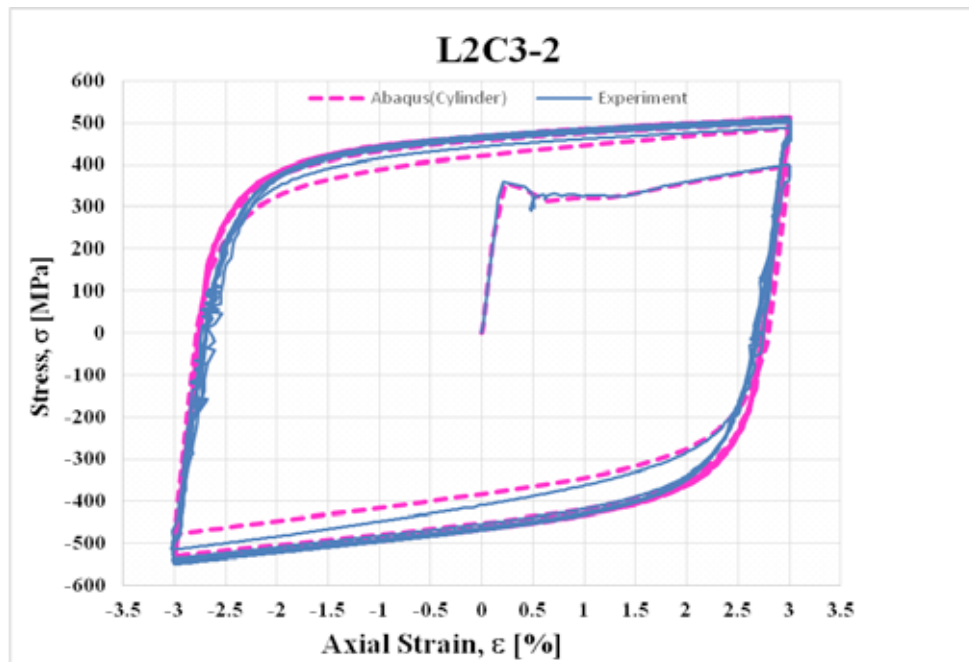


Figure 6. 23: Stress-Strain response comparison of L2C3-2 for the cylinder

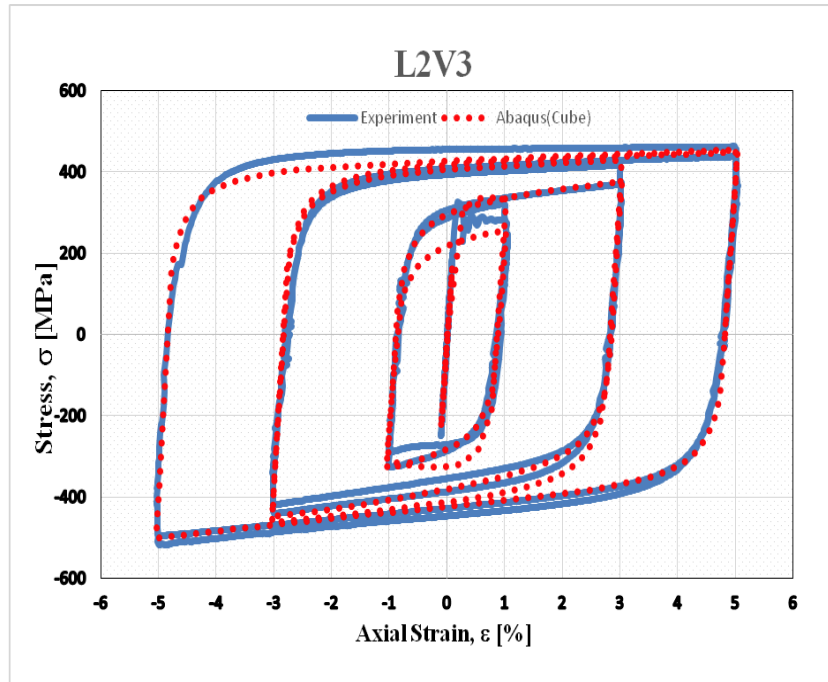


Figure 6. 24: Stress-Strain response comparison of L2V3 for the cube

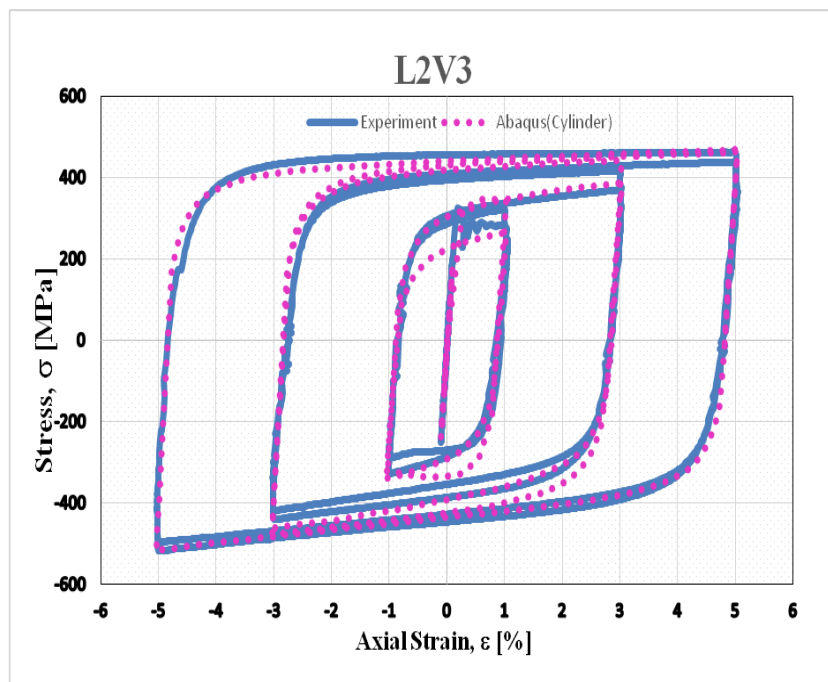


Figure 6. 25: Stress-Strain response comparison of L2V3 for the cylinder

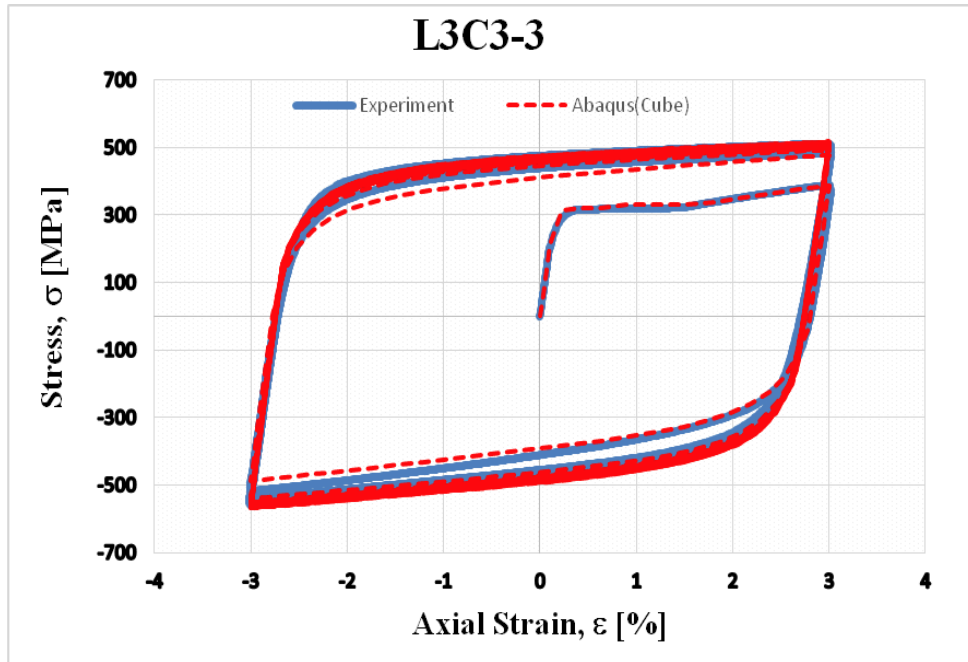


Figure 6. 26: Stress-Strain response comparison of L3C3-3 for the cube

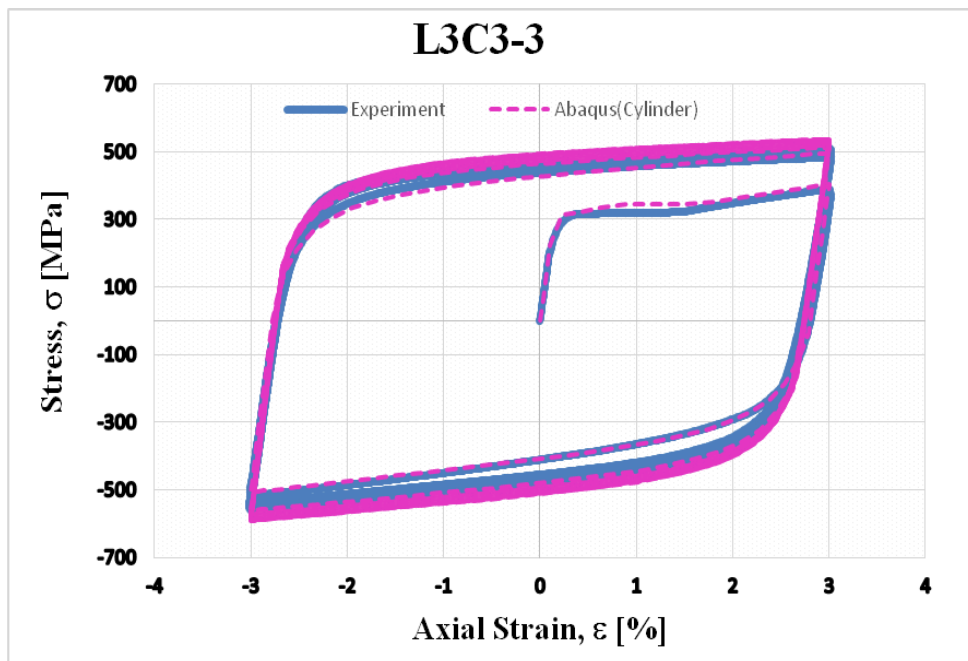


Figure 6. 27: Stress-Strain response comparison of L3C3-3 for the cylinder

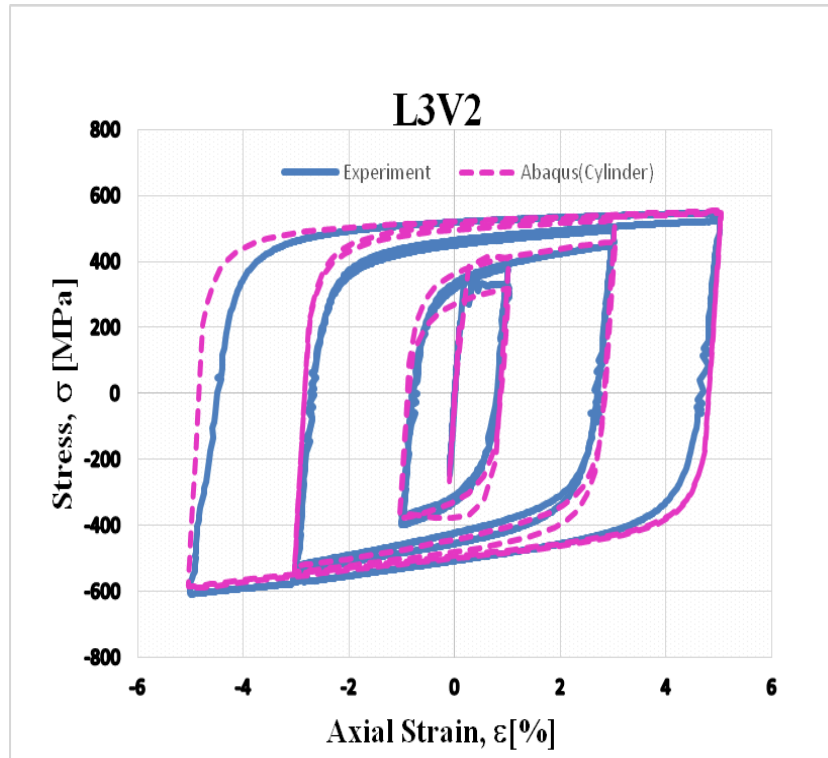


Figure 6. 28: Stress-Strain response comparison of L3V2 for the cylinder

## SECTION 7

### CONCLUSIONS AND COMMENTS

The aim of the study was to experimentally investigate the stress-strain and low cycle fatigue behaviour of four European mild carbon steel grades subjected to repeated cyclic plastic deformations and then to find parameters for material modelling in Abaqus in order to validate the results. Based on the experimental and numerical results, the following conclusions can be drawn:

- 1) For the monotonic tensile tests, the ductility of all the considered steel grades reduced with strength increase.
- 2) For the variable strain amplitude tests, cyclic hardening, which is characterized by stress increase from one cycle to the next, was evident for all the steels except for the high strength steel (S690) for which both cyclic hardening and cyclic softening were evident.
- 3) Also, the highest normalized stress ratio has been recorded for S275 while the lowest for S690. The normalized stress ratio is an indicator of the achieved resistance of the steels.
- 4) For the constant strain amplitude tests, all the steel grades exhibited transient behavior meaning that changes in cyclic deformation behavior were more pronounced at the beginning of each cyclic loading, but the materials gradually stabilized with continued cycling (steady-state).
- 5) A close correlation was observed among all the steel grades considering their cyclic strain hardening exponent.
- 6) For the Charpy Impact tests, all the steel grades satisfied the minimum energy absorption capacity. They exhibited high tensile toughness with good ductility.
- 7) The fatigue strain-life of all the steel grades exhibited nearly similar behavior.



- 8) All the numerical results for the tests modeling on both cube and cylinder revealed close agreement with the experimental results for the selected specimens.
- 9) Compared to the experimental results, more consistent numerical results have been obtained for constant than variable strain amplitude. However, within the strain range corresponding to the data considered to find the parameters for the modeling of variable strain amplitude materials, numerical results were close to the experimental results.
- 10) For the cyclic tests, material calibration is tricky, complex and mostly done by trial and error. Future research work can elaborate simple procedures particularly for selecting the peak tensile stresses, the compressive stresses, and the yield stresses.

### **Acknowledgement**

*The research leading to these results has received funding from the European Community's Research Fund for Coal and Steel (RFCS) under grant agreement no RFSR-CT-2013-00021 "European pre-qualified steel joints (EQUALJOINTS). This support is gratefully acknowledged.*

## SECTION 8

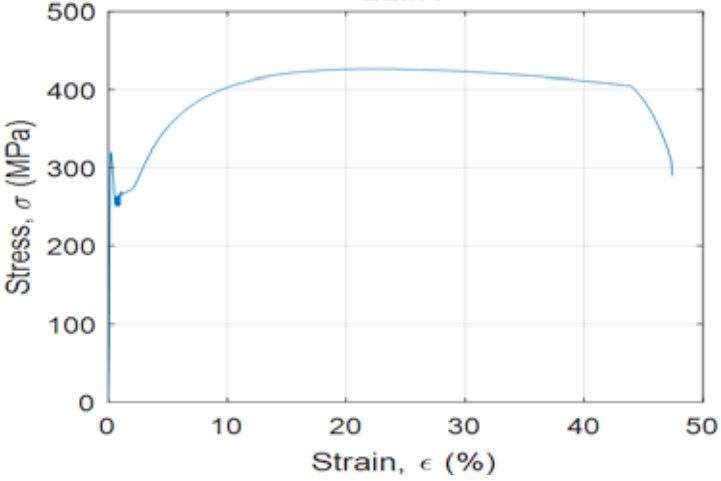

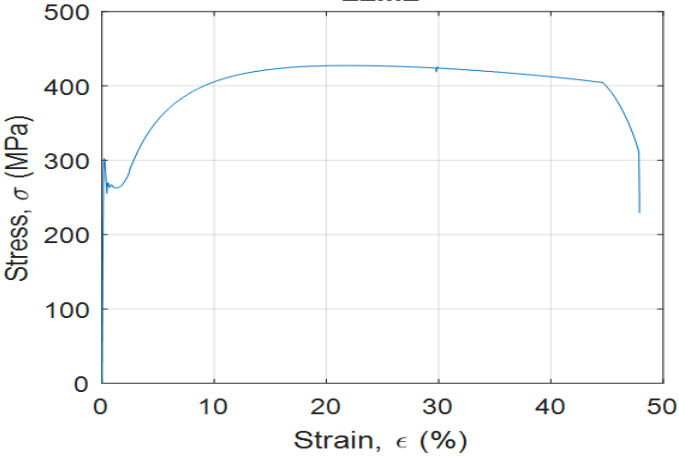

### REFERENCES

- [1] David Hoepfner, W. “Cyclic Loading and Cyclic Stress”. *Encyclopedia of Tribology*, pp .691-698, 2013.
- [2] Richa, A., Rashmi, U. and Pramod, P. “Low Cycle Fatigue Life Prediction”. *International Journal of Emerging Engineering Research and Technology*, Vol. 2 (4), pp. 5-15, 2014.
- [3] Taylor, A. “The Northridge Earthquake: 20 Years Ago Today”. *The Atlantic*. Retrieved 2016-02-18.
- [4] Nastar, N. “Effects of Low-Cycle Fatigue on a Ten-Story Steel Building”. Retrieved 2016-02-18.
- [5] CEN (2004). EN10025. Hot Rolled products of structural steels, Brussels, Belgium.
- [6] BS EN 10025-6: 2004+A1:2009, Hot rolled products of structural steels, Part 6: Technical delivery conditions for flat products of high yield strength structural steels in the quenched and tempered condition, BSI.
- [7] Oliver, H., Georges, A., and Boris, D. “The right choice of steel according to the Eurocode”.
- [8] “Material Selection and Product Specification”. Internet: [http://www.steelconstruction.info/Material\\_selection\\_and\\_product\\_specification#Yield\\_strength](http://www.steelconstruction.info/Material_selection_and_product_specification#Yield_strength).
- [9] Ali Fatemi- University of Toledo; Chapter 5-“Cyclic Deformation & e-N Approach”.
- [10] Saad Abdullah, A.”Cyclic plasticity and creep of power plant materials”. PhD thesis, University of Nottingham, 2012.
- [11] “Stress-Strain Curve”. Internet: [http://en.wikipedia.org/wiki/Stress%E2%80%93strain\\_curve](http://en.wikipedia.org/wiki/Stress%E2%80%93strain_curve), Jan. 8, 2017.
- [12] “Bauschinger Effect”. Internet: [http://en.wikipedia.org/wiki/Bauschinger\\_effect](http://en.wikipedia.org/wiki/Bauschinger_effect), May. 24, 2016.

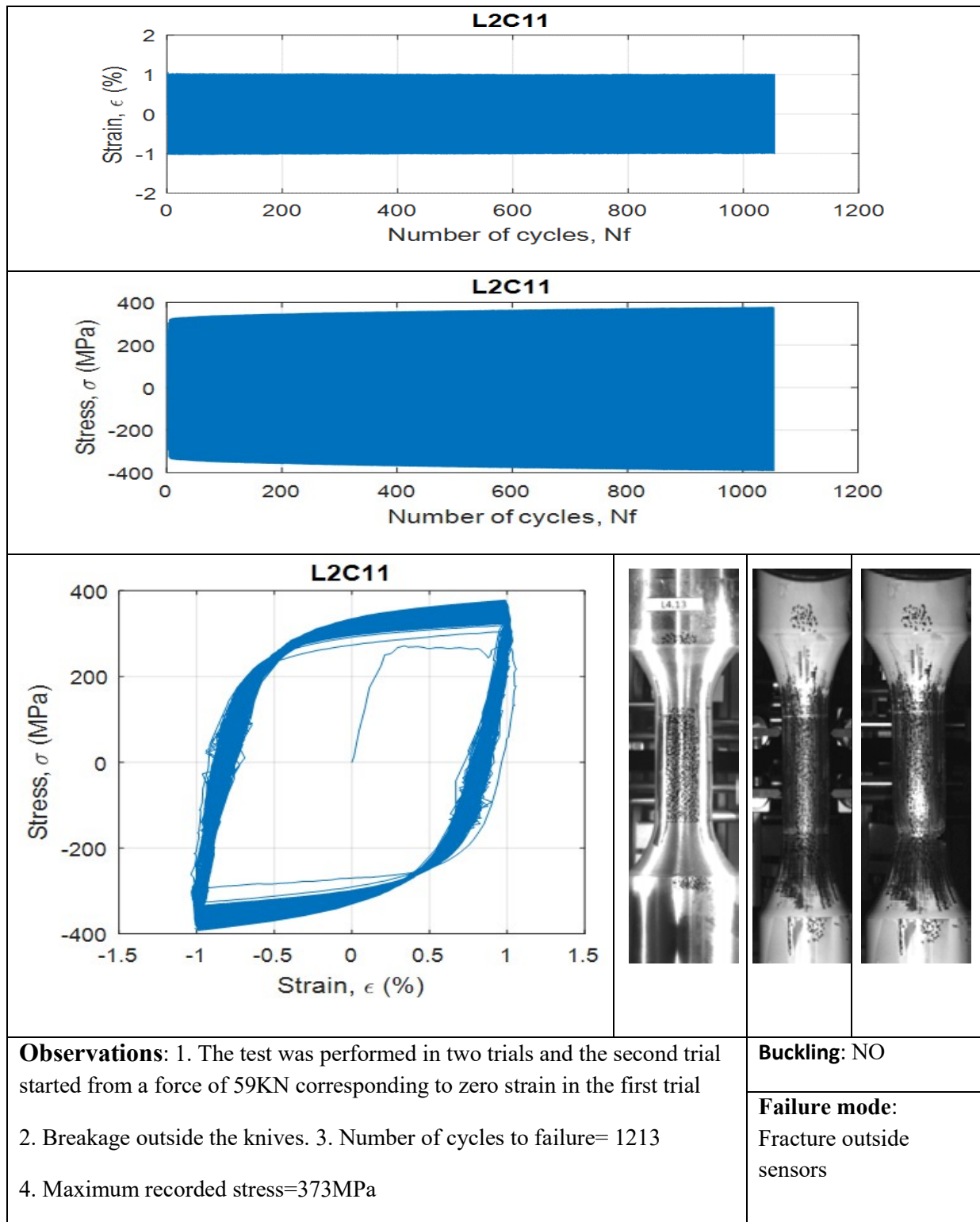
- [13] Tarigopula, V., Hopperstad, O., Langseth, M., and Clausen, H. “An evaluation of a combined isotropic-kinematic hardening model for representation of complex strain-path changes in dual-phase steel”. *European Journal of Mechanics - A/Solids*, Vol. 28 (4), pp. 792–805, Jul. – Aug. 2009.
- [14] David, L., and Lallit, A. “A large deformation theory for rate-dependent elastic–plastic materials with combined isotropic and kinematic hardening”. *International Journal of Plasticity*, Vol. 25, pp. 1833–1878, 2009.
- [15] Ramberg, W., and Osgood, W. R. “Description of stress–strain curves by three parameters”. *Technical Note No. 902*, National Advisory Committee For Aeronautics, Washington DC, 1943.
- [16] Peter, D., Ahmad Itani, M., Ian Buckle, G. “Cyclic response and low cycle fatigue characteristics of plate steels”. *Technical Report MCEER-06-0013*, Nov. 1, 2006.
- [17] Abílio de Jesus, M.P., Rui, M., Bruno Fontoura, F.C., Carlos, R., Luis da Silva, S., and Milan, V. “A comparison of the fatigue behavior between S355 and S690 steel grades”. *Journal of Constructional Steel Research*, Vol. 79, pp. 140–150, 2012.
- [18] “EN Standards Steel”. Internet: <http://www.simplexmetal.com/sheets-plates-types-industrial-sheet-plate/EN-Standards-Steel-Plates.htm>.
- [19] “Structural Steels: Chemical Composition, Mechanical Properties and Common Applications”. Internet: <http://www.azom.com/article.aspx?ArticleID=8067#4>.
- [20] Roessle, M.L. and Fatemi, A. (2000). “Strain-controlled fatigue properties of steels and some simple approximations”. *International Journal of Fatigue*, Vol. 22, pp. 495–511.
- [21] NKS-150. “A Procedure to Generate Input Data of Cyclic Softening and Hardening for FEM Analysis from Constant Strain Amplitude Fatigue Tests in LCF Regime”. *Electronic Report*. ISBN 978-87-7893-213-6, 2007.
- [22] Abaqus documentation version 6.6. Models for metals subjected to cyclic loading. <http://50.16.225.63/v2016/books/usb/default.htm?startat=pt05ch23s02abm18.html>

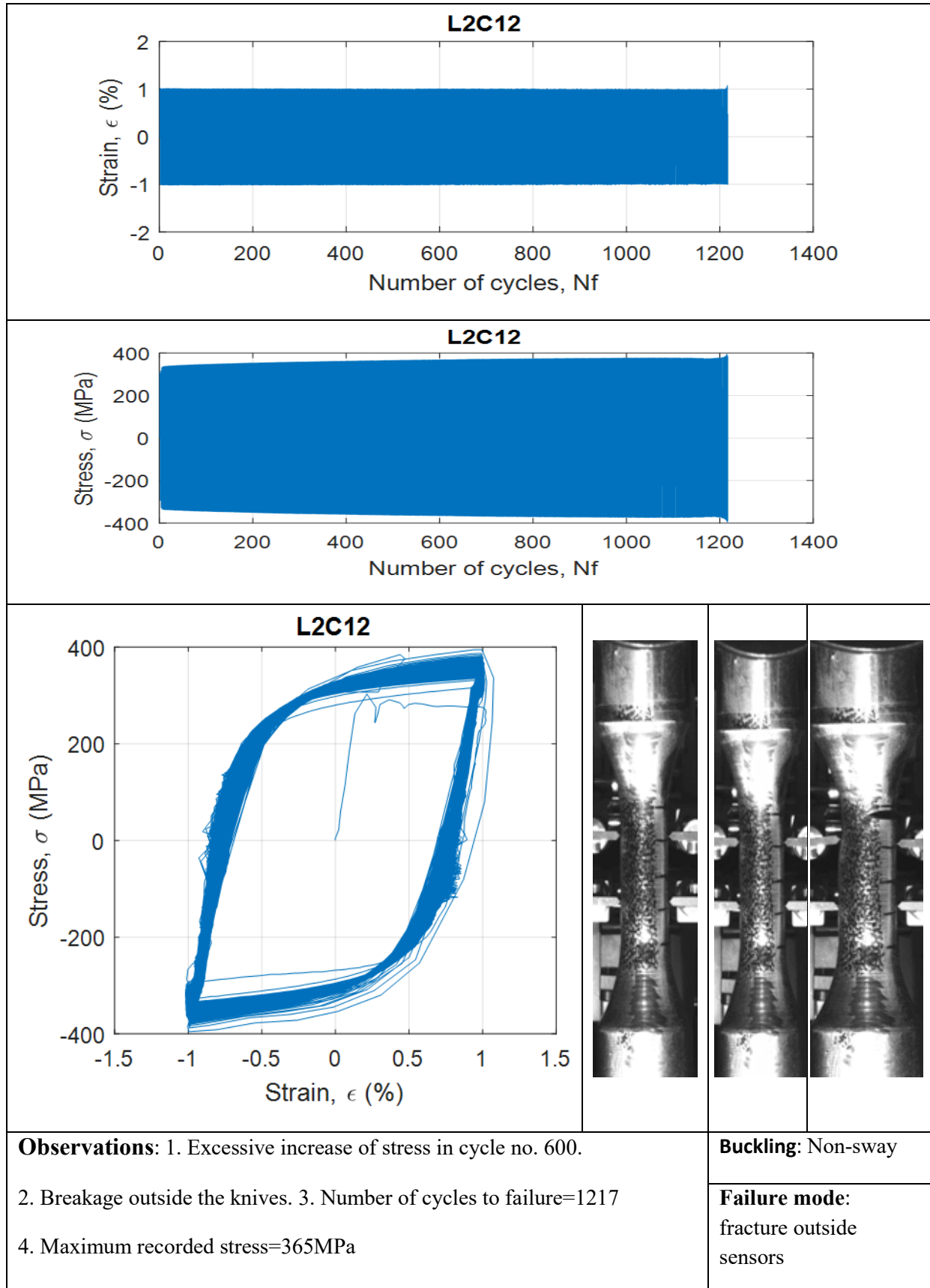
# APPENDIX

## 1. Results from monotonic tensile tests for S275

<p style="text-align: center;"><b>L2M1</b></p> 		
<p><b>Observations:</b> 1. Car paint exfoliation at 25% strain amplitude 2. Largest strain amplitude recorded=47% 3. Maximum recorded stress=426MPa</p>		<p><b>Buckling:</b> N/A</p> <p><b>Failure mode:</b> Fracture between sensors</p>
<p style="text-align: center;"><b>L2M2</b></p> 		
<p><b>Observations:</b> 1. Breakage between sensors 2. Largest strain amplitude recorded=48% 3. Maximum recorded stress=427MPa</p>		<p><b>Buckling:</b> N/A</p> <p><b>Failure mode:</b> Fracture between sensors</p>

## 2. Results from constant strain amplitude tests for S275





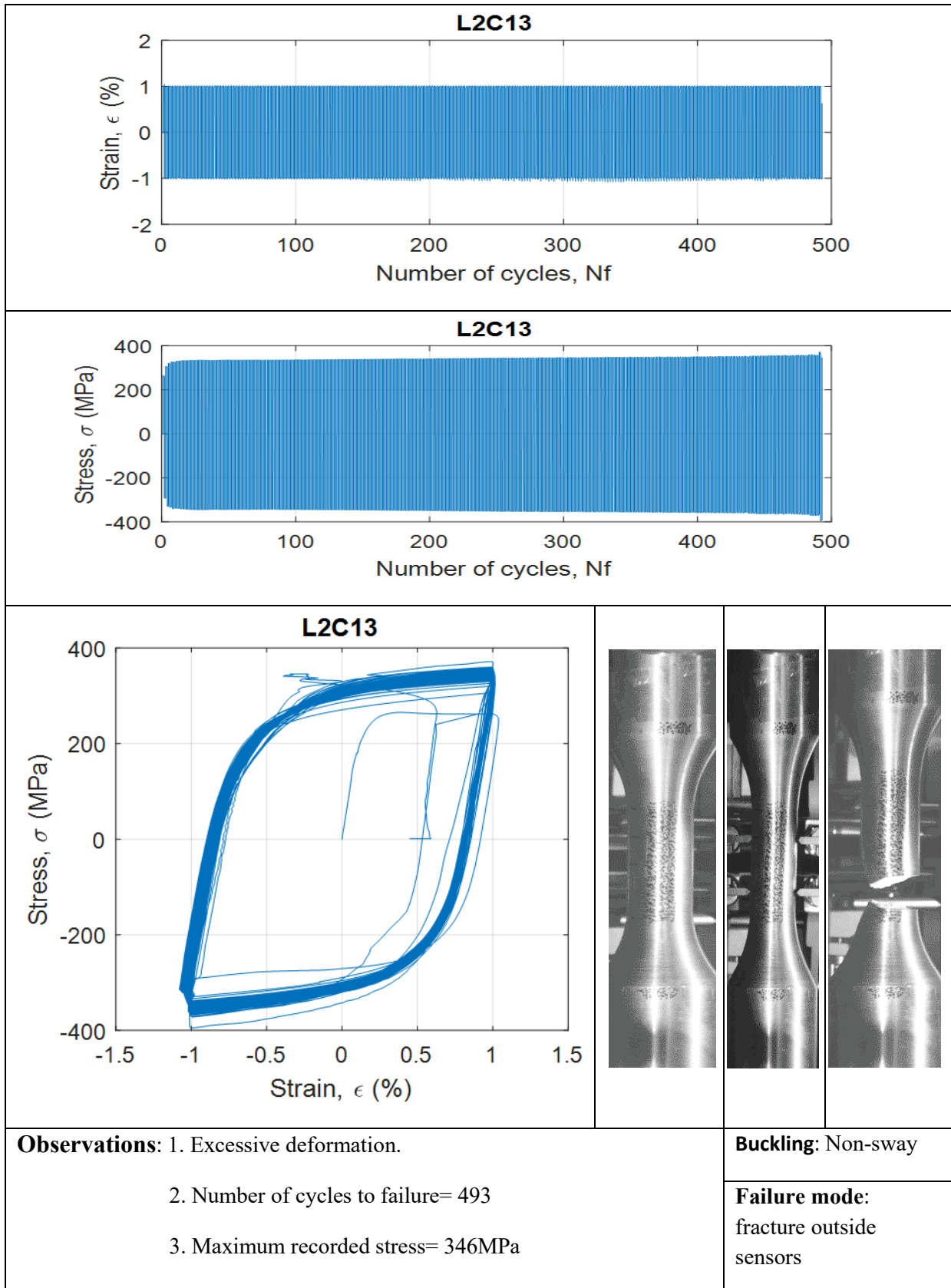
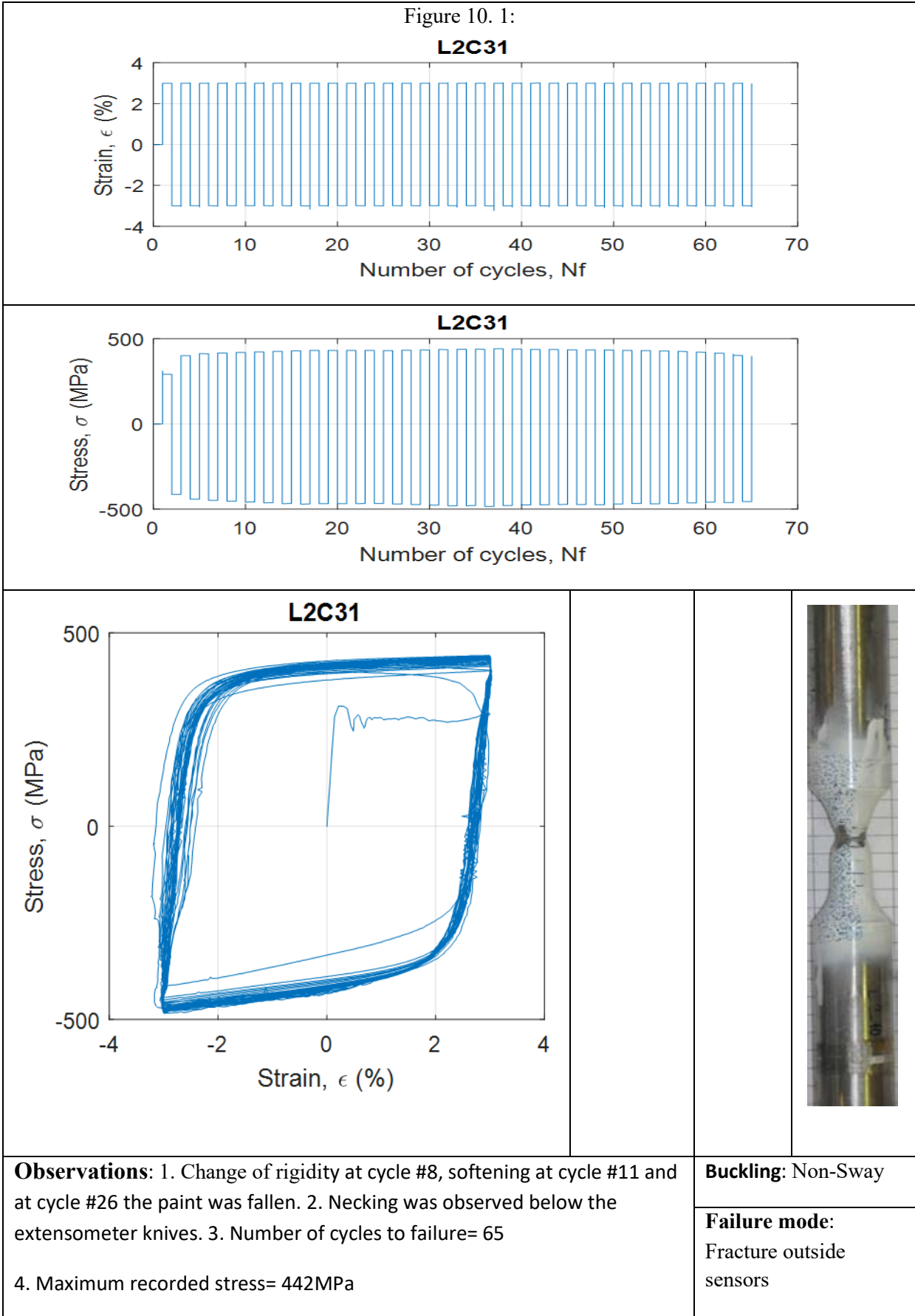
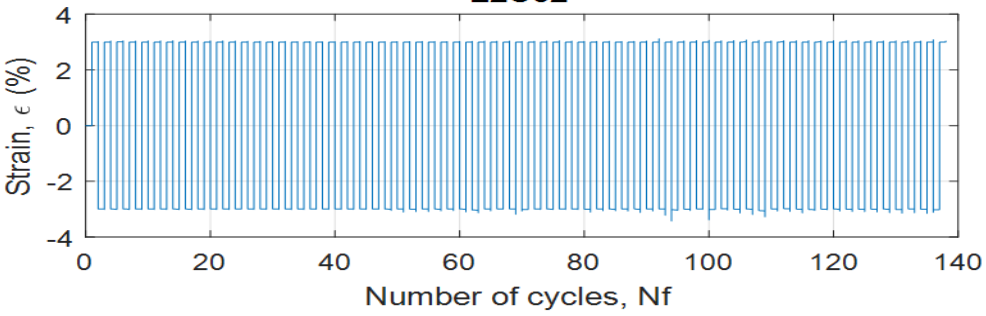
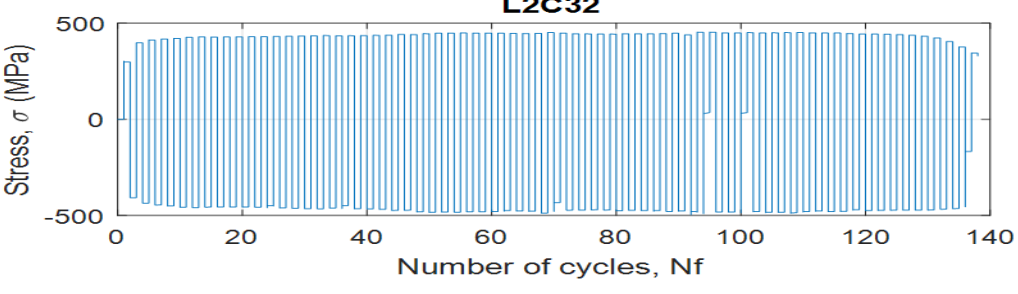
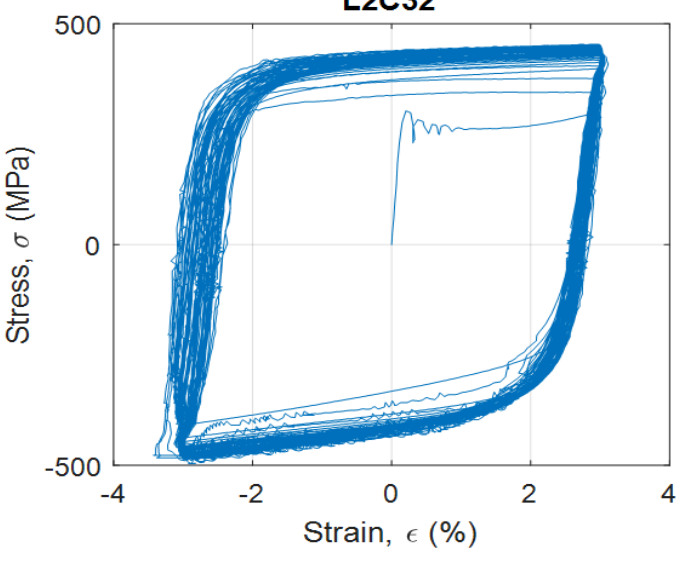

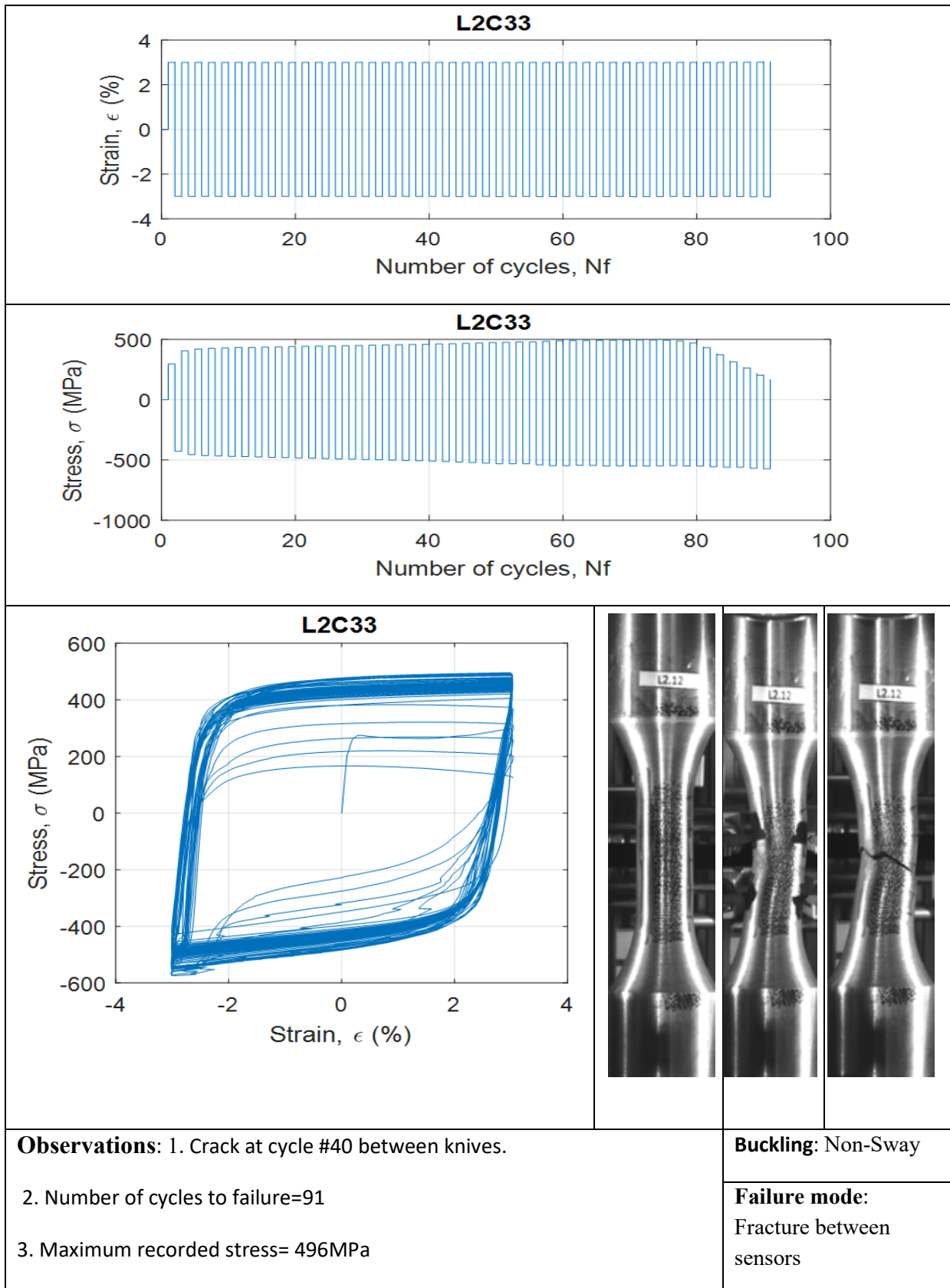


Figure 10. 1:

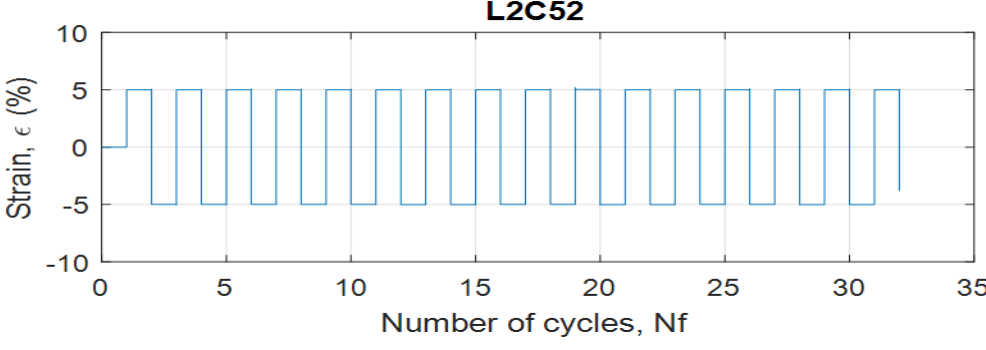
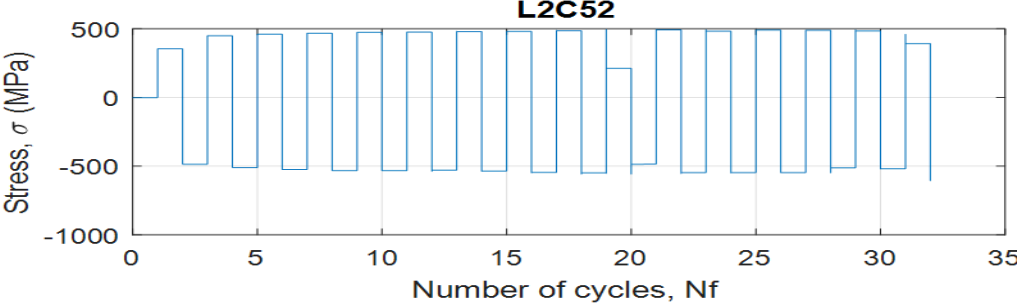
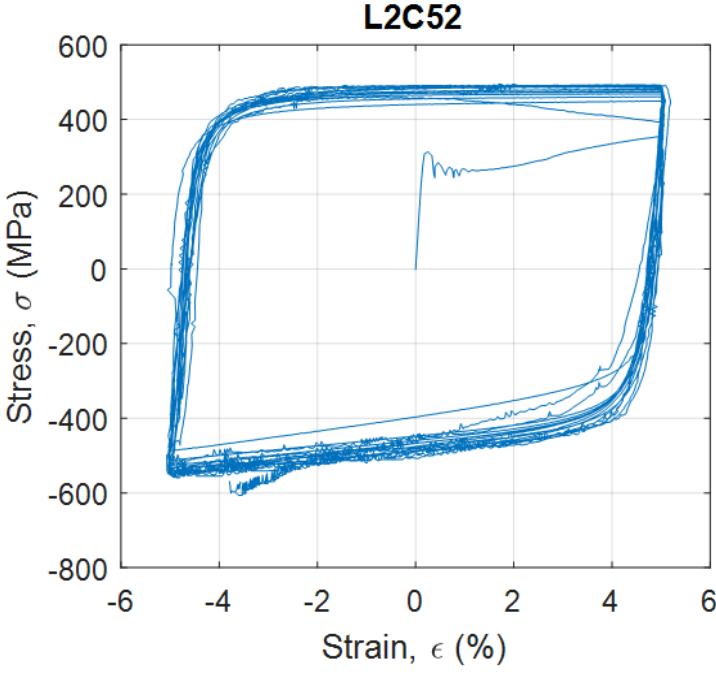



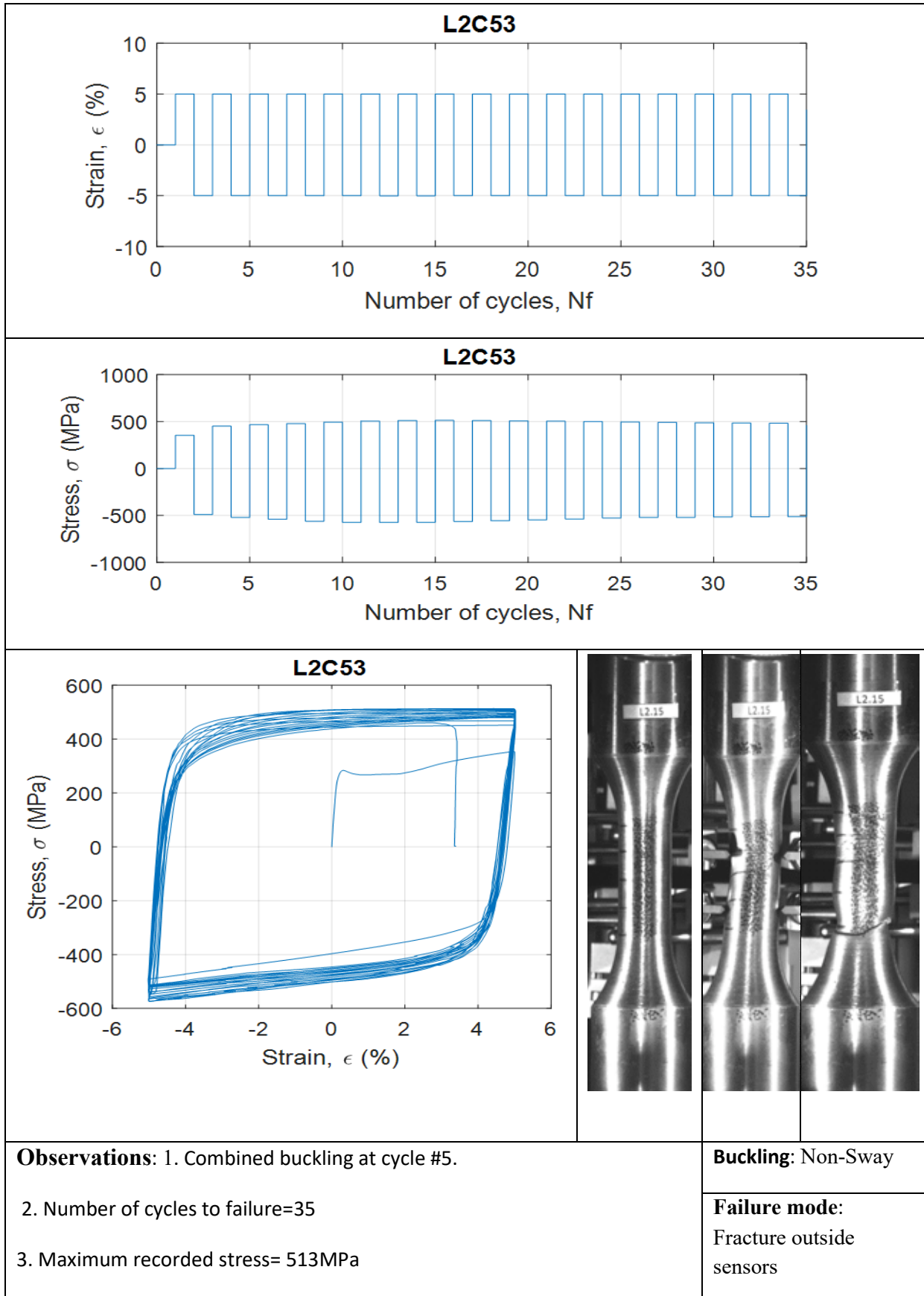


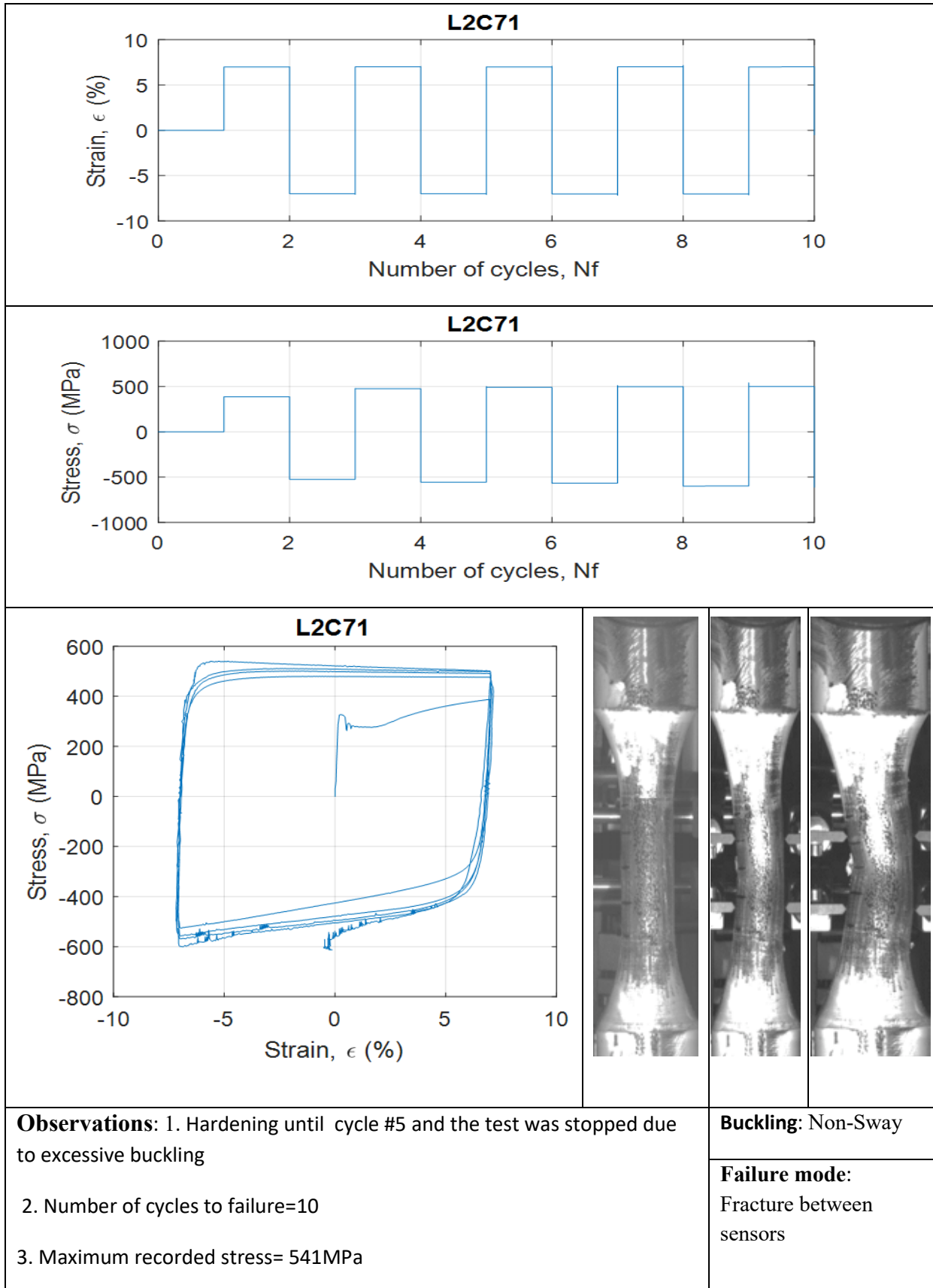
			
			
			
<p><b>Observations:</b> 1. Hardening for the first 6 cycles. 2. At cycle #26, visible buckling. 3. At cycles #58 and #68, cracks and breakage respectively.</p> <p>4. Number of cycles to failure=138</p> <p>5. Maximum recorded stress= 454MPa</p>		<p><b>Buckling:</b> Non-Sway</p> <p><b>Failure mode:</b> Fracture between sensors</p>	



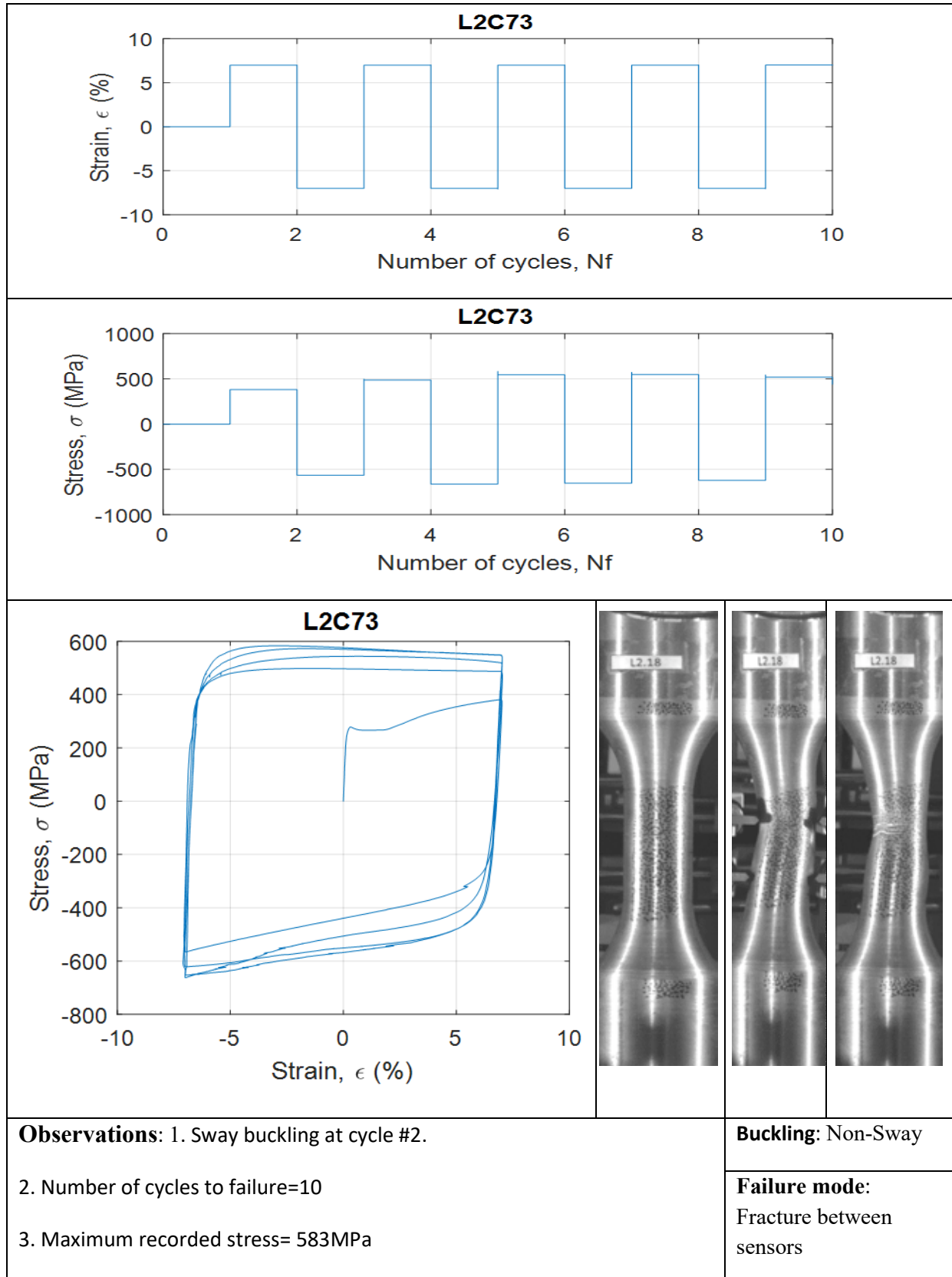
<p><b>Observations:</b> 1. At cycles #7, #12 and #16, buckling initiation, paint exfoliation and crack initiation respectively.</p> <p>2. Excessive deformation</p> <p>3. Number of cycles to failure=36</p> <p>4. Maximum recorded stress= 490MPa</p>	
	<p><b>Buckling:</b> Non-Sway</p> <p><b>Failure mode:</b> Fracture between sensors</p>

			
			
			
<p><b>Observations:</b> 1. Hardening for the 1<sup>st</sup> 6 cycles and crack at cycle #14 between knives. 2. Visible necking at cycle #16.</p> <p>3. Number of cycles to failure=32</p> <p>4. Maximum recorded stress= 495MPa</p>			
		<p><b>Buckling:</b> Non-Sway</p> <p><b>Failure mode:</b> NO</p>	



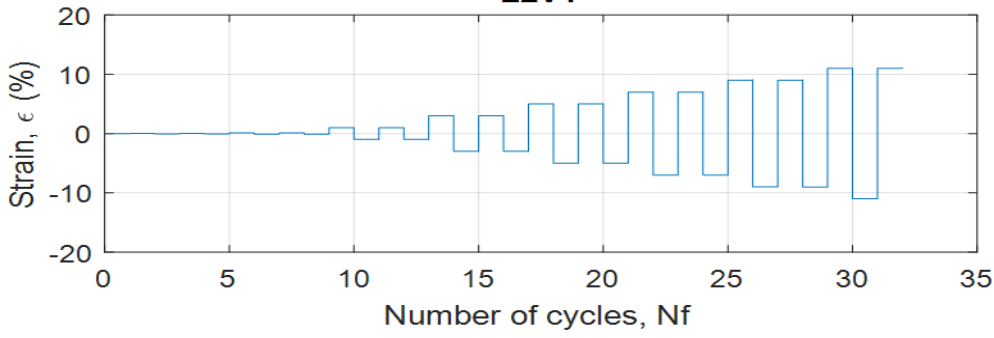
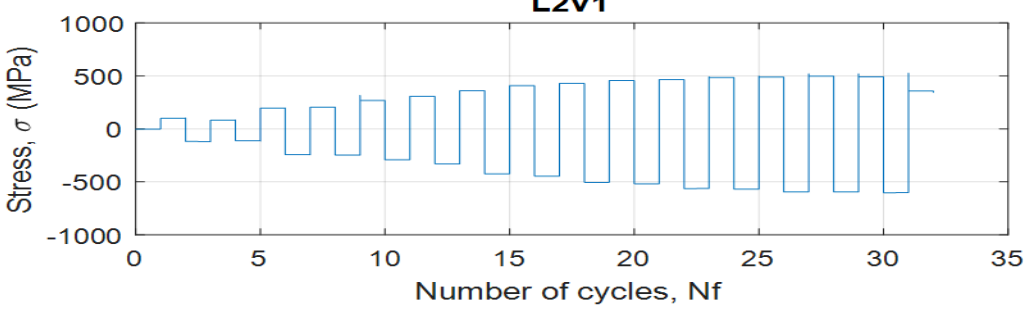
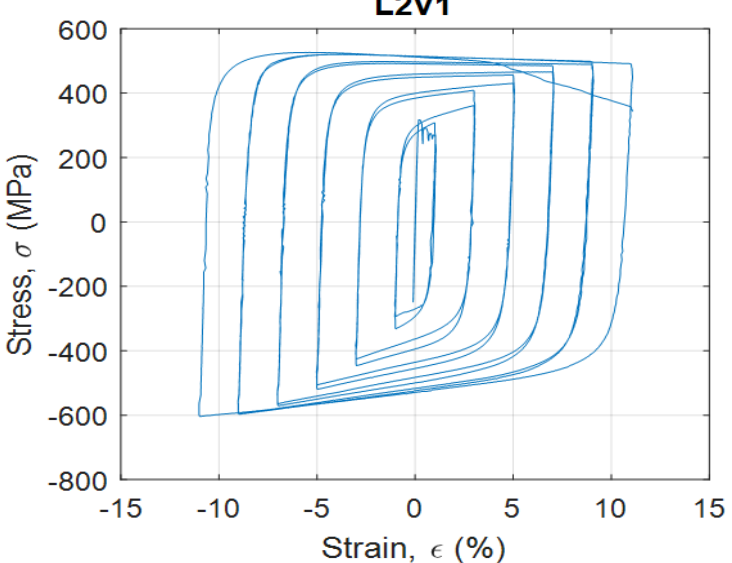



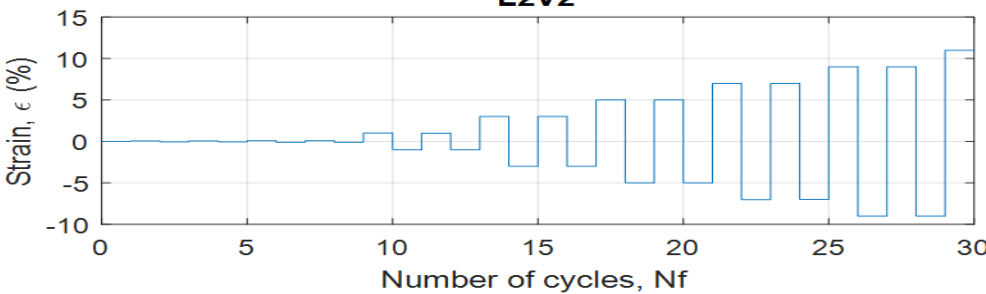
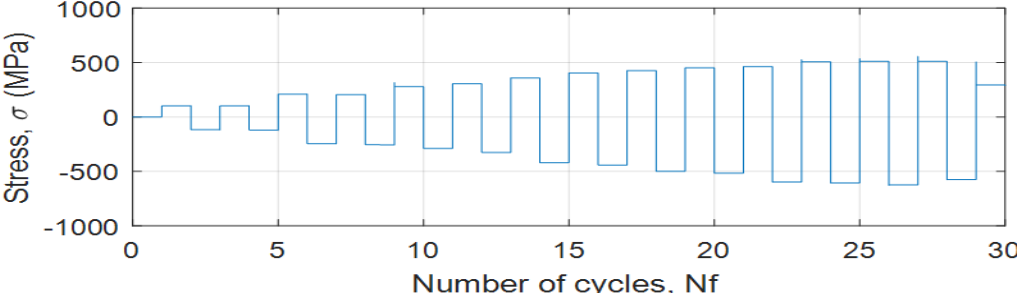
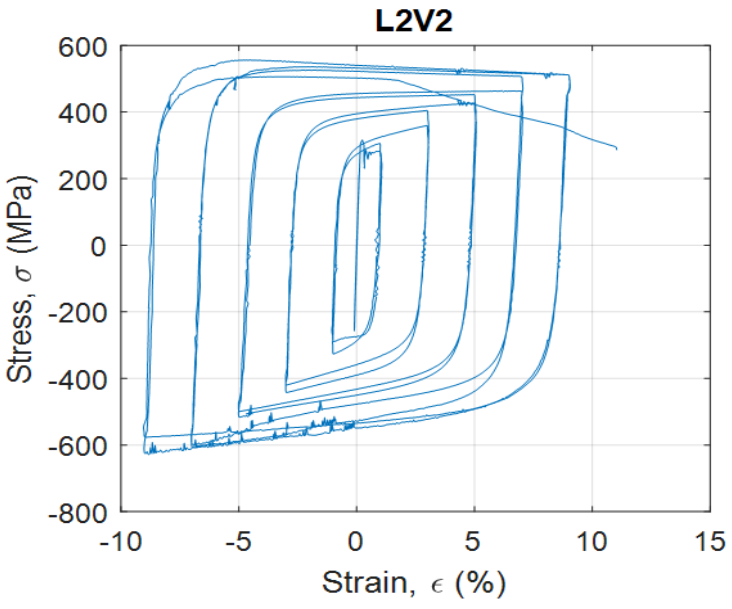

<p><b>Observations:</b> 1. Notched at the chamfer radius.                  2. Crack appearance at cycle #5 between knives                  3. Number of cycles to failure=15                  4. Maximum recorded stress= 512MPa</p>		<p><b>Buckling:</b> NO</p> <p><b>Failure mode:</b>                  Fracture between sensors</p>

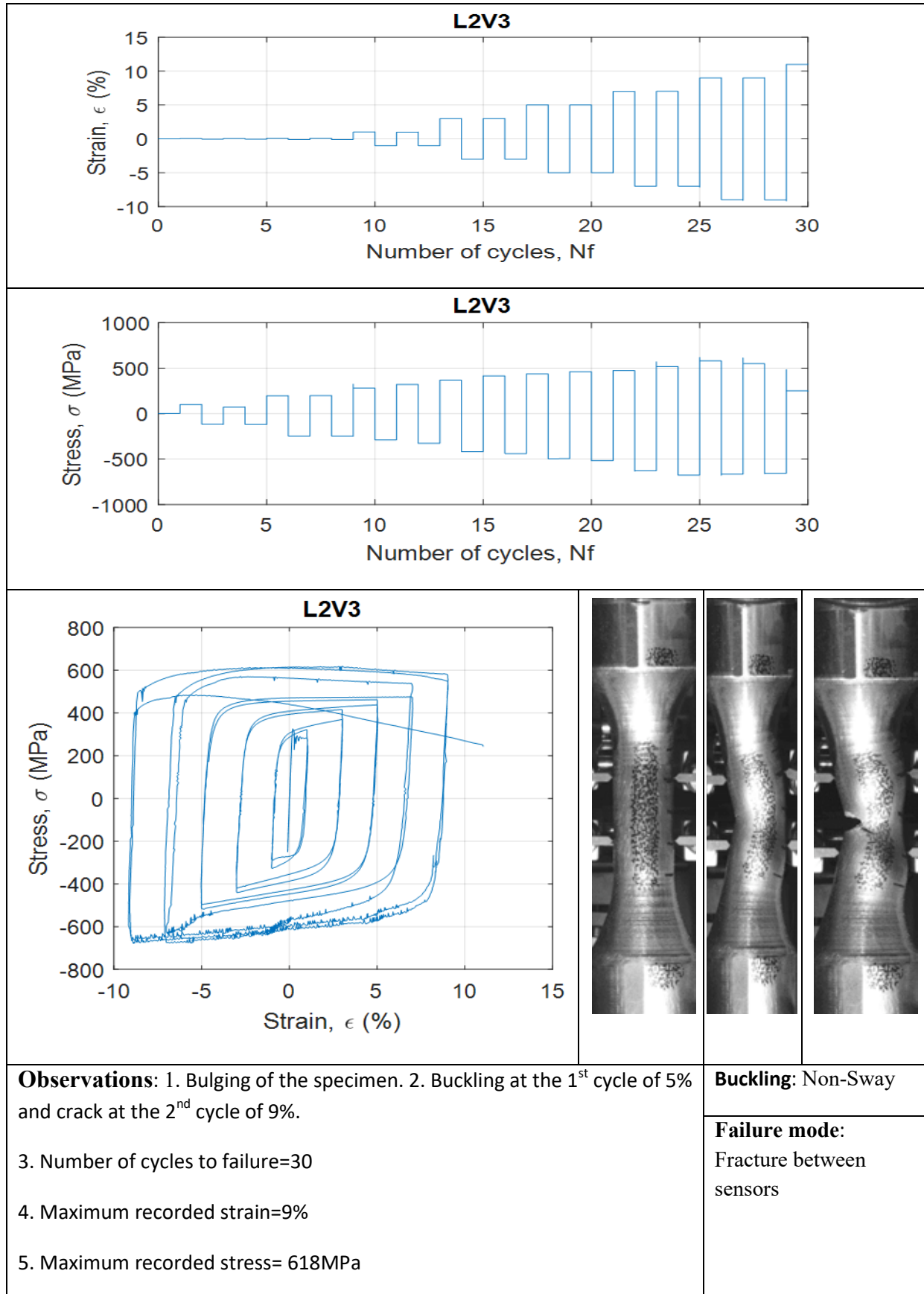




### 3. Results from variable strain amplitude tests for S275

			
			
			
<p><b>Observations:</b> 1. At cycle #9, car paint exfoliation and rotation of the knives. 2. Breakage between knives at the 2<sup>nd</sup> cycle of 11%.</p> <p>3. Number of cycles to failure=32</p> <p>4. Maximum recorded strain=11%</p> <p>5. Maximum recorded stress= 526MPa</p>		<p><b>Buckling:</b> NO</p> <p><b>Failure mode:</b> Fracture between sensors</p>	

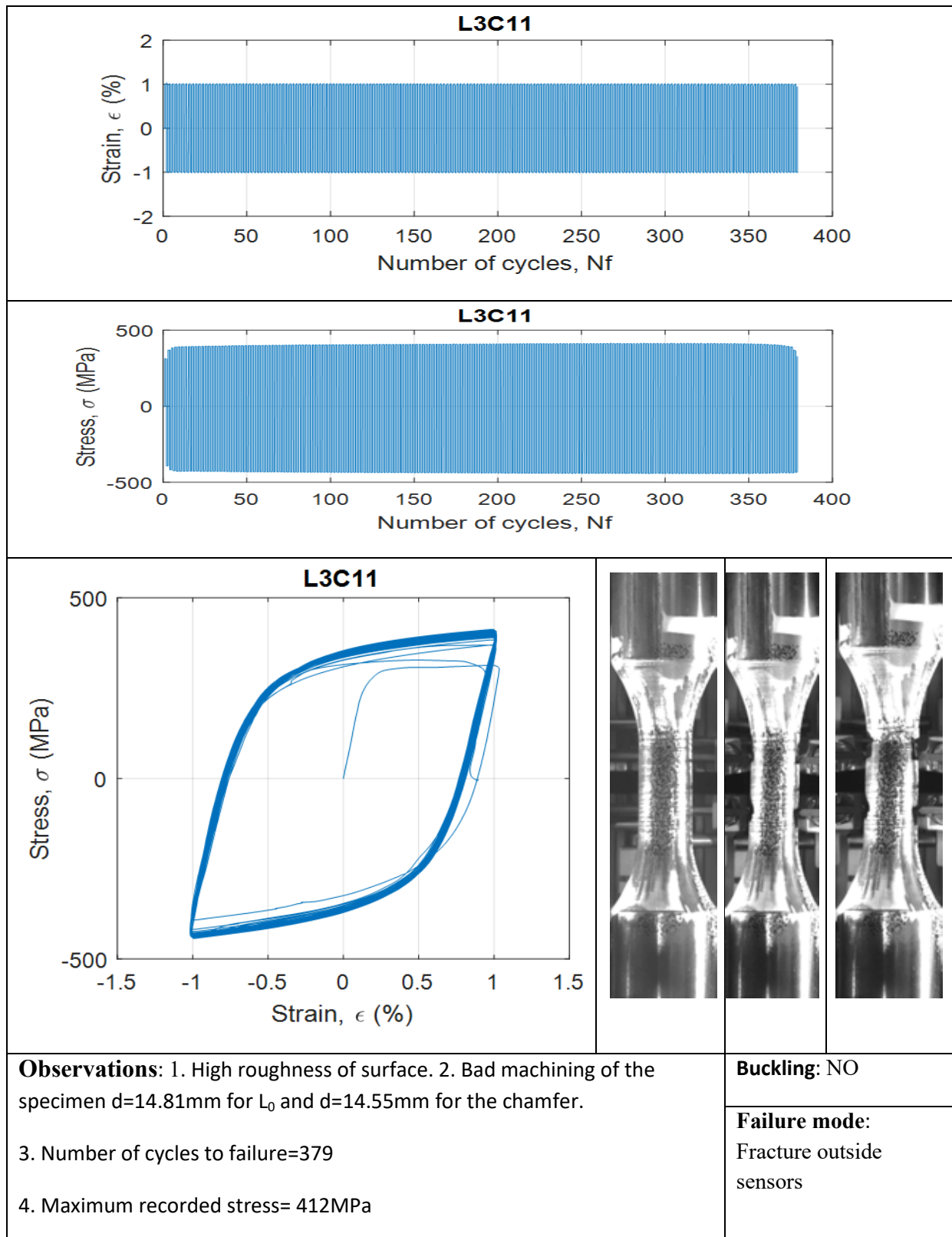
			
			
			
<p><b>Observations:</b></p> <ol style="list-style-type: none"> <li>At 1<sup>st</sup> cycle of 7%, necking between knives.</li> <li>At 1<sup>st</sup> cycle of 9%, crack appearance</li> <li>Number of cycles to failure=30</li> <li>Maximum recorded strain=9%</li> <li>Maximum recorded stress= 556MPa</li> </ol>		<p><b>Buckling:</b> Non-Sway</p> <p><b>Failure mode:</b> Fracture between sensors</p>	
			



### 4. Results from monotonic tensile tests for S355

<p style="text-align: center;"><b>L3M1</b></p>		
<p><b>Observations:</b> 1. Primer for wood                  2. Largest strain amplitude recorded=39%                  3. Maximum recorded stress= 522MPa</p>		<p><b>Buckling:</b> N/A  <b>Failure mode:</b>                  Fracture between sensors</p>
<p style="text-align: center;"><b>L3M2</b></p>		
<p><b>Observations:</b> 1. VIC recording failed                  2. Largest strain amplitude recorded=39%                  3. Maximum recorded stress=526MPa</p>		<p><b>Buckling:</b> N/A  <b>Failure mode:</b>                  Fracture between sensors</p>

### 5. Results from constant strain amplitude tests for S355

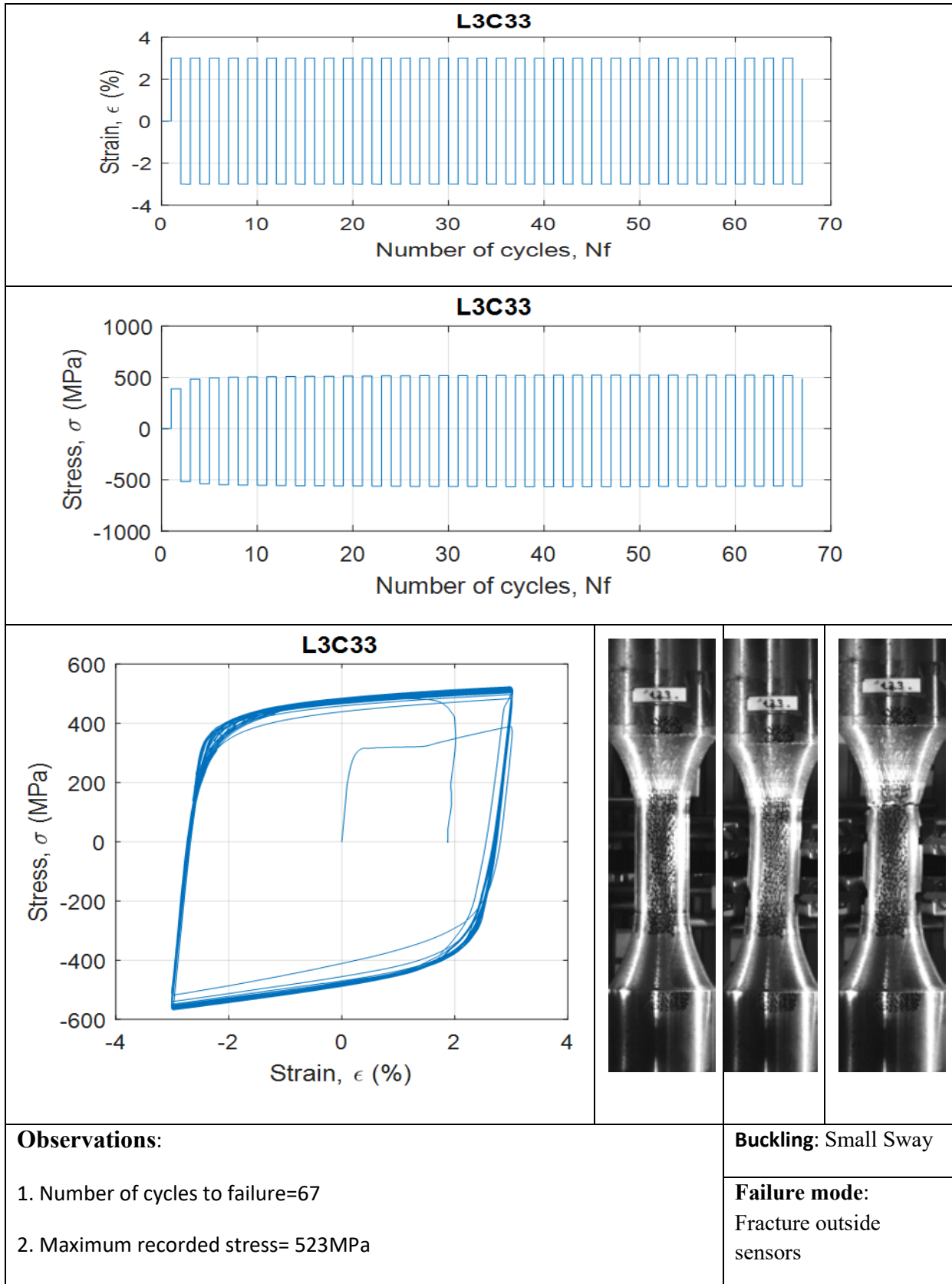


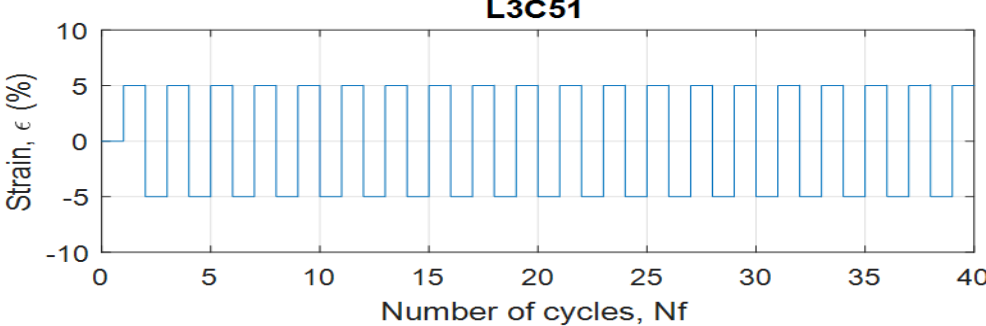
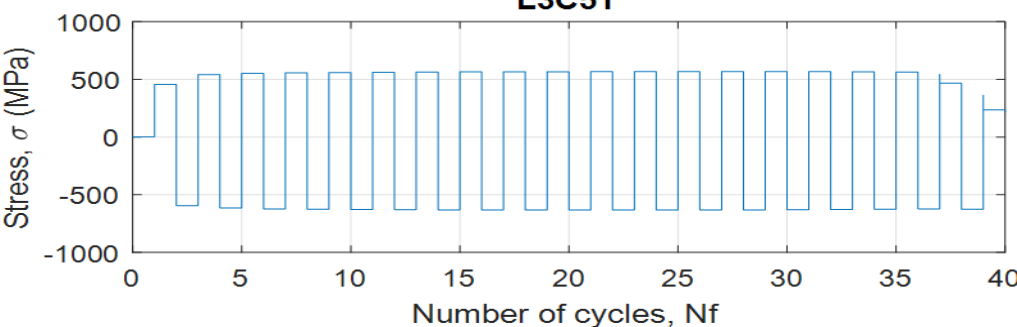
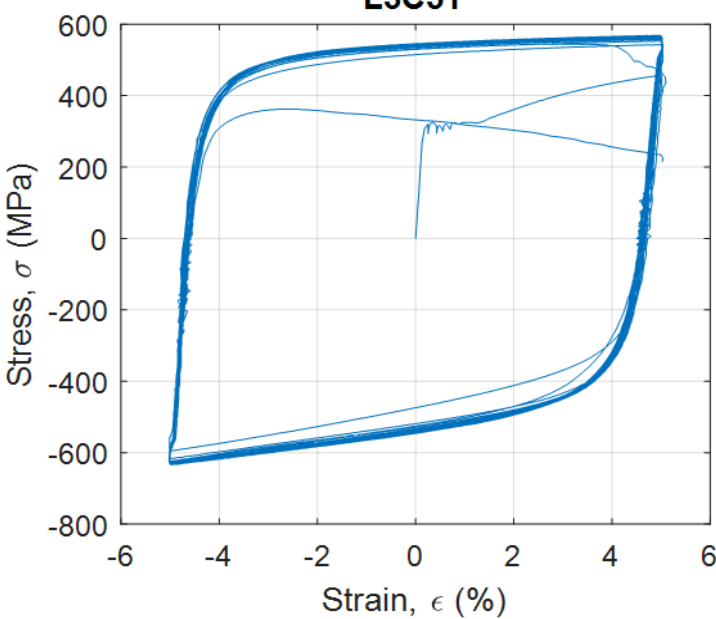

<p><b>Observations:</b> 1. At cycle #426, crack initiation.</p> <p>2. Number of cycles to failure=925</p> <p>3. Maximum recorded stress= 413MPa</p>		<p><b>Buckling:</b> NO</p> <p><b>Failure mode:</b> Fracture outside sensors</p>

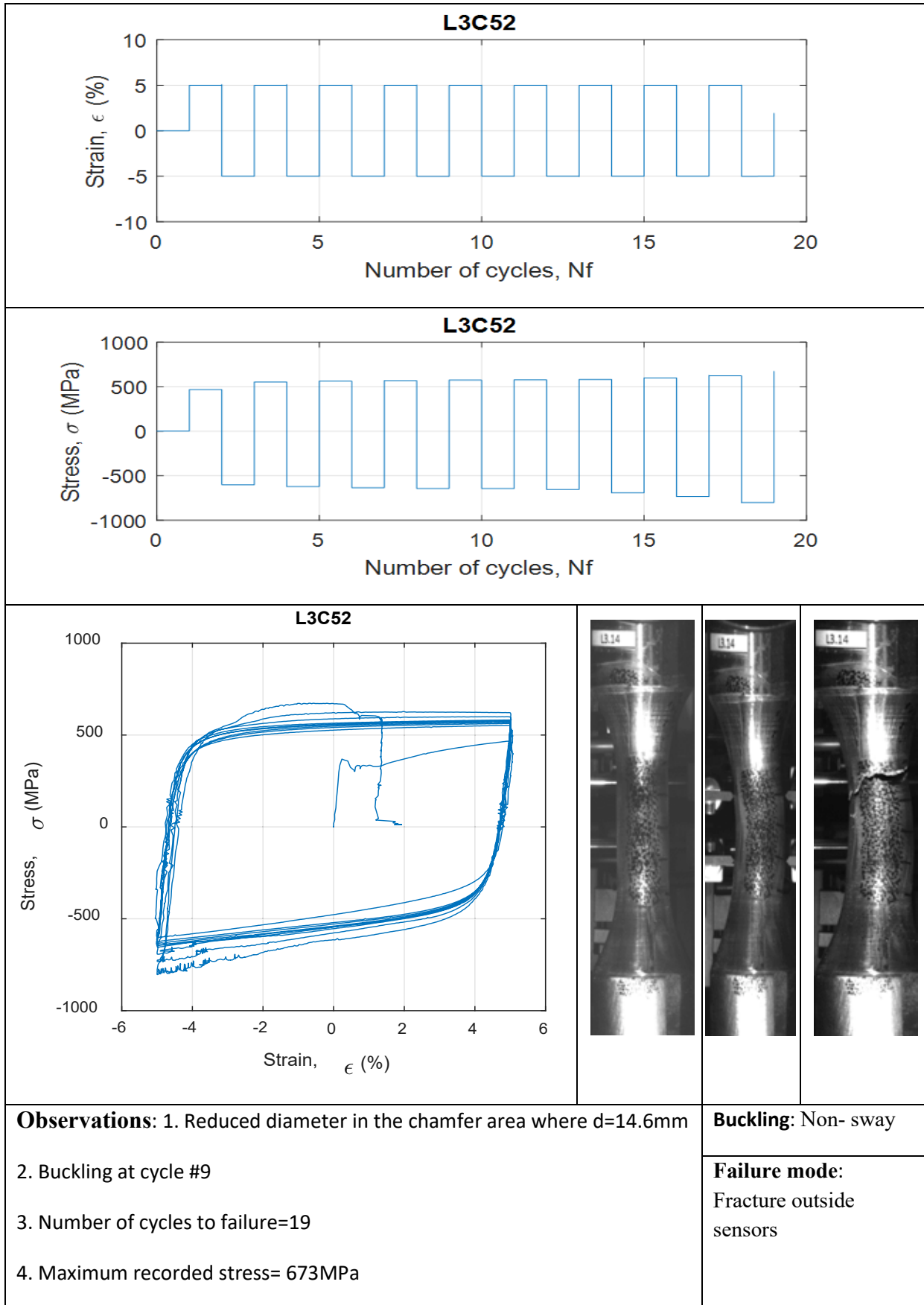
<p><b>Observations:</b> 1. Primer for wood and at cycle #54 the primer cracks.                  2. Sequential failure                  3. Number of cycles to failure=142                  4. Maximum recorded stress= 413MPa</p>		<p><b>Buckling:</b> NO</p> <p><b>Failure mode:</b>                  Fracture between sensors</p>

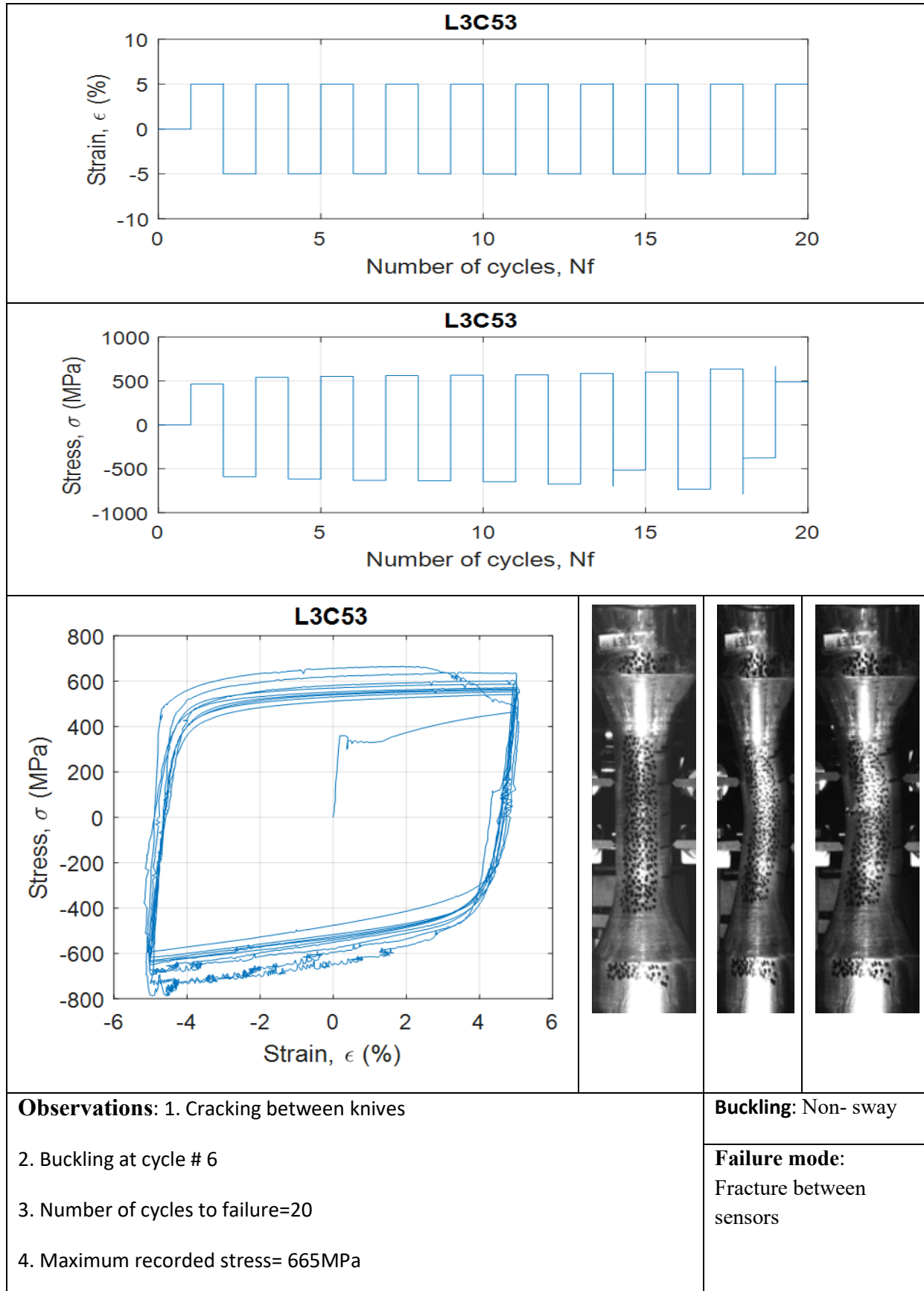
<p><b>Observations:</b> 1. Reduced diameter for the chamfer area for which <math>d=14.57\text{mm}</math>.</p> <p>2. Crack outside the knives</p> <p>3. Number of cycles to failure=99</p> <p>4. Maximum recorded stress= 533MPa</p>		<p><b>Buckling:</b> NO</p> <p><b>Failure mode:</b> Fracture outside sensors</p>



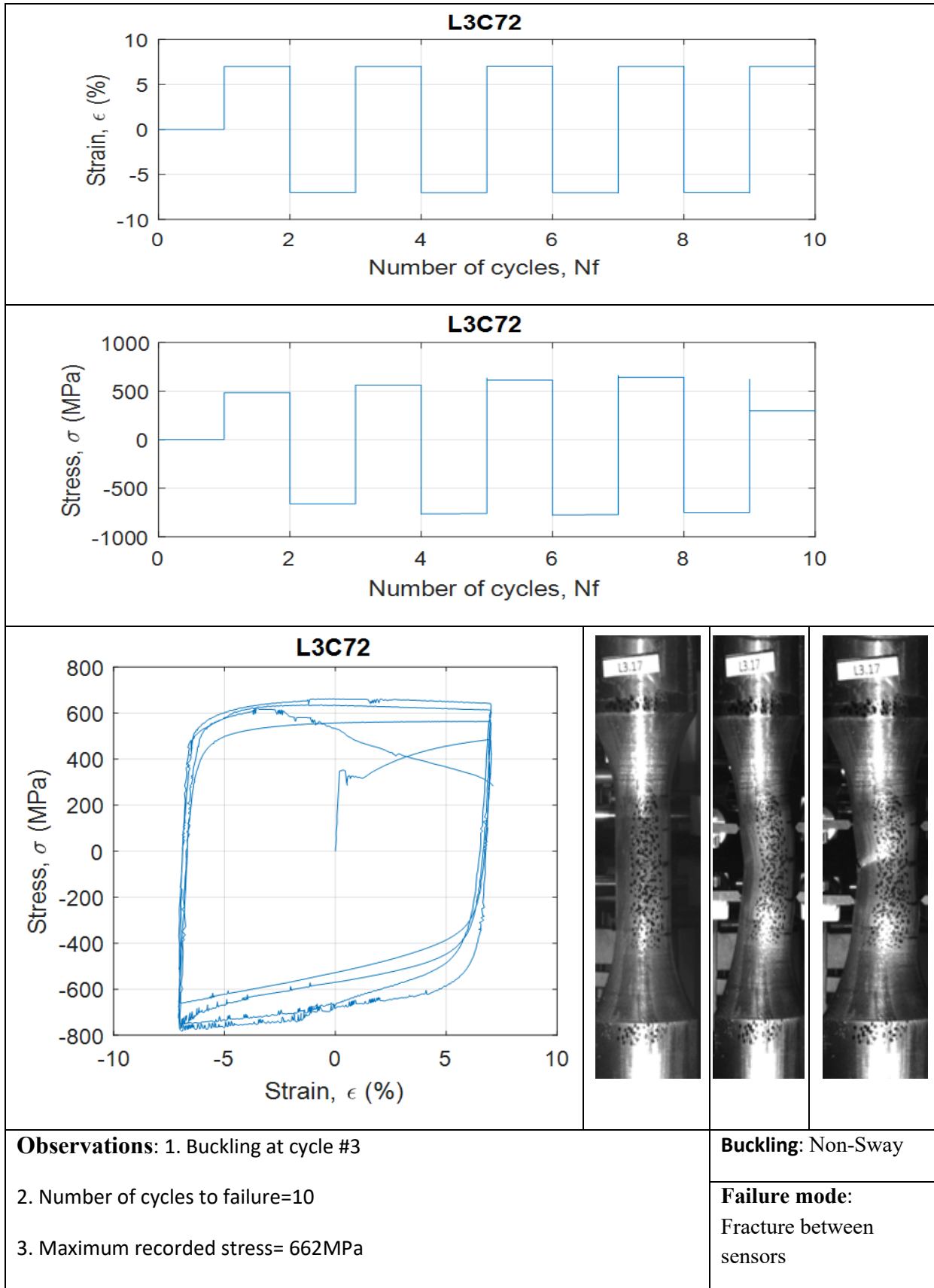


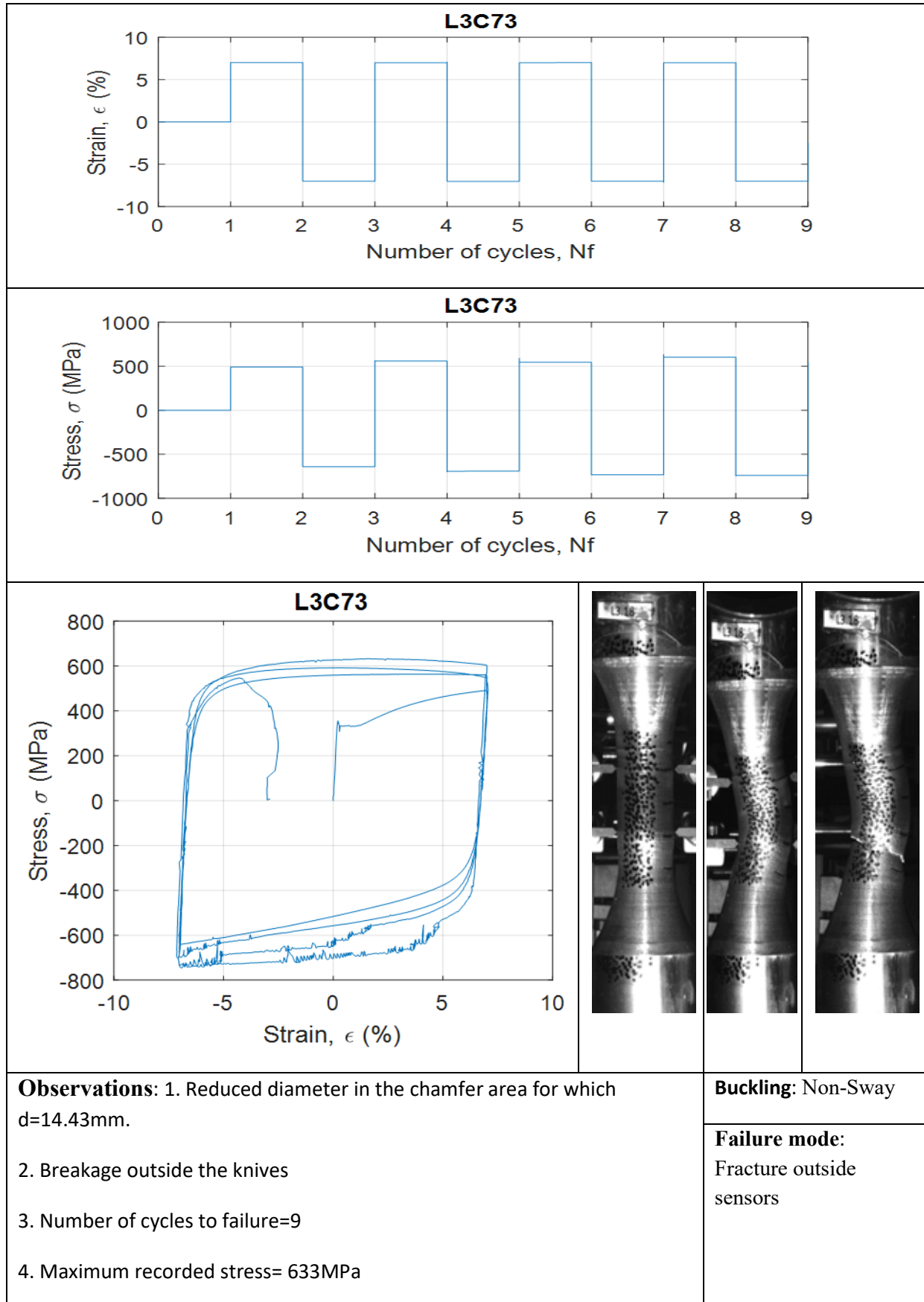
			
			
			
<p><b>Observations:</b> 1. Wood primer</p> <p>2. Number of cycles to failure=40</p> <p>3. Maximum recorded stress= 569MPa</p>		<p><b>Buckling:</b> Non- sway</p> <p><b>Failure mode:</b> Fracture between sensors</p>	



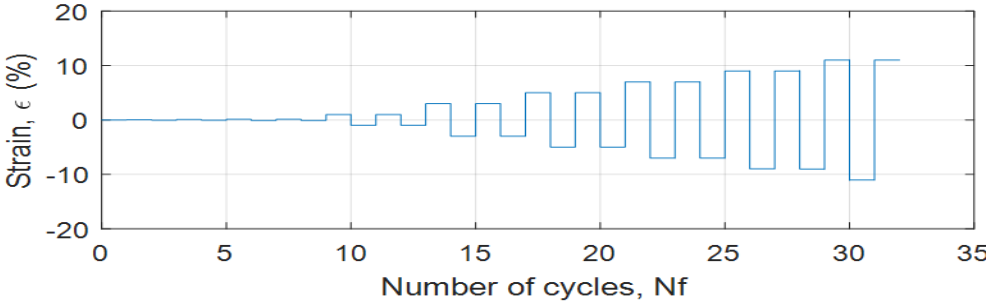
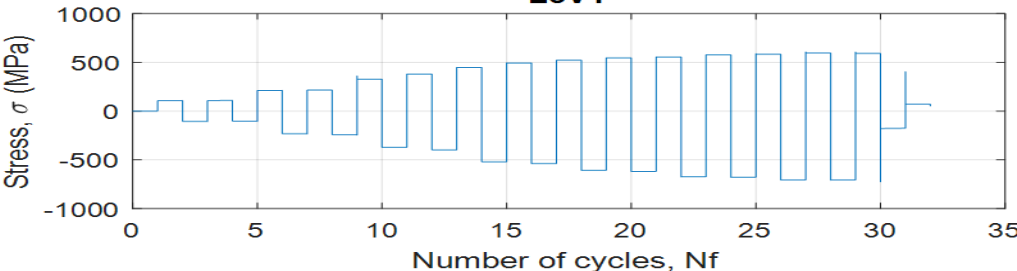
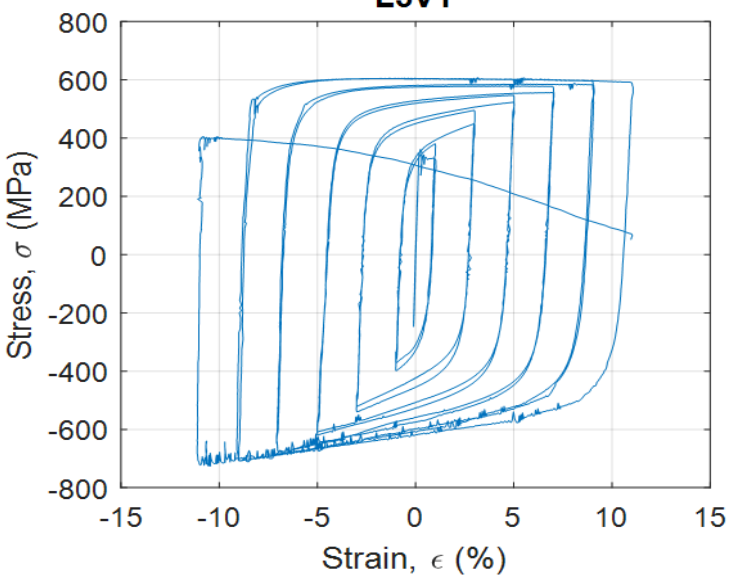



<p><b>Observations:</b> 1. Wood prime. 2. For the 2<sup>nd</sup> -7% cycle, the curve shows an additional stress.</p> <p>3. At the 4<sup>th</sup> cycle, buckling outside the testing machine plan</p> <p>4. Number of cycles to failure=14</p> <p>5. Maximum recorded stress= 631MPa</p>	<p><b>Buckling:</b> Small Sway</p> <p><b>Failure mode:</b> Fracture near sensors</p>

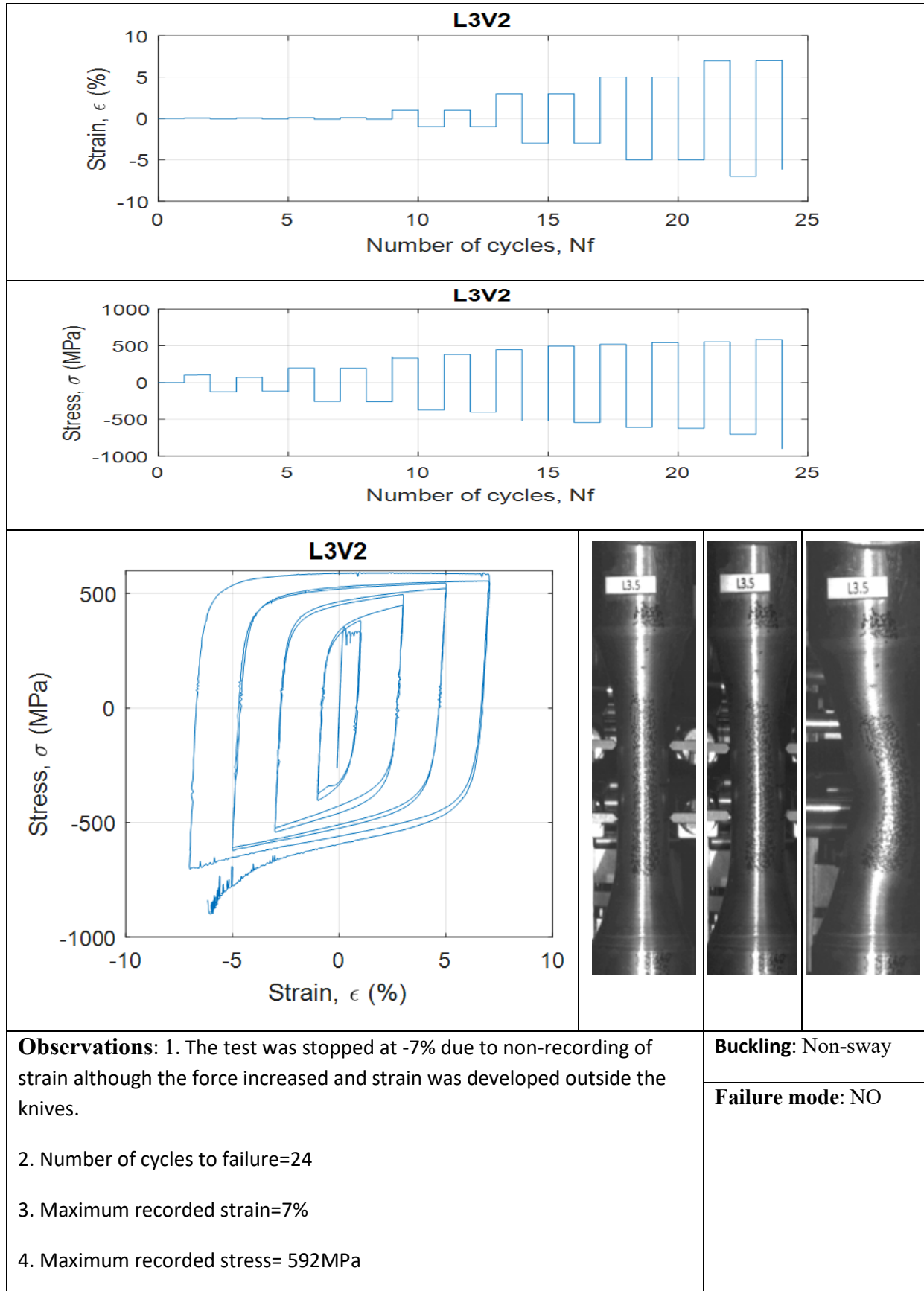




### 6. Results from variable strain amplitude tests for S355

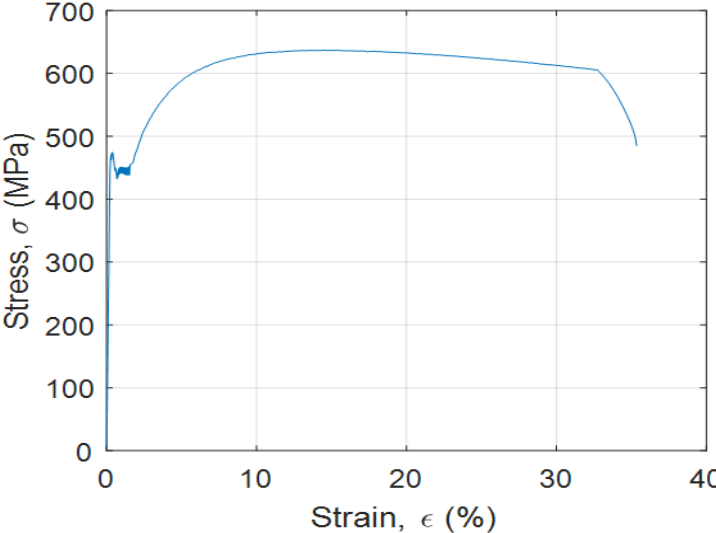
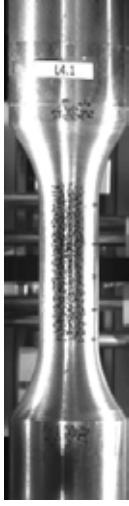
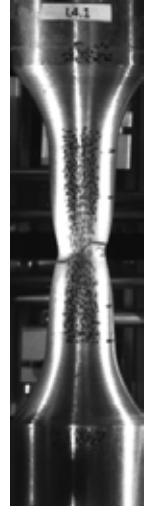
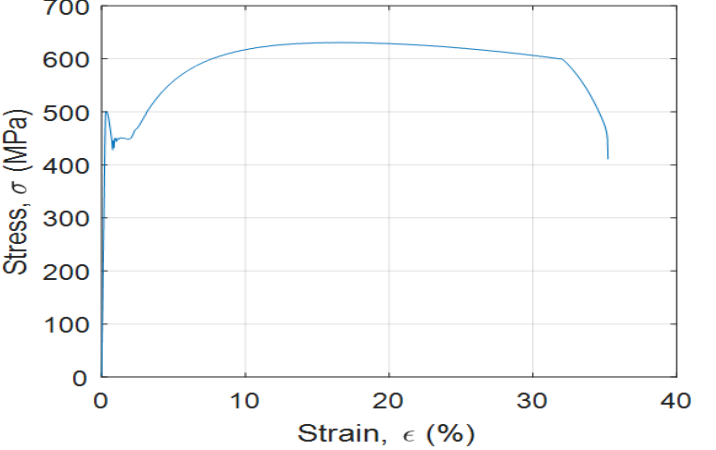

		
		
		
<p><b>Observations:</b> 1. Wood primer. 2. Buckling at 7% and rotation of knives.</p> <p>3. Crack appearance at -11%</p> <p>4. Number of cycles to failure=32</p> <p>5. Maximum recorded strain=11%</p> <p>6. Maximum recorded stress= 607MPa</p>		<p><b>Buckling:</b> Non-Sway</p> <p><b>Failure mode:</b> Fracture between sensors</p>



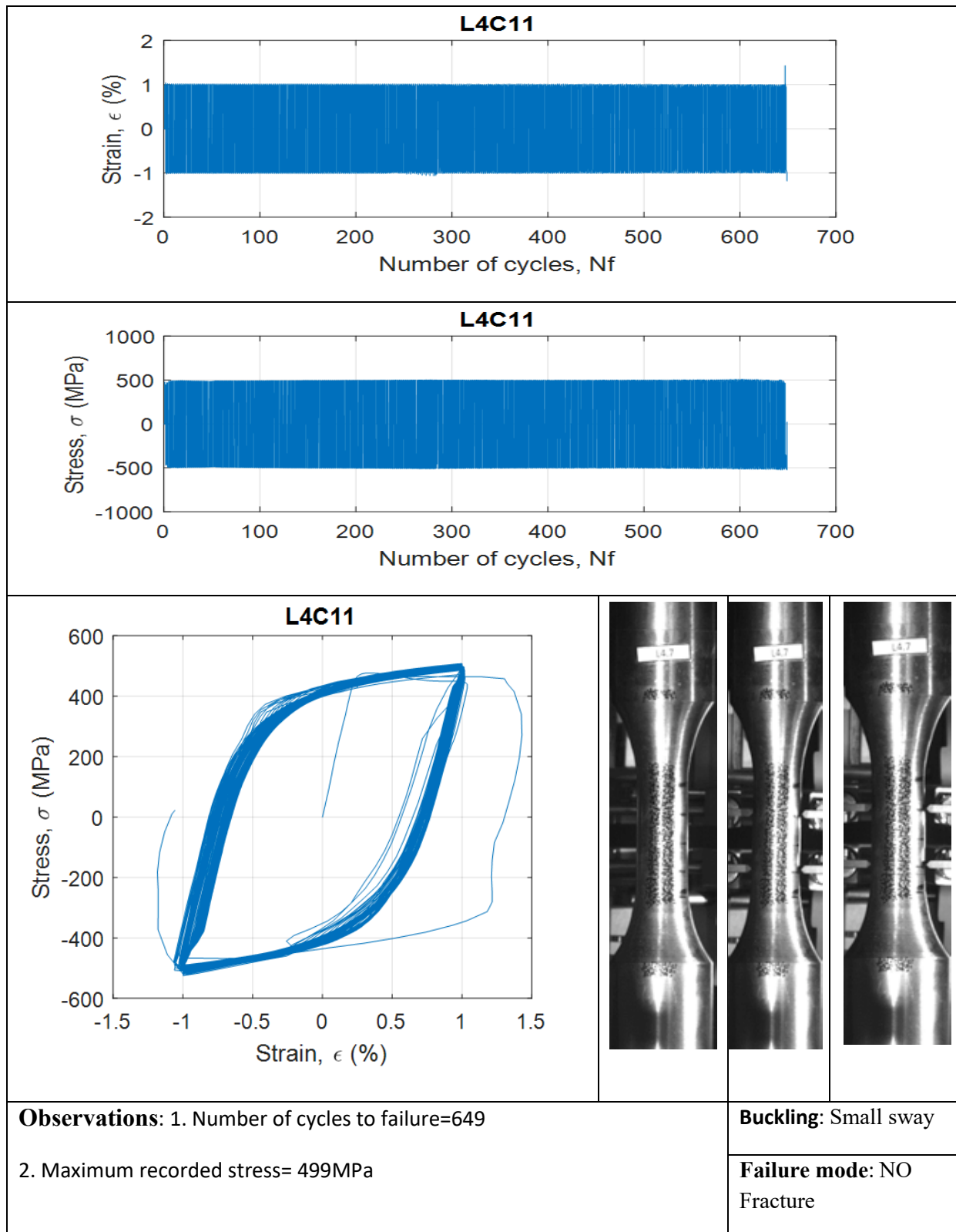


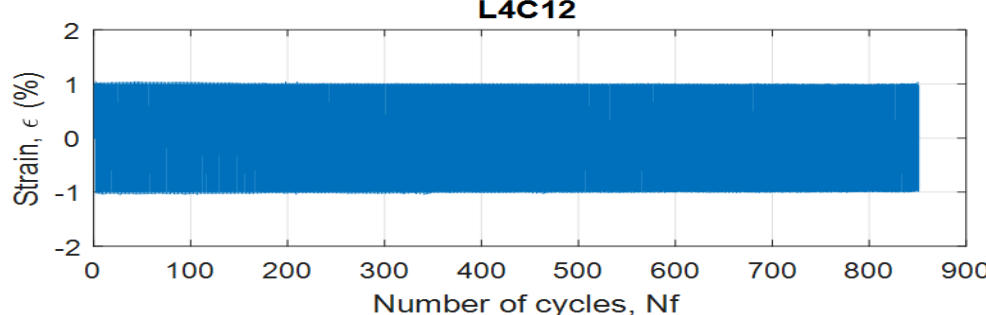
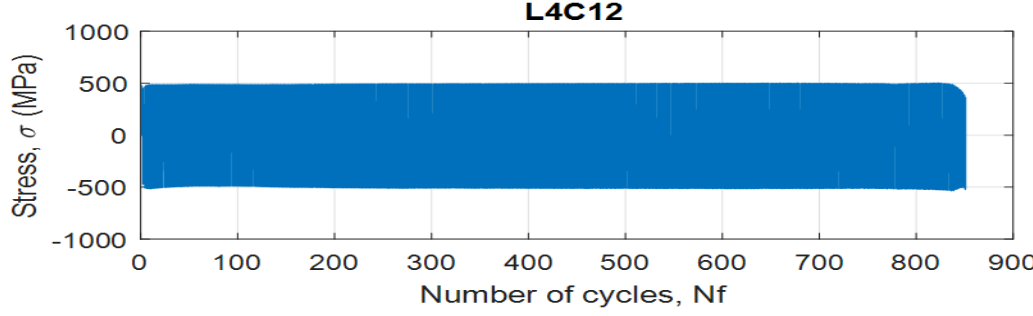
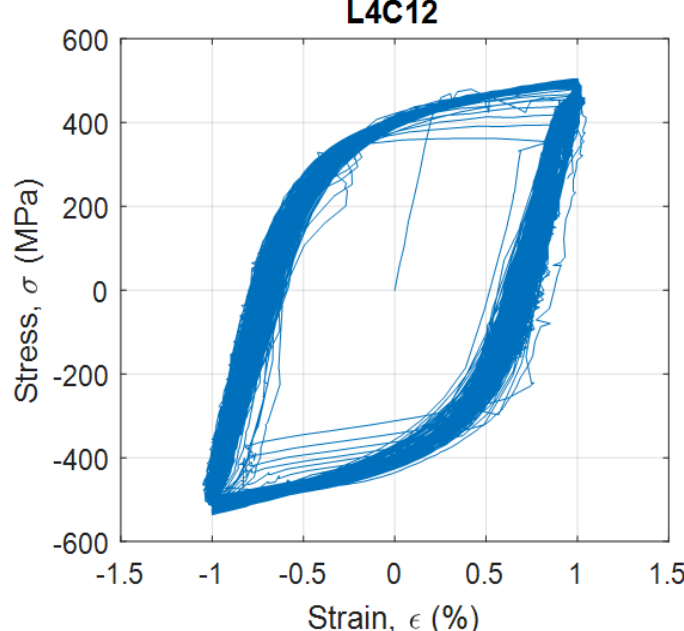

<p><b>Observations:</b> 1. Reduced diameter for the chamfer area where <math>d=14.88\text{mm}</math></p> <p>2. At 2<sup>nd</sup> cycle of -7%, horizontal displacement of 1mm</p> <p>3. Number of cycles to failure=31</p> <p>4. Maximum recorded strain=11%</p> <p>5. Maximum recorded stress= 611MPa</p>		<p><b>Buckling:</b> Small sway</p> <p><b>Failure mode:</b> Fracture between sensors</p>

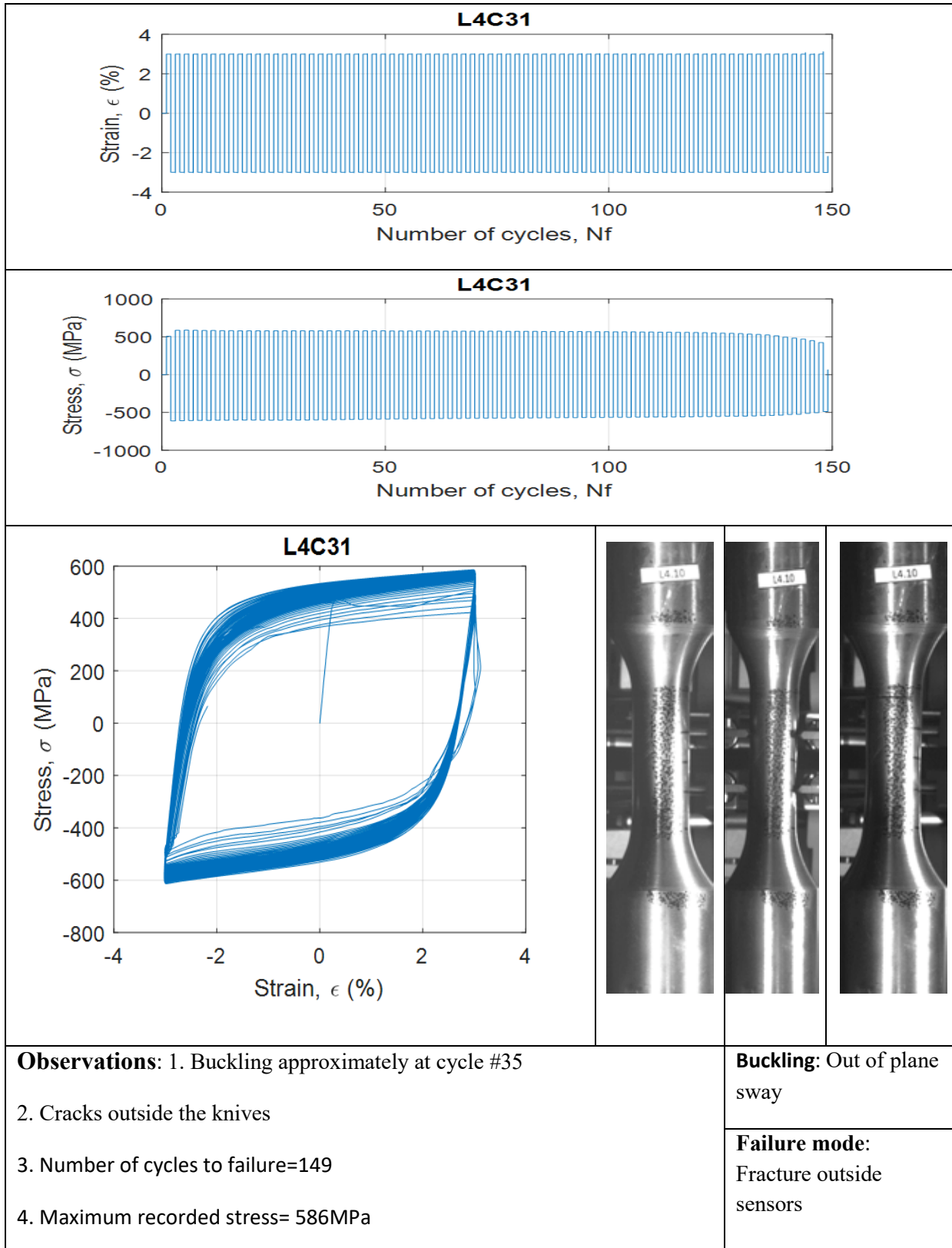
### 7. Results from monotonic tensile tests for S460

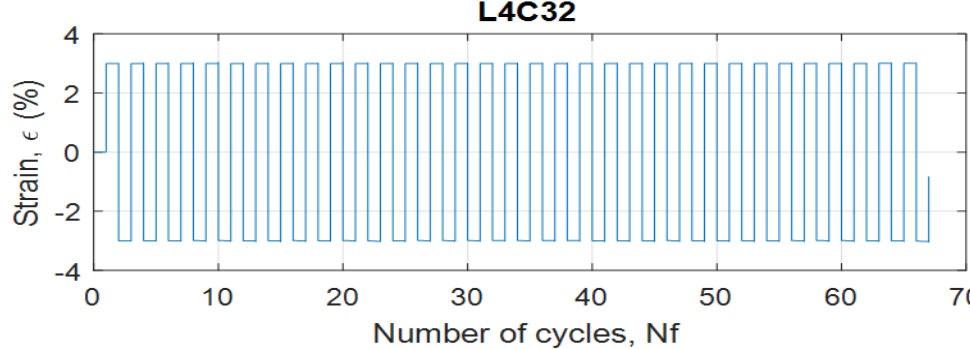
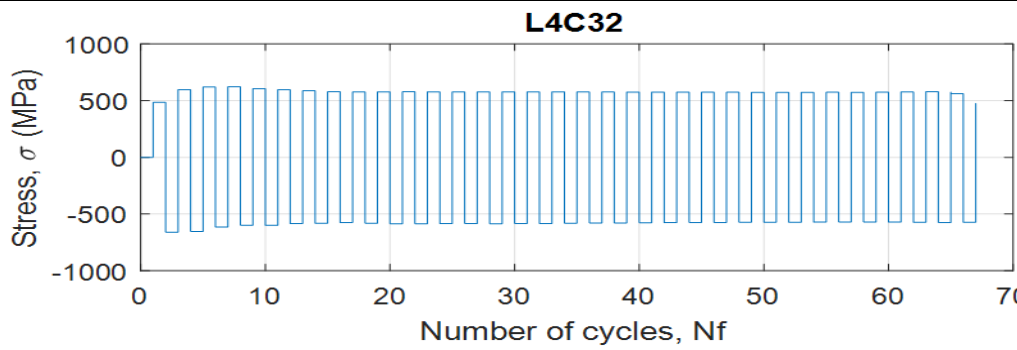
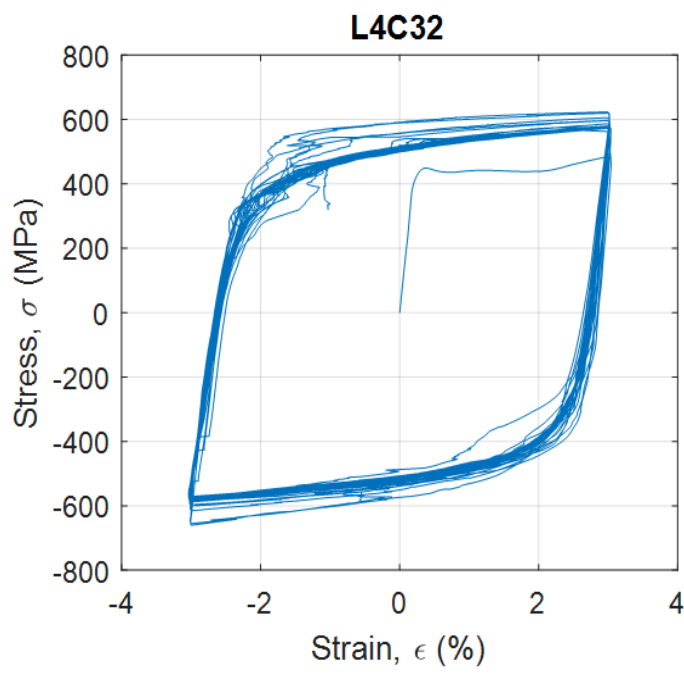
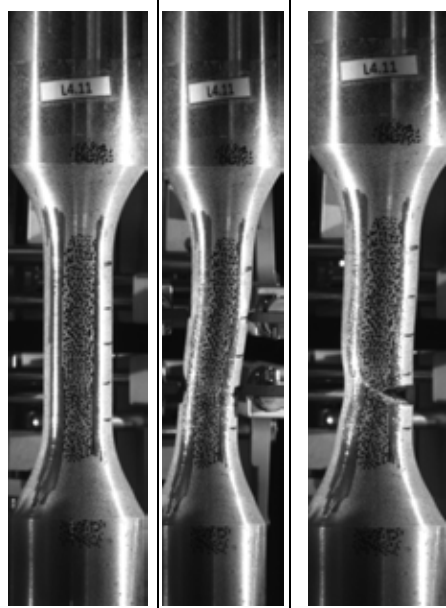
<p style="text-align: center;"><b>L4M1</b></p>  <p style="text-align: center;">Stress, <math>\sigma</math> (MPa)</p> <p style="text-align: center;">Strain, <math>\epsilon</math> (%)</p>		
<p><b>Observations:</b></p> <ol style="list-style-type: none"> <li>1. Largest strain amplitude recorded=35%</li> <li>2. Maximum recorded stress= 637MPa</li> </ol>	<p><b>Buckling:</b> N/A</p>	
	<p><b>Failure mode:</b> Fracture between sensors</p>	
<p style="text-align: center;"><b>L4M2</b></p>  <p style="text-align: center;">Stress, <math>\sigma</math> (MPa)</p> <p style="text-align: center;">Strain, <math>\epsilon</math> (%)</p>		
<p><b>Observations:</b></p> <ol style="list-style-type: none"> <li>1. Largest strain amplitude recorded=35%</li> <li>2. Maximum recorded stress= 631MPa</li> </ol>	<p><b>Buckling:</b> N/A</p>	
	<p><b>Failure mode:</b> Fracture between sensors</p>	

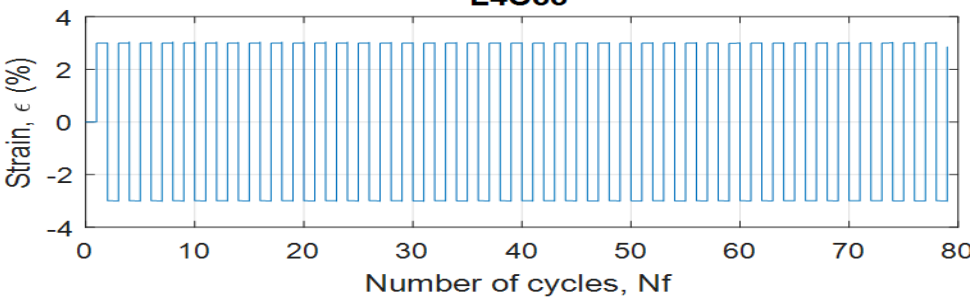
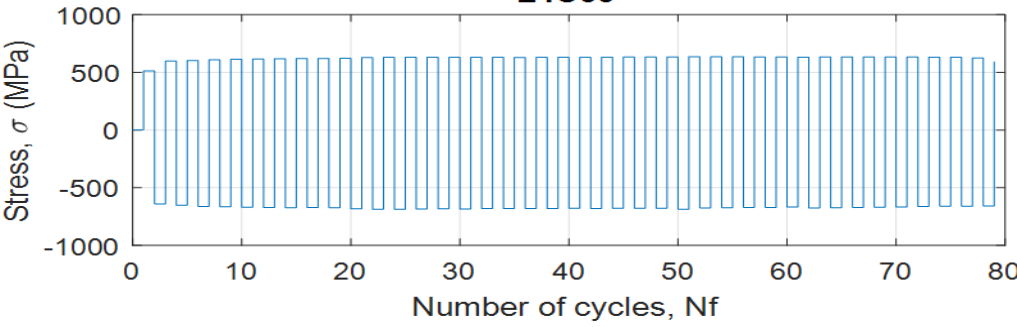
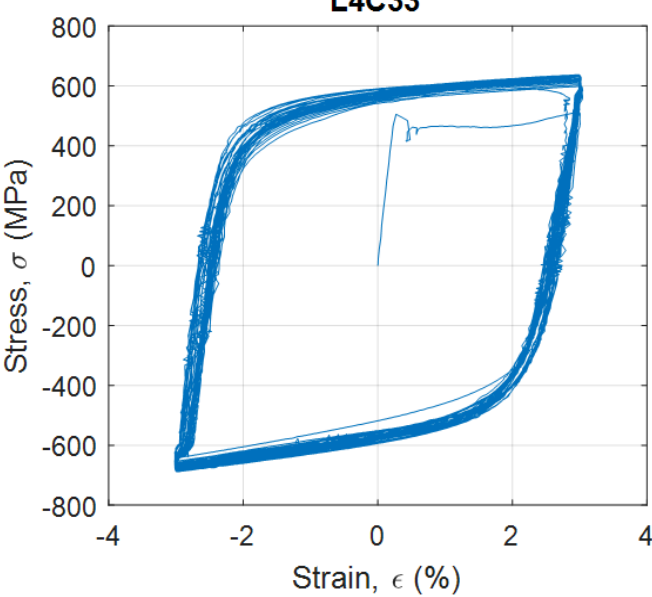

### 8. Results from constant strain amplitude tests for S460



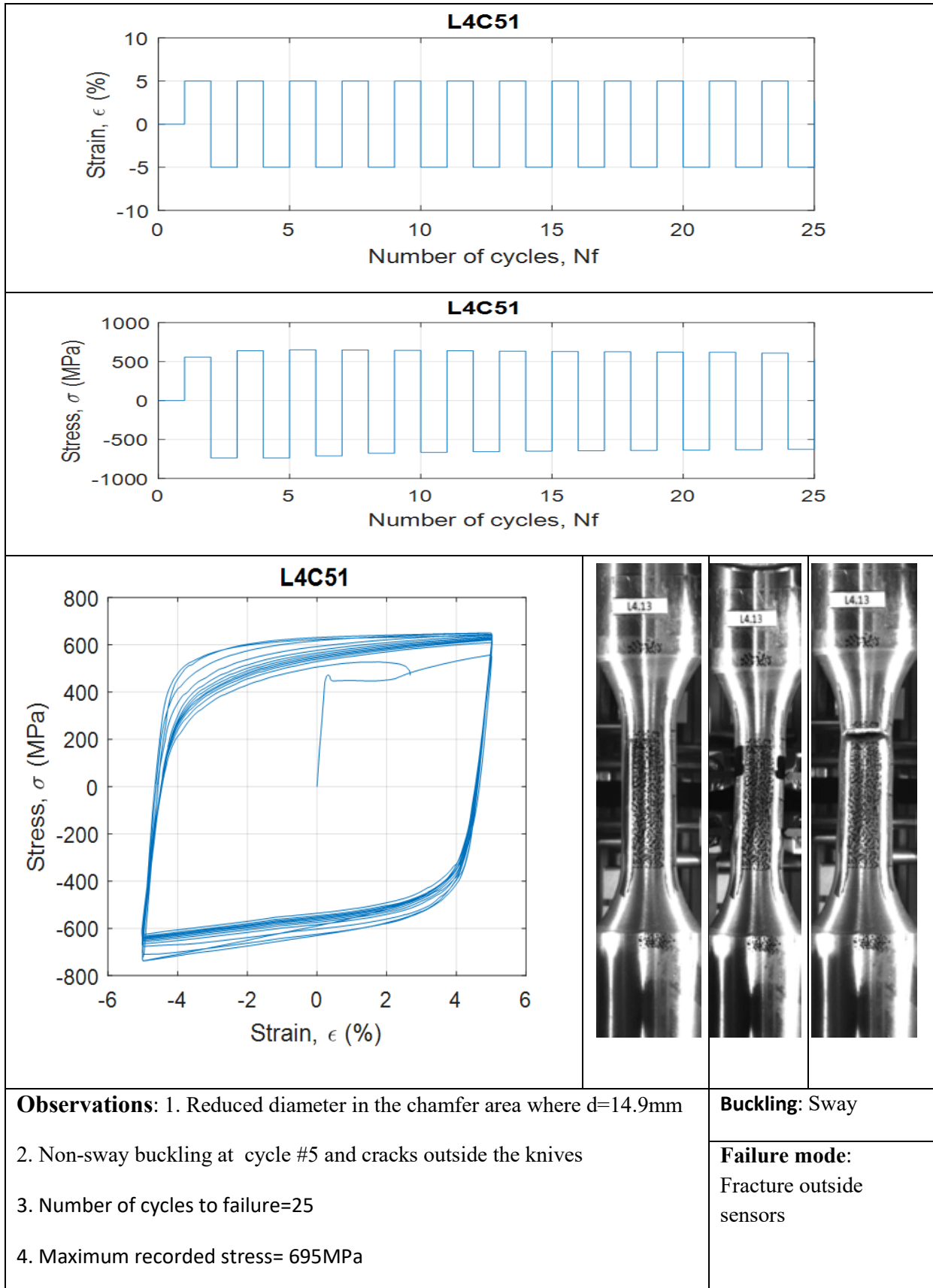
			
			
			
<p><b>Observations:</b> 1. The test lasted 4 hours.</p> <p>2. At cycle #420, crack appearance below the knives</p> <p>3. Number of cycles to failure=851</p> <p>4. Maximum recorded stress= 500MPa</p>		<p><b>Buckling:</b> NO</p> <p><b>Failure mode:</b> Fracture outside sensors</p>	



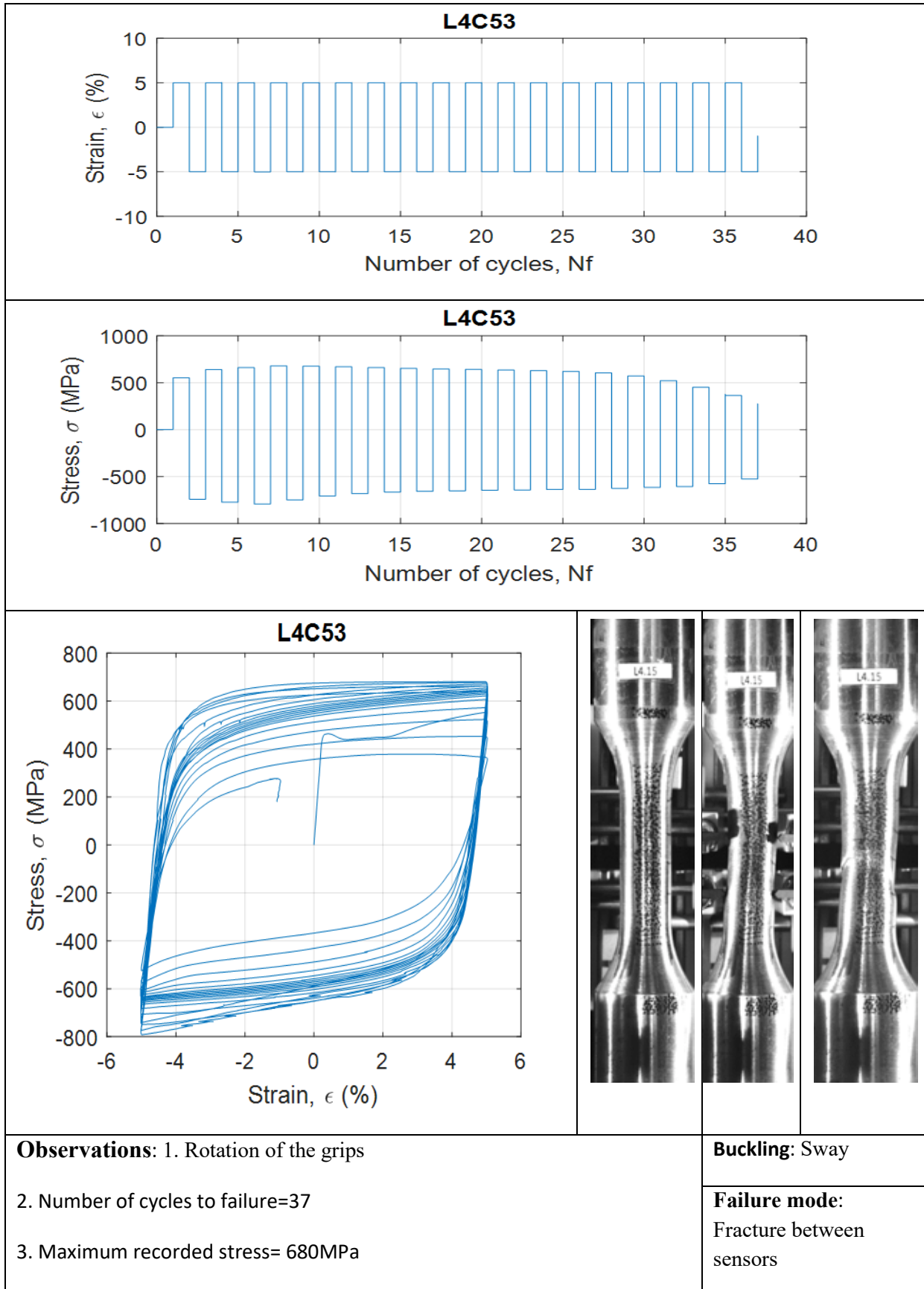
	
	
	
<p><b>Observations:</b> 1. A jump in the strain for the 1<sup>st</sup> cycle of -3%</p> <p>2. Shifting of the hysteresis loop</p> <p>3. Number of cycles to failure=67</p> <p>4. Maximum recorded stress= 623MPa</p>	
<p><b>Buckling:</b> Sway</p> <p><b>Failure mode:</b> Fracture outside sensors</p>	

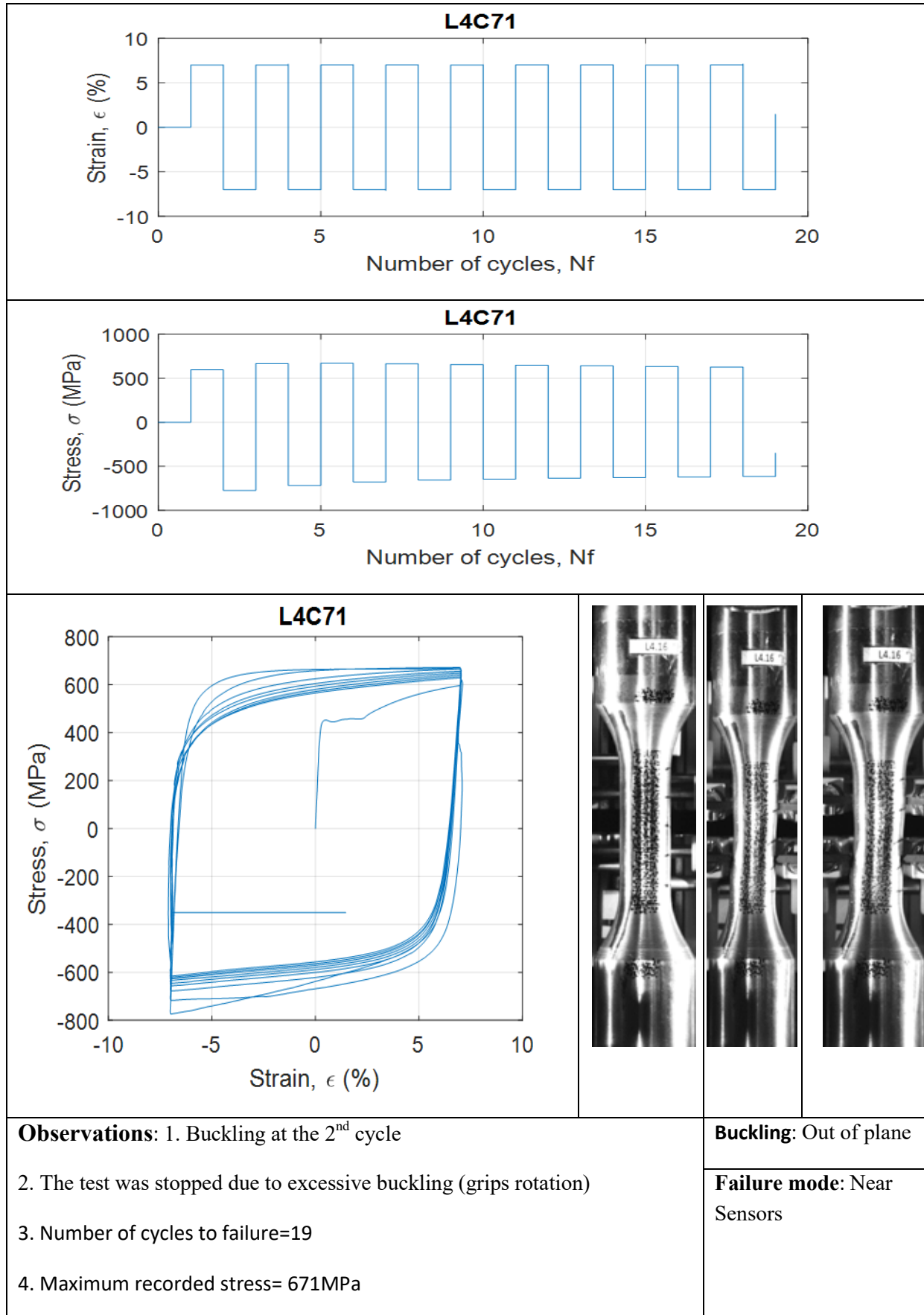
			
			
			
			
<p><b>Observations:</b> 1. A small notch occurred at the chamfer radius</p> <p>2. At cycle #14, breakage below the knives</p> <p>3. Number of cycles to failure=79</p> <p>4. Maximum recorded stress= 637MPa</p>		<p><b>Buckling:</b> Sway</p> <p><b>Failure mode:</b> Fracture outside sensors</p>	





<p><b>Observations:</b> 1. Notch occurred at the chamfer radius and buckling at cycle #5</p> <p>2. At cycle #6, the hysteresis loop is shifted to the left</p> <p>3. Number of cycles to failure=18</p> <p>4. Maximum recorded stress= 741MPa</p>		<p><b>Buckling:</b> Non-Sway</p> <p><b>Failure mode:</b> Fracture between sensors</p>	

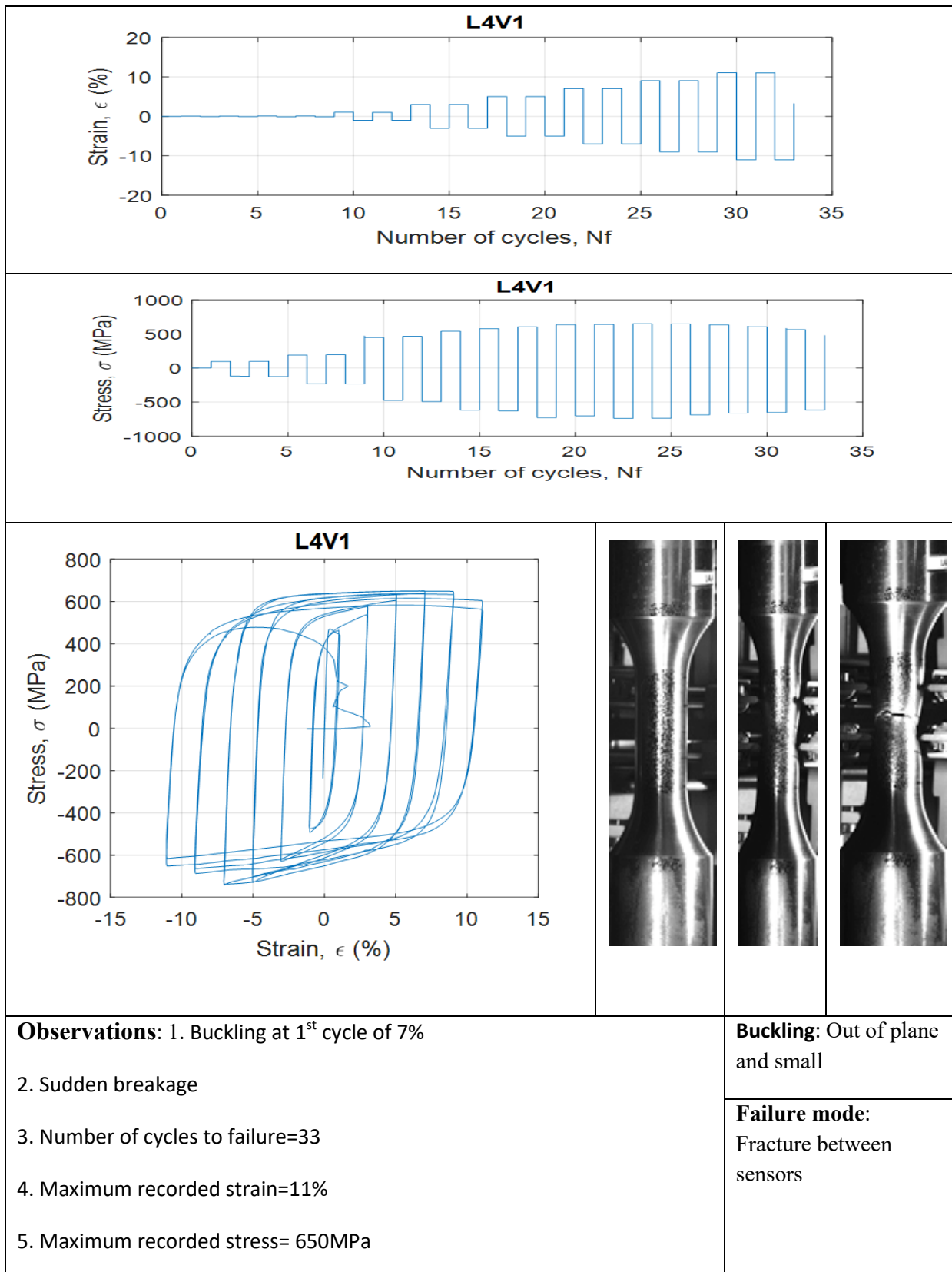




<p><b>Observations:</b> 1. Buckling at cycle #3 and breakage at cycle #6</p> <p>2. Necking between knives</p> <p>3. Number of cycles to failure=15</p> <p>4. Maximum recorded stress= 669MPa</p>		<p><b>Buckling:</b> Non-Sway</p> <p><b>Failure mode:</b> No Fracture</p>	

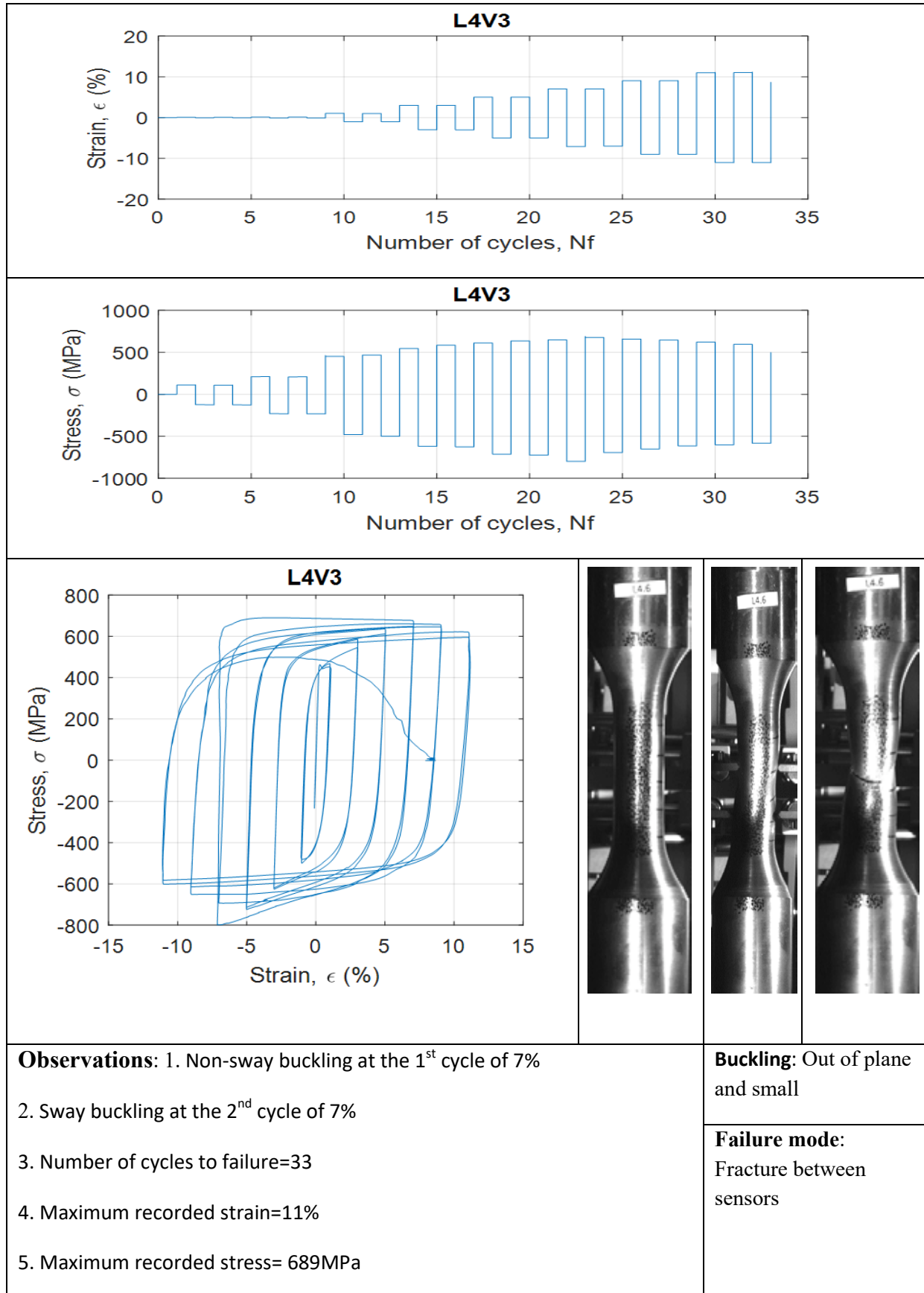
<p style="text-align: center;"><b>L4C73</b></p> <p style="text-align: center;">Number of cycles, Nf</p>		
<p style="text-align: center;"><b>L4C73</b></p> <p style="text-align: center;">Number of cycles, Nf</p>		
<p style="text-align: center;"><b>L4C73</b></p> <p style="text-align: center;">Stress, <math>\sigma</math> (MPa)</p> <p style="text-align: center;">Strain, <math>\epsilon</math> (%)</p>		<p><b>Buckling:</b> Non-sway + Sway</p> <hr/> <p><b>Failure mode:</b> No Fracture</p>
<p><b>Observations:</b></p> <ol style="list-style-type: none"> <li>1. Number of cycles to failure=5</li> <li>2. Maximum recorded stress= 737MPa</li> </ol>		

### 9. Results from variable strain amplitude tests for S460

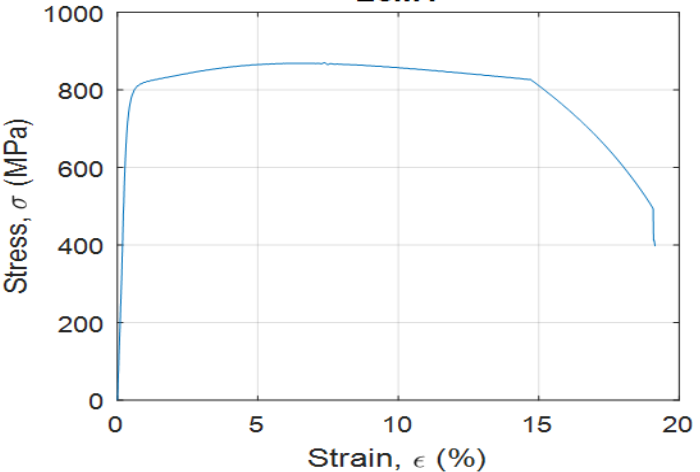
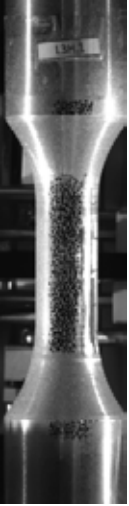

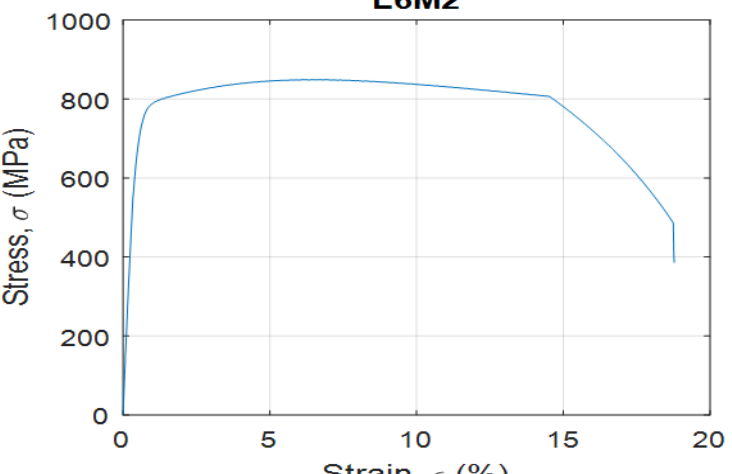
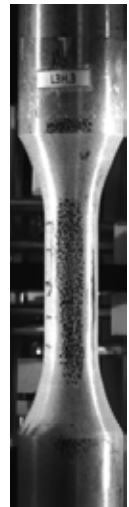



<p><b>Observations:</b> 1. A jump occurred in the curve at cycle #7.</p> <p>2. At cycle #10, buckling initiation and the roller fallen and breakage between knives at cycle #15</p> <p>3. Number of cycles to failure=37</p> <p>4. Maximum recorded strain=12%</p> <p>5. Maximum recorded stress= 690MPa</p>			
		<p><b>Buckling:</b> Sway</p> <p><b>Failure mode:</b> Fracture between sensors</p>	

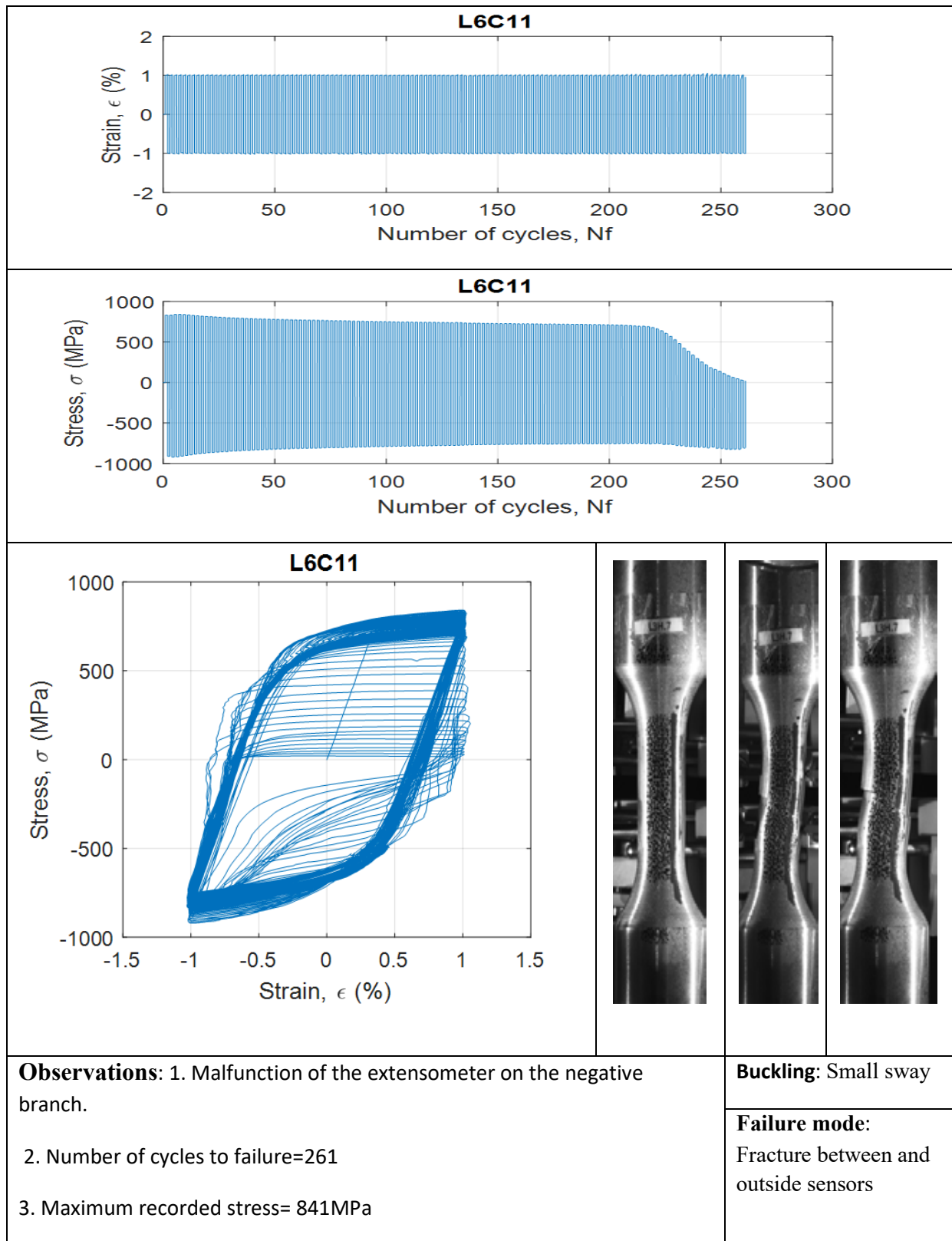


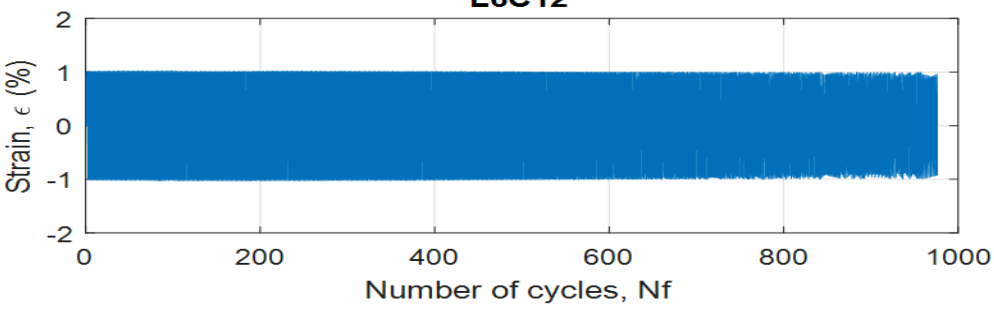
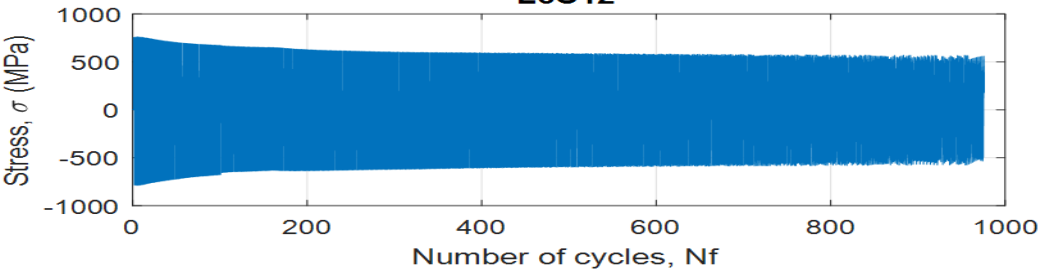
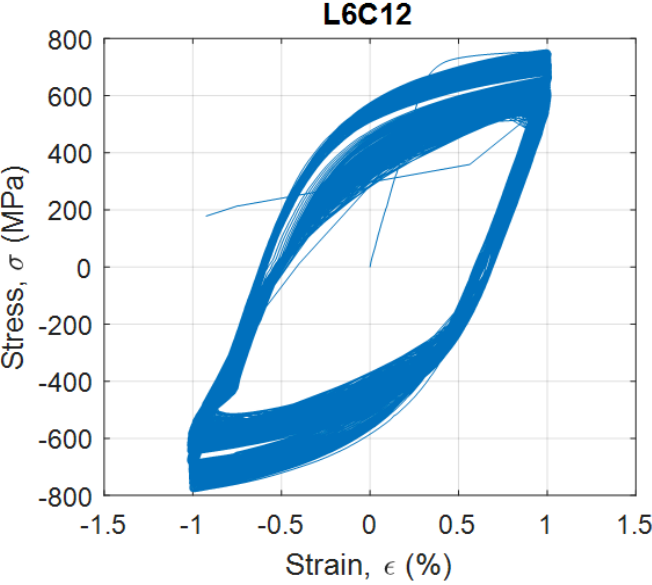



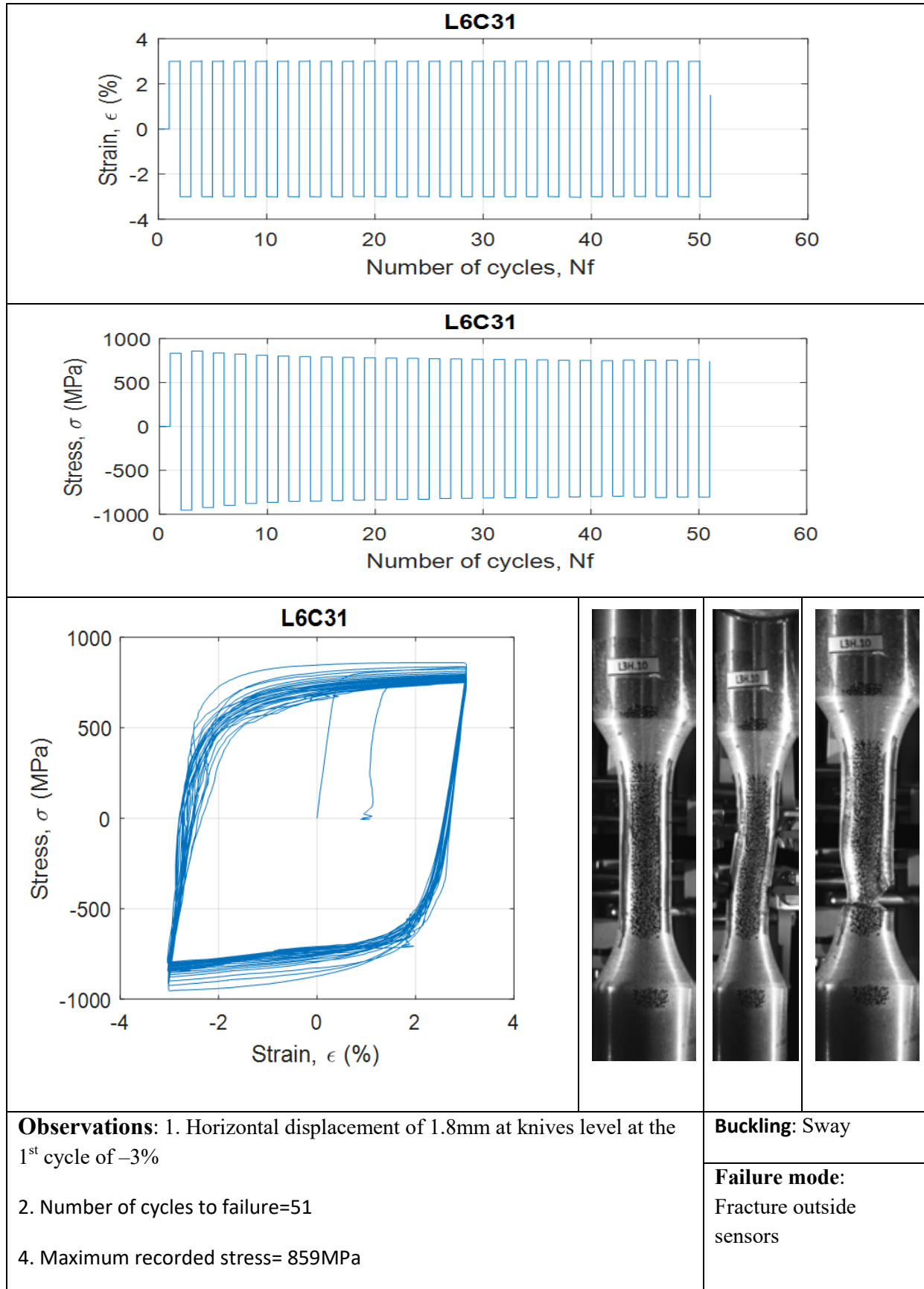
### 10. Results from monotonic tensile tests for S690

<p style="text-align: center;"><b>L6M1</b></p>  <p>Stress, <math>\sigma</math> (MPa)</p> <p>Strain, <math>\epsilon</math> (%)</p>		
<p><b>Observations:</b> 1. Breakage between knives</p> <p>2. Largest strain amplitude recorded=19%</p> <p>3. Maximum recorded stress= 870MPa</p>	<p><b>Buckling:</b> N/A</p> <p><b>Failure mode:</b> Fracture between sensors</p>	
<p style="text-align: center;"><b>L6M2</b></p>  <p>Stress, <math>\sigma</math> (MPa)</p> <p>Strain, <math>\epsilon</math> (%)</p>		
<p><b>Observations:</b> 1. Breakage between knives</p> <p>2. Longitudinal crack appearance</p> <p>2. Largest strain amplitude recorded=19%</p> <p>3. Maximum recorded stress=849MPa</p>	<p><b>Buckling:</b> N/A</p> <p><b>Failure mode:</b> Fracture between sensors</p>	

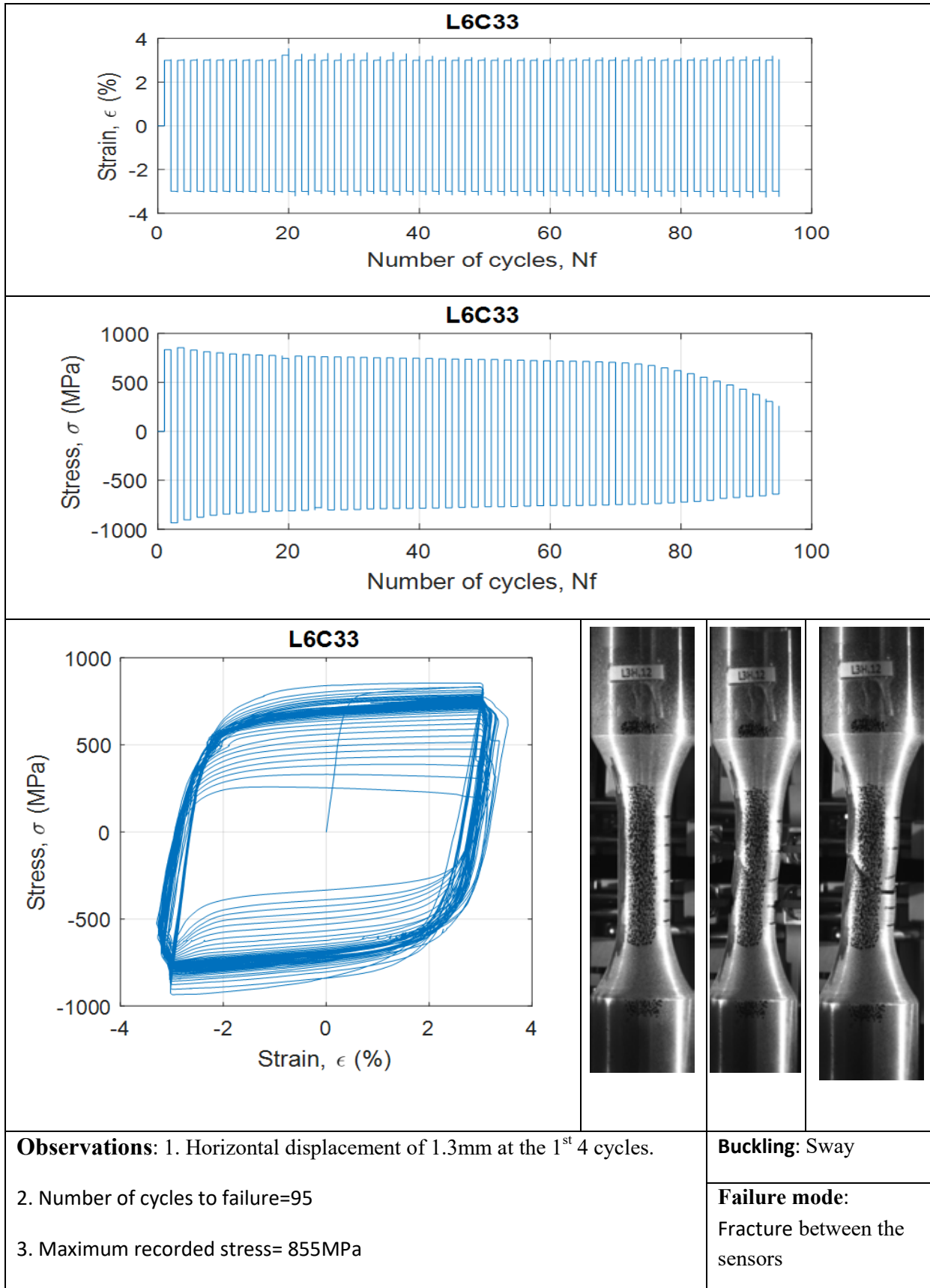
## 11. Results from constant strain amplitude tests for S690

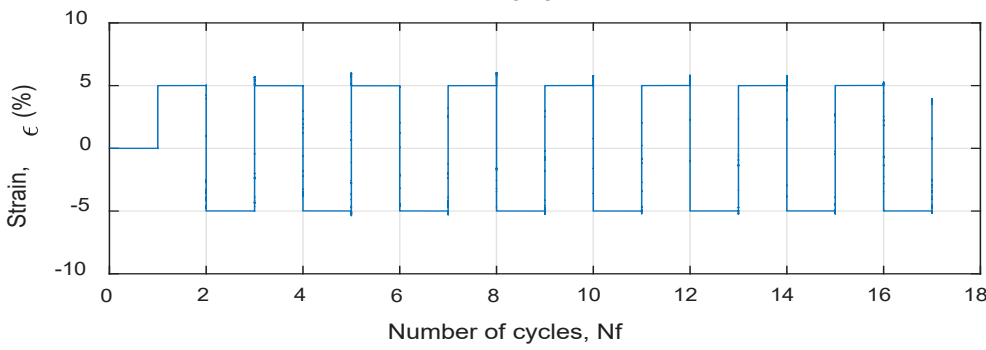
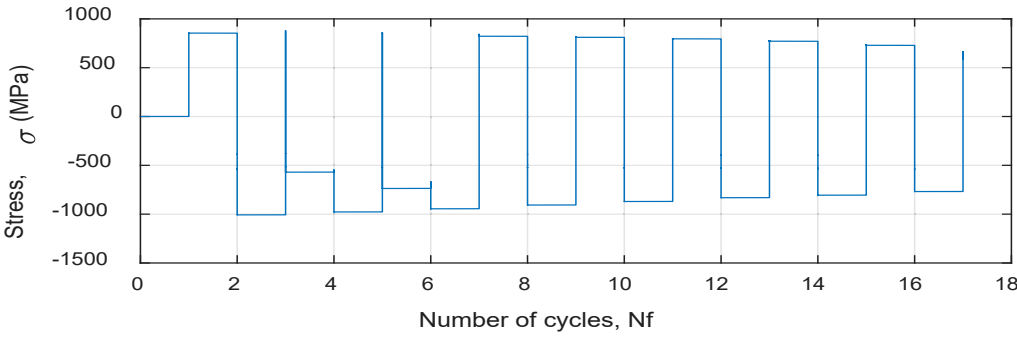
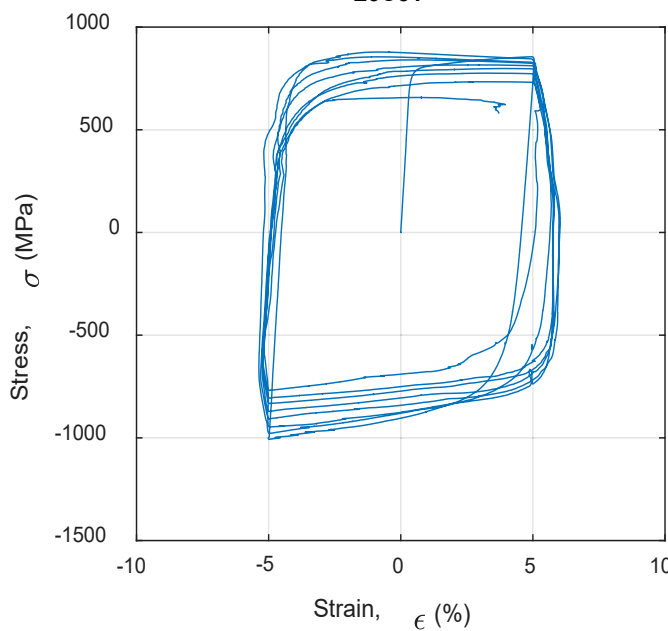
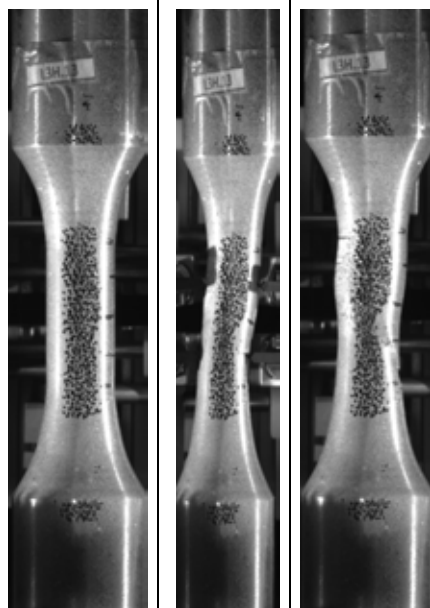


		
		
		
<p><b>Observations:</b> 1. At cycle #51 a sudden jump in strain leading the VIC recordings to shifted strains and the deformation of the specimen was no longer axial from cycle #51.</p> <p>2. The nominal strain decreased such that the cycle may not represent the real plus minus 1% and one of the rollers fallen down at cycle #488</p> <p>3. Number of cycles to failure=973</p> <p>4. Maximum recorded stress= 760MPa</p>		<p><b>Buckling:</b> NO</p> <p><b>Failure mode:</b> Fracture outside sensors</p>

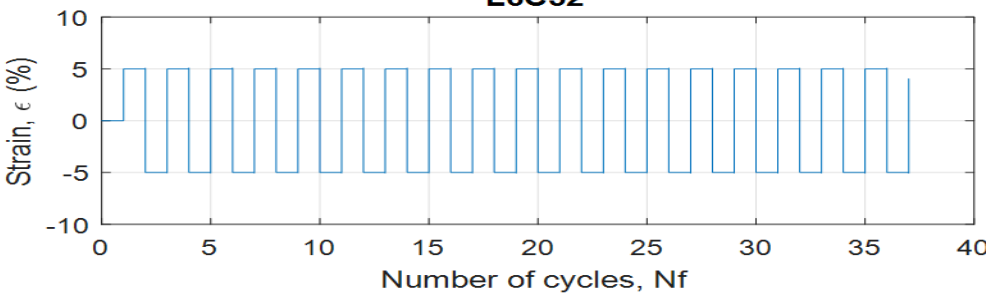
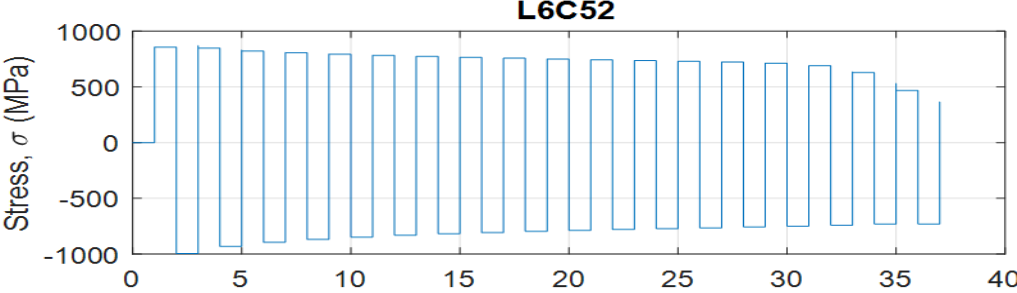
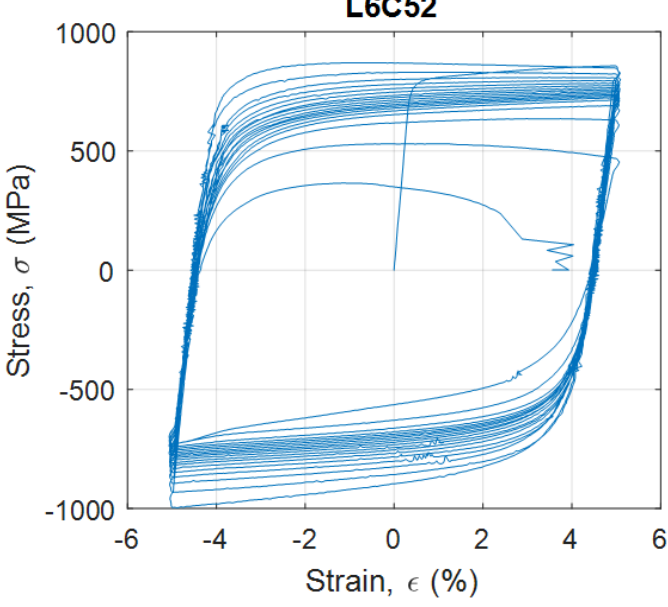



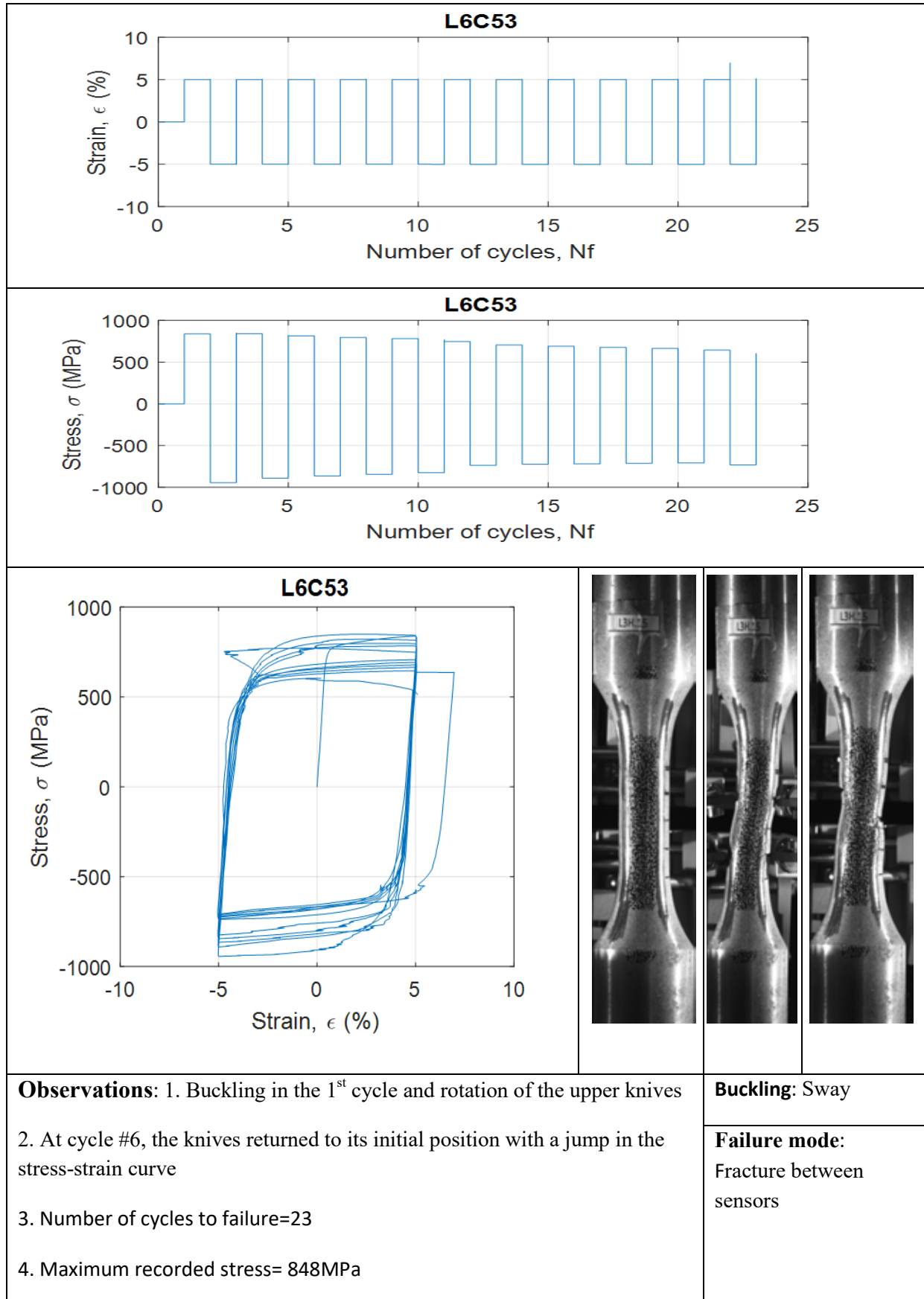
<p><b>Observations:</b> 1. A small notch at the chamfer radius</p> <p>2. At cycle # 22 necking between knives and at cycle #26 crack initiation</p> <p>3. Number of cycles to failure=96</p> <p>4. Maximum recorded stress= 858MPa</p>		<p><b>Buckling:</b> Sway</p> <p><b>Failure mode:</b> Fracture between sensors</p>

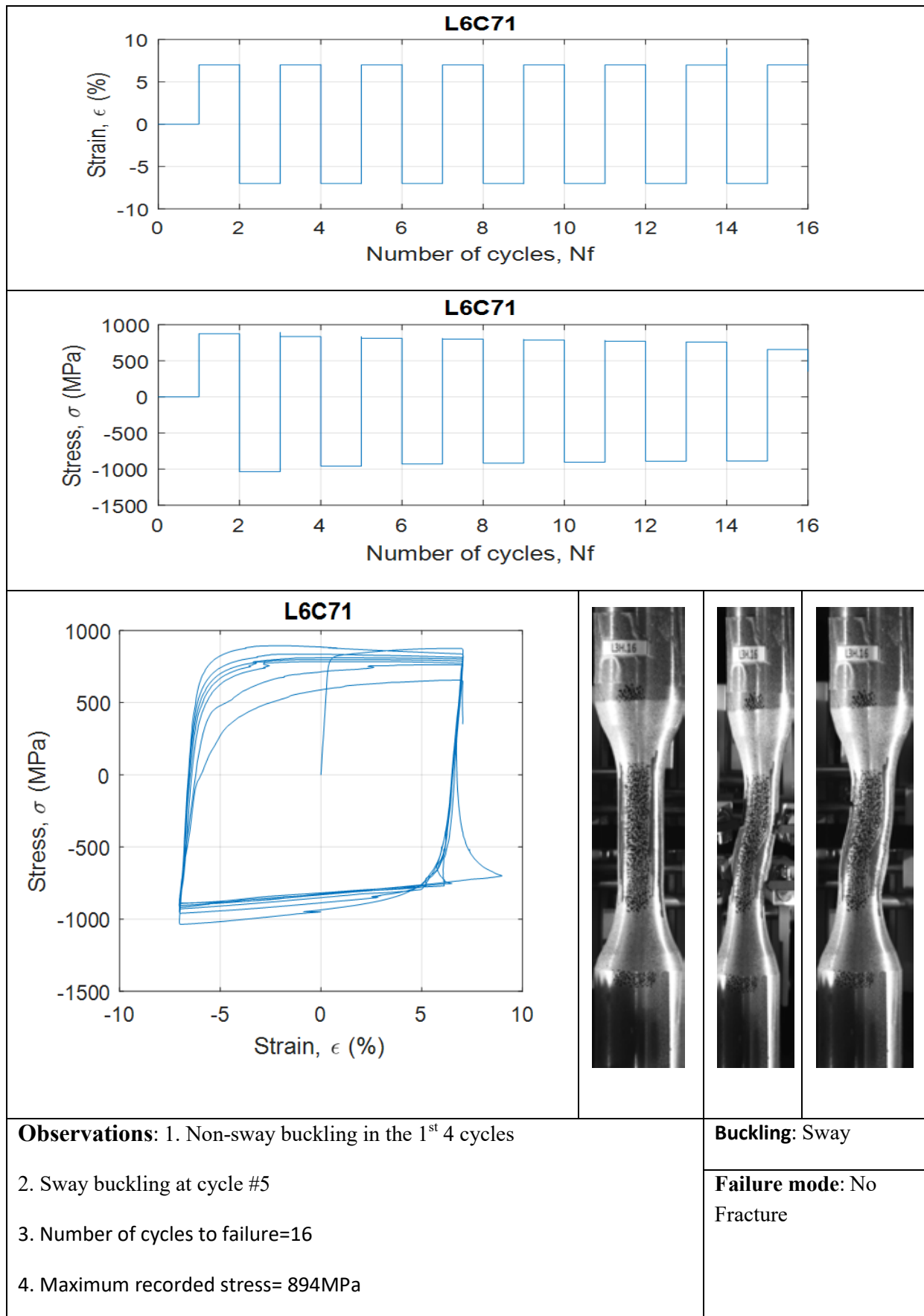


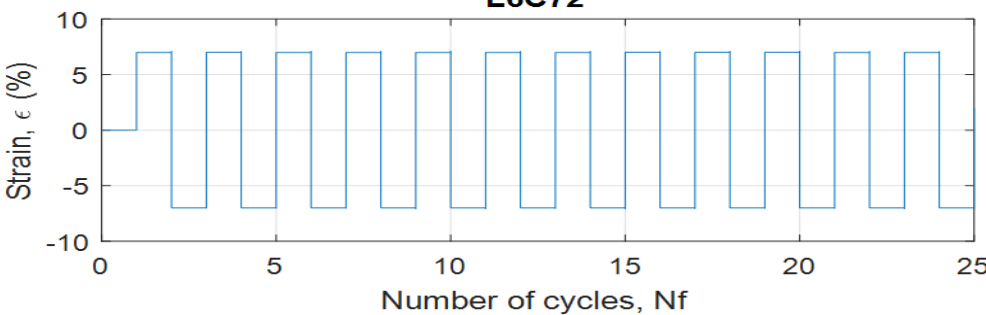
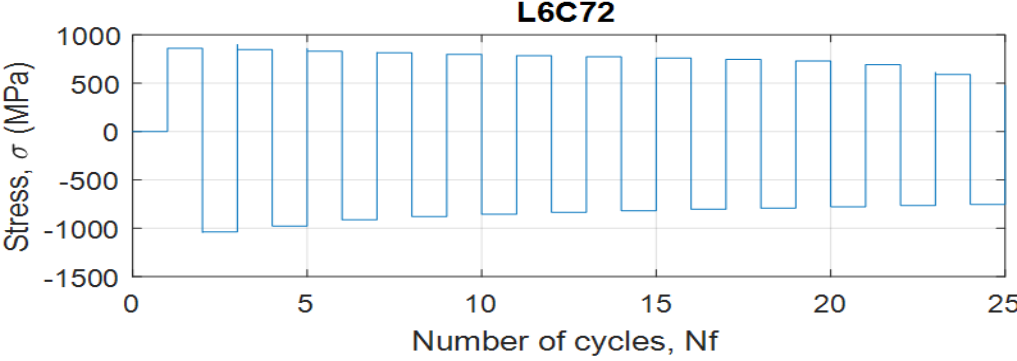
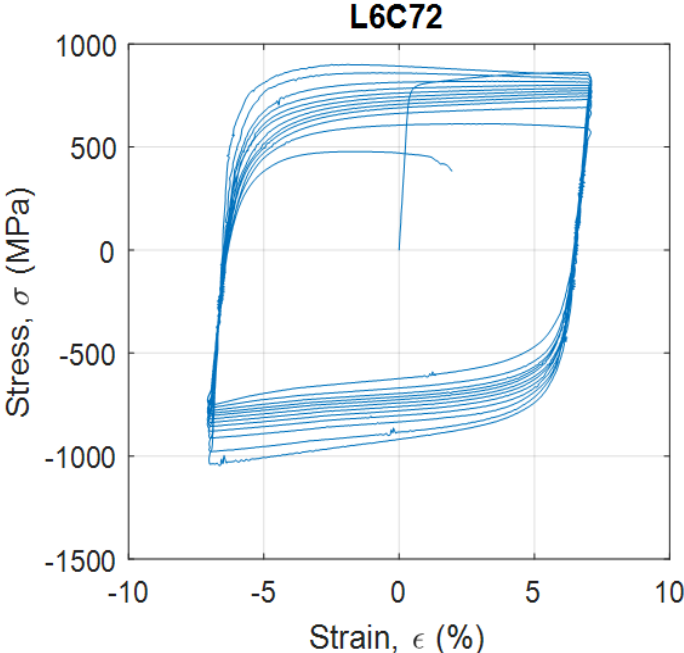

		
		
		
<p><b>Observations:</b> 1. Cracks outside the knives                  2. Number of cycles to failure=17                  3. Maximum recorded stress= 878MPa</p>		<p><b>Buckling:</b> Sway  <b>Failure mode:</b> Fracture near sensors</p>



			
			
			
<p><b>Observations:</b> 1. Softening at cycle #2 and buckling at cycle #4.</p> <p>2. Cracks above upper knives</p> <p>3. Number of cycles to failure=37</p> <p>4. Maximum recorded stress= 870MPa</p>			
		<p><b>Buckling:</b> Sway</p>	
		<p><b>Failure mode:</b> Fracture between sensors</p>	

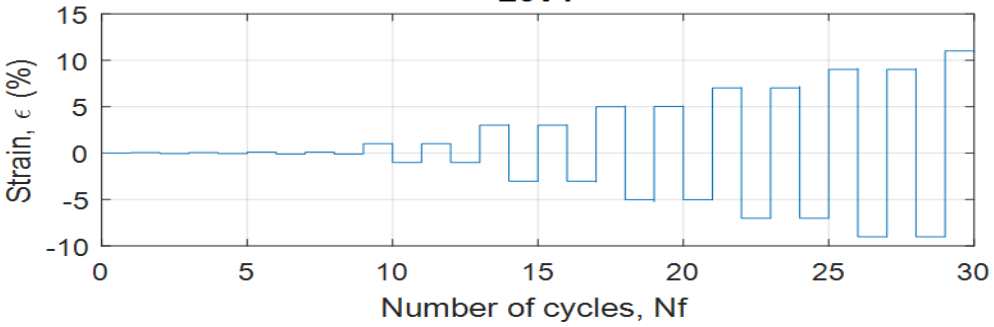
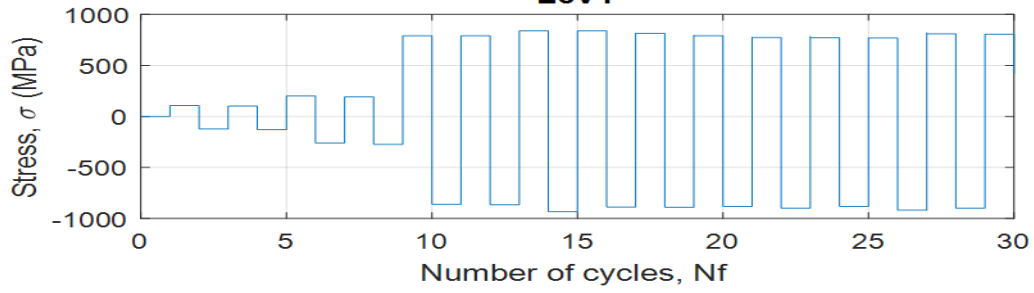
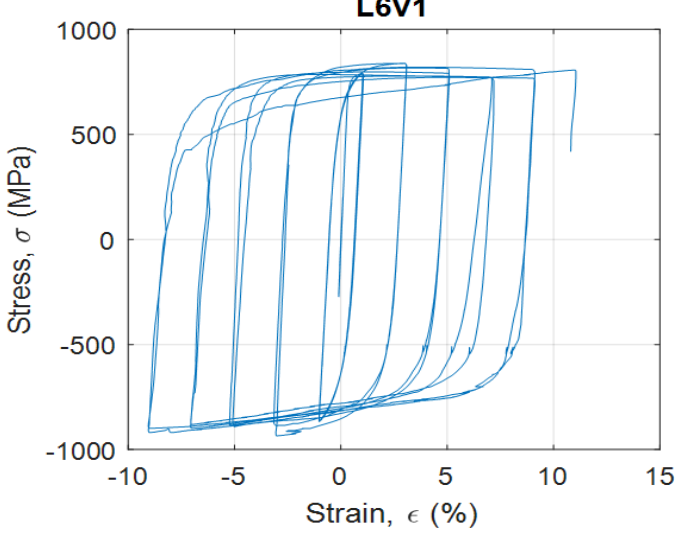
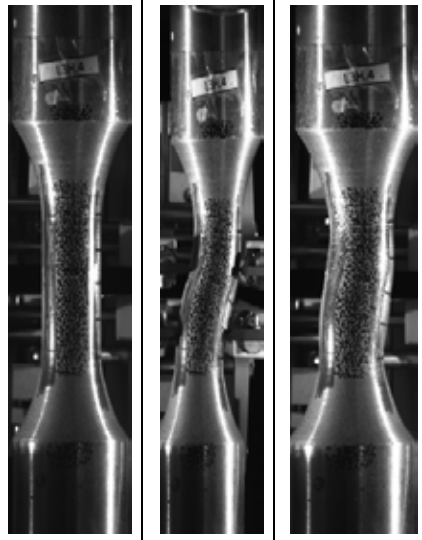




		
		
		
<p><b>Observations:</b></p> <ol style="list-style-type: none"> <li>1. Small imperfection at the chamfering radius</li> <li>2. Buckling initiation at cycle #2 and crack appearance at cycle #6</li> <li>3. Number of cycles to failure=25</li> <li>4. Maximum recorded stress= 901MPa</li> </ol>		<p><b>Buckling:</b> Sway</p> <p><b>Failure mode:</b> Fracture between sensors</p>

<p><b>Observations:</b> 1. Initial lateral deformation</p> <p>2. Breakage at the knives level</p> <p>3. Number of cycles to failure=15</p> <p>4. Maximum recorded stress= 869MPa</p>		<p><b>Buckling:</b> Sway</p> <p><b>Failure mode:</b> Fracture near sensors</p>

## 12. Results from variable strain amplitude tests for S690

		
		
		
<p><b>Observations:</b></p> <ol style="list-style-type: none"> <li>1. Reduced diameter in the chamfer area</li> <li>2. The test was stopped due to excessive buckling</li> <li>3. Number of cycles to failure=30</li> <li>4. Maximum recorded strain=9%</li> <li>5. Maximum recorded stress= 839MPa</li> </ol>		<p><b>Buckling:</b> Sway</p> <p><b>Failure mode:</b> No Fracture</p>

<p><b>Observations:</b> 1. More stable on the elastic cycles</p> <p>2. At cycle #4, decrease of the slope and the maximum force. 3. At cycle #6, buckling initiation. 4. Necking between knives and microcracks above knives</p> <p>5. Number of cycles to failure=38</p> <p>6. Maximum recorded strain=12%</p> <p>7. Maximum recorded stress= 795MPa</p>		<p><b>Buckling:</b> NO</p> <p><b>Failure mode:</b> Fracture between sensors</p>	

